Rapid community-driven development of a SARS-CoV-2 tissue simulator

Michael Getz[1,**], Yafei Wang[1,**], Gary An[2,*], Andrew Becker[2,*], Chase Cockrell[2,*], Nicholson Collier[3,4,*], Morgan Craig[5,6*], Courtney L. Davis[7,*], James Faeder[8,*], Ashlee N. Ford Versypt[9,10,*],Juliano F. Gianlupi[1,*], James A. Glazier[1,*], Sara Hamis[11,*], Randy Heiland[1,*], Thomas Hillen[12,*], Dennis Hou[13,*], Mohammad Aminul Islam[9,*], Adrianne Jenner[5,6,*], Furkan Kurtoglu[1,*], Bing Liu[8,*,†], Fiona Macfarlane[11,*], Pablo Maygrundter[14,*], Penelope A Morel[15,*], Aarthi Narayanan[16,*], Jonathan Ozik[3,4,*], Elsje Pienaar[17,*], Padmini Rangamani[18,*], Jason Edward Shoemaker[19,*], Amber M. Smith[20,*], Paul Macklin[1,***]

[1] Department of Intelligent Systems Engineering, Indiana University. Bloomington, IN USA
[2] The University of Vermont Medical Center, Burlington, VT USA
[3] Decision and Infrastructure Sciences, Argonne National Laboratory. Lemont, IL USA
[4] Consortium for Advanced Science and Engineering, University of Chicago. Chicago, IL USA
[5] Department of Mathematics, University of Montreal. Montreal, QC Canada
[6] CHU Sainte-Justine Research Centre, Montreal, QC Canada
[7] Natural Science Division, Pepperdine University, Malibu, CA USA
[8] Department of Computational and Systems Biology, University of Pittsburgh. Pittsburgh, PA USA
[9] School of Chemical Engineering, Oklahoma State University, Stillwater, OK USA
[10] Oklahoma Center for Respiratory and Infectious Diseases, Oklahoma State University, Stillwater, OK USA
[11] School of Mathematics and Statistics, University of St Andrews, St Andrews, Scotland.
[12] Department of Mathematical and Statistical Sciences, University of Alberta. Edmonton, AB Canada
[13] Department of Mathematics, Rutgers University. New Brunswick, NJ USA
[14] Citizen scientist. Austin, TX USA
[15] Department of Immunology, University of Pittsburgh. Pittsburgh, PA USA
[16] National Center for Biodefense and Infectious Disease, George Mason University. Manassas, VA USA
[17] Weldon School of Biomedical Engineering, Purdue University. West Lafayette, IN USA
[18] Department of Mechanical and Aerospace Engineering, University of California. San Diego, CA USA
[19] Department of Chemical and Petroleum Engineering, University of Pittsburgh. Pittsburgh, PA USA
[20] Department of Pediatrics, University of Tennessee Health Science Center, Memphis, TN USA

* contributed equally to this work
** equally contributing lead authors
† in memoriam
*** corresponding author: macklinp@iu.edu, @MathCancer

Note: This is a rapid prototyping project. For the very latest, see http://COVID-19.physicell.org

Abstract:

The 2019 novel coronavirus, SARS-CoV-2, is an emerging pathogen of critical significance to international public health. Knowledge of the interplay between molecular-scale virus-receptor interactions, single-cell viral replication, intracellular-scale viral transport, and emergent tissue-scale viral propagation is limited. Moreover, little is known about immune system-virus-tissue interactions and how these can result in low-level (asymptomatic) infections in some cases and acute respiratory distress syndrome (ARDS) in others, particularly with respect to presentation in different age groups or pre-existing inflammatory risk factors like diabetes. Given the nonlinear interactions within and among each of these processes, multiscale simulation models can shed light on the emergent dynamics that lead to divergent outcomes, identify actionable "choke points" for pharmacologic interventions, screen potential therapies, and identify potential biomarkers that differentiate patient outcomes. Given the complexity of the problem and the acute need for an actionable model to guide therapy discovery and optimization, we introduce and iteratively refine a prototype of a multiscale model of SARS-CoV-2 dynamics in lung tissue. The first prototype model was built and shared internationally as open source code and an online interactive model in under 12 hours, and community domain expertise is driving rapid refinements with a two-to-four week release cycle. In a sustained community effort, this consortium is integrating data and expertise across virology, immunology, mathematical biology, quantitative systems physiology, cloud and high performance computing, and other domains to accelerate our response to this critical threat to international health.

Introduction

The ongoing pandemic caused by the novel severe acute respiratory syndrome coronavirus 2 (SARS-CoV-2) has illuminated the global public health threat posed by highly pathogenic coronaviruses that emerge from zoonotic sources. With the majority of the world's population immunologically naïve and no available antivirals or vaccines, over 14,000,000 infections and 600,000 deaths amassed by the end of July 2020[1]. Coronavirus disease 2019 (COVID-19)—caused by SARS-CoV-2 infection—is characterized by a range of respiratory symptoms, including fever and cough[2,3], that can progress to acute respiratory distress syndrome (ARDS) in some patients[4,5]. Age and comorbidities appear to be the main risk factors for development of severe disease[6-8]. However, the dynamics of virus replication, interaction with host immune responses, and spread within the respiratory tract are still being established. Because a vaccine may not be available for 9-18 months, there is a critical need to further understand the infection in order to quickly identify pharmacologic interventions and optimal therapeutic designs that work to lessen virus replication and disease severity. However, this requires an international community effort that integrates expertise across a variety of domains and a platform that can be iteratively updated as new information and data arises.

To aid this effort, we have assembled an international, multi-disciplinary coalition to rapidly develop an open source, multi-scale tissue simulator that can be used to investigate mechanisms of intracellular viral replication, infection of epithelial cells, host immune response, and tissue damage. The aim of this project is to concentrate community modeling efforts to create a comprehensive multiscale simulation framework that can subsequently be calibrated, validated, and used to rapidly explore and optimize therapeutic interventions for COVID-19. Once the prototype has been completed (after several design iterations), this coalition will transition to maintain and support the simulation framework and aggregate calibrated/validated parameter values.

To address the acute need for rapid access to an actionable model, we are using a community-driven coalition and best open science practices to build and iteratively refine the model:

(1) **Open source and GitHub:** All simulation source code is shared as open source on GitHub, with well-defined, versioned, and documented releases, and Zenodo-generated archives and DOIs.
(2) **Interactive cloud-hosted models:** Every prototype version is rapidly transformed into a cloud-hosted, interactive model to permit faster scientific communication across communities, particularly with virologists, immunologists, pharmacologists, and others who have essential insights but ordinarily would not directly run the simulation models.
(3) **Social media and virtual feedback:** We enlist community participation (feedback, modeling contributions, software contributions, and data contributions) through social media, virtual seminars, web forms, a dedicated Slack workspace, and weekly team meetings. We particularly encouraging feedback and data contributions by domain experts in virology, epidemiology, immunology, and mathematical biology.
(4) **Frequent preprint updates:** Each model iteration is accompanied by a cloud-hosted, interactive app (see #2) and an updated preprint on *bioRxiv*.
(5) **Integration of feedback:** All community feedback is evaluated to plan the next set of model refinements and recorded in an updated *bioRxiv* preprint.

Our first test of this workflow saw a first proof-of-concept software release (Steps 1-2) in 12 hours, and the first integration of community feedback and preprint dissemination was complete within a week. We have begun integrating community feedback, and it is our intention to continue rapid iteration, with a new candidate model release every few weeks.

Goals and guiding principles

This project is community-driven, including the following contributions:

1) **Community priorities:** The community helps define the driving research questions, set the project scope, and select the critical biological components to be modeled.
2) **Consensus hypotheses:** The community drives a shared, clearly-written consensus specification of the underlying biological hypotheses.

3) **Mathematical modeling:** The community helps develop, review, and refine the mathematical interpretation of the biological hypotheses.
4) **Computational implementation:** The computational implementation is shared as open source with community definition of specifications, unit tests, coding, and code review.
5) **Community feedback:** Community feedback on the model realism, hypotheses, mathematics, computational implementation, and techniques is encouraged throughout the development process.
6) **Community parameters and data:** Community contributions of parameter estimates and data contributions are aggregated to assist in model development and constraint.

Project scope

While by definition the project scope can be refined by the community, the initial project scope is to:

1) Develop the general computational framework sufficiently to address many of the community-driven research questions.
2) Deliver a working simulation framework for use by others to perform calibration and validation. That is, the prototyping aims of this project are complete once the model is capable of demonstrating essential biological behaviors qualitatively.
3) To provide a software framework whose underlying hypotheses, mathematics, and computational implementation have been rigorously assessed by appropriate domain experts.

In particular, while this project will work to constrain, estimate, and calibrate parameters to the greatest extent possible, it is *not* within scope to delay software release until full calibration and validation. Those tasks are within scope of fully funded teams with dedicated experiments.

This project aims to deliver software that one can reasonably expect to calibrate and validate, thus freeing funded investigations from expensive early software development while providing a broad community consensus on key biological hypotheses. By rapidly prototyping this software, we aim to accelerate many funded research efforts.

Essential model components

As part of defining the project scope, we have identified the following critical model components:

1) Virus dissemination in epithelial tissue
2) Virus binding, endocytosis, replication, and exocytosis
3) Infected cell responses, including changes to metabolism, secreted signals, and death
4) Inflammatory response
5) Ramp up of the immune response (particularly in lymph nodes)
6) Immune cell infiltration
7) Immune cell predation of infected and other cells
8) Tissue damage by death of cells due to infection or host response; serves as a surrogate marker for organ dysfunction

Guiding principles

The coalition aims to model not merely the disease endpoints, but the disease *dynamics*. This will allow scientists to investigate mechanistic “what if” questions on potential interventions: *What if* we could inhibit endocytosis? *What if* we could introduce a cytokine early or late in the disease course? *What if* the infected cell apoptosis could be accelerated or delayed?

To accomplish this, we use a modular design: an overall tissue-scale model integrates an array of targeted *submodels* that simulate critical processes (e.g., receptor binding and trafficking and virus replication). Each submodel is clearly specified to enable interoperability and to make it feasible for subteams to simultaneously develop and test the model components in parallel. Throughout development, we use open source methodologies that enhance communication, transparency, and reproducibility. See Box 1.

Guiding principles: motivation

- The model should investigate the dynamics of infection and treatment, not merely endpoints.
- The model should help the community ask "what if" questions to guide experiments and interventions[9,10].

Guiding principles: approach

- Community consensus will be gathered and efforts pooled into a "standardized" model that captures key SARS-CoV-2 dynamics. The model will be supplied to the community for parallel studies by multiple labs.
- The model framework will be built with relatively sparse data, relying upon domain expertise and observations to choose its general form and assess its qualitative behavior.
- The model will be modular. Each submodel will have well-defined inputs and outputs, allowing parallel development and replacement of submodels with improved versions without change to the overall integrated model or other submodels.
- As part of the model formulation, documentation, and dissemination, we will craft clearly delineated "conceptual model and hypotheses" to encourage development of independent models with distinct methodologies and software frameworks.
- The submodels will be independently executable and verifiable, allowing parallel development.
- The overall model framework will be released periodically released numbered versions (distributions) that bundle the best working version of each submodel as it exists at the time of release, allowing end-users (the community) to use well-defined, well-tested snapshots of the project.
- The model (and known parameter values) will be made publicly available as open source for maximum public benefit.
- The model will be made publicly available as an interactive web app to encourage community participation, to accelerate scientific dissemination, and to increase public educational benefit.
- Rapid prototyping will be used to encourage a fast develop-test-refine cycle, build expertise, and gain community feedback.
- Data and parameter sharing is encouraged throughout this effort for use in the user community following the model's "completion."
- The model will be developed to a point that it has correct qualitative behavior so that calibration is likely to succeed. This is the "product" for use in subsequent investigations by multiple teams. See the ***scoping*** statements above.
- After the model prototyping is complete (the goal of this paper), a maintenance and support phase will be entered to fix bugs, support scientist users, and add features identified by the user community.

Box 1: Guiding principles for the rapid prototyping a modular, multiscale model.

Critical questions for the model framework

The community identified a series of driving biological questions concerning COVID-19 to guide the development of the model framework (see **Box 2**). It is expected that the model will not initially be able to address all of the questions listed; rather, the development plan envisions that with each iteration of the model framework it will expand in its representational capacity as directed by the topics listed in Box 2. Furthermore, as with all modeling projects, we anticipate that as the framework develops it will generate new questions and/or be responsive to the rapidly evolving knowledge-base concerning COVID-19.

1. What are the critical "choke points" in viral infection, replication, and propagation?
2. Which interventions could most effectively leverage identified vulnerabilities in viral replication?
3. What unanticipated dynamics can emerge from a single molecular-scale inhibition?
4. Does the initial level of exposure to the virus affect the severity of the progression of the disease and how could this be ameliorated?
5. What are the key points of virus-immune interactions that drive mild versus severe (e.g., ARDS) responses?
6. What are key differences at the target cell level during innate versus adaptive immune responses?
7. Are there threshold levels of infection at the cellular or tissue level that indicate a switch from asymptomatic to symptomatic or from mild to severe disease in a patient?
8. Through what mechanisms do certain patient characteristics, pre-existing conditions, or background medications increase the likelihood of adverse outcomes?
9. What interventions could accelerate immunity?
10. What interventions can reduce or reverse adverse immune reactions?
11. At what stage is an intervention most beneficial?
12. How does viral mutagenicity affect the robustness of a therapy or a therapeutic protocol?
13. How does cellular heterogeneity affect infection dynamics?
14. How does the nearby tissue environment, such as the mucus layer, affect infection dynamics?
15. How does the infection spread from its initial locus of infection to other tissues (in particular, from upper respiratory tract to the bronchi, bronchioles, and alveoli within lungs)? How does stochasticity impact these dynamics?
16. How do tissues recover after clearance of local infection? Can scarring be minimized to reduce long-term adverse effects in recovered patients?
17. How do adverse effects in SARS-CoV-2 infected epithelia differ (mechanistically) from other infections and other modes of epithelial dysfunction?

Box 2: Community-selected scientific questions driving the model's development.

Key biology for the simulation model

This rapid prototyping effort brings together specialists from a broad variety of domains: virology and infectious

diseases, mathematical biology, computer science, high performance computing, data science, and other disciplines. Therefore, it is critical that all members of the project have access to a clear description of underlying biology that drive the model's assumptions. In this section we outline key aspects of viral replication and host response in functional terms needed for development of agent-based, multi-scale and multi-physics models.

Cell infection and viral replication

The key cell-level process is viral infection of a single cell, followed by replication to create new virions:

1. SARS-CoV-2 is a single-stranded enveloped RNA virus[11]. A virion (single virus particle) has a lipid coating (envelope) that protects the virus when outside a cell (or host). Each virus has dozens of spike glycoproteins that bind to ACE2 (receptors) on select cell membranes[3,11].
2. Virions travel in the tissue microenvironment to reach a cell membrane. The spike binds to an available ACE2 receptor on the cell membrane. Prior to binding to the ACE2 receptor, the spike is cleaved by the protease, TMPRSS2, which is required for efficient cell entry[12]. Multiple modes of transport (e.g., passive diffusion in fluids and porous tissues, mucociliary clearance, chemotaxis, ultrafiltration driven by hydrostatic and oncotic pressure through permeable cell junctions, and cellular active transport) may play a role at slow and fast time scales. There may also be surface contact transmission between neighboring cells.
3. The cell internalizes the adhered virus via endocytosis into a vesicle.
4. The endocytosed virion—now residing in a vesicle with lowered pH—is uncoated to release its mRNA contents into the cell cytoplasm.
5. Copying viral RNA creates a (-) RNA template, which is used for (+) RNA production.
6. RNA is used to synthesize viral RNA and proteins.
7. Viral proteins are transported to the interior surface of the cell membrane.
8. Viral proteins at the cell membrane are assembled into virions.
9. Assembled virions are exported from the cell by exocytosis.
10. When a cell dies and lyses, some or all partly and fully assembled virions can be released into the tissue microenvironment.

Once infected, an individual cell cannot "recover" (e.g., by actively degrading viral RNA and stopping endocytosis) to return to normal function. Rather, the cell is irreversibly committed to eventual death. For further detail, see review articles on RNA virus replication dynamics[13,14].

Infected cell responses

Although infected cells (e.g., type 1 or type 2 alveolar cells in the lung) cannot recover, their respond can slow viral replication and reduce infection of nearby cells. Infected cells do this by secreting type I interferons (IFN-α,β), which diffuse and bind to receptors on nearby cells to reduce viral replication following infection, activate an inflammatory response, and induce gene transcription[15] to minimize cycling and/or induce apoptosis in these cells[16]. Secreted IFN-α,β are important activators and regulators of the innate and adaptive immune responses[16]. Many respiratory viruses, including influenza and SARS-CoVs[17], have evolved to inhibit IFN activation[18], and evidence is emerging that certain non-structural proteins produced by SARS-CoV-2 infected cells interfere with IFN-α, β and chemokines by inhibiting production and suppressing signaling[17,18].

Eventually, infected cells die (by apoptosis, necroptosis, or pyroptosis[19]), lyse, and release unassembled viral components[19]. While the mechanism of cell death in SARS-CoV-2 is currently unknown, in other RNA virus infections, cells can undergo apoptotic, necrotic, or pyroptotic death over the course of viral infection[20]. Disruption of cell metabolism and competition for critical substrates may also contribute to cell death[21,22].

Inflammatory and immune responses

Lethal SARS and MERS in humans has been correlated with elevated IFN-α,β [23], myeloid activity, and impaired T and B cells[24,25], with the timing of IFN-α,β critical[26,27]. IFN-α,βs secreted by infected cells or by immune cells diffuse to surrounding cells and recruit innate immune cells, such as macrophages and neutrophils, to the area. Recent studies comparing SARS-CoV-2 with SARS-CoV have revealed that SARS-CoV-2 replicates more efficiently in pneumocytes and alveolar macrophages, but IFN-α,β secretion is blunted in SARS-CoV-2 infected cells[28]. In COVID-19 patients, decreased numbers of T cells, natural killer (NK) cells, and, to a lesser extent, B cells occur, and the extent of depletion of T cells has been correlated with disease severity[2,3,29]. Rapid inhibition of viral replication requires early and high levels of IFN-α,β secretion and activation[30]. The production of excess inflammatory cytokines, such as IL-1, IL-6 and TNF-α and other chemokines by infected cells results in increased macrophage and neutrophil presence, which correlates with lung dysfunction[31,32]. Delayed IFN-α,β production also promotes inflammatory macrophage recruitment that contributes to vascular leakage and impaired T-cell function[26,27]. Activated macrophages also produce other proinflammatory cytokines like IL-1, IL-6, and TNF-α, among others, that enhance infiltration of immune cells and interact with endothelial cells to cause vasodilation[33]. The excess production of IL-1 and IL-6 may be related to several viral proteins shown to directly activate the inflammasome pathway, the innate immune response responsible for IL-1β secretion[34-36]. Moreover, epithelial tissue death can reduce tissue integrity, contributing to further immune infiltration, fluid leakage and edema, and acute respiratory distress[37-39].

In severe cases, a “cytokine storm” of pro-inflammatory cytokines (e.g., IL-2, IL-7, IL-10, G-CSF, IP-10, MCP-1, MIP-1A, and TNF-α) induces extensive tissue damage[31]. During influenza virus infection, there is some evidence that ARDS is correlated with the extent of infection in the lower respiratory tract and increased cytokine activity resulting from exposure of the endothelium[40]. Increases in neutrophil counts and the neutrophil-to-lymphocyte ratio (NLR) have been observed in patients with severe COVID-19[41]. The NLR has also been shown to be an important clinical predictor of disease severity[42], as it reflects the innate to adaptive immune response. Neutrophils generally produce reactive oxygen species ROS, which can induce the death of infected and healthy cells in the local environment, further contributing to tissue damage[37].

Coronaviruses have been shown to evade and modulate various host immune responses[43-45]. In addition to those discussed above, some evidence suggests that an antibody to spike protein enhances disease during SARS-CoV infection by inducing macrophage switching from a wound healing phenotype to an inflammatory phenotype[46]. Furthermore, influenza viruses and other SARS-CoVs are known to infect macrophages and T cells[3,47], raising the possibility for SARS-CoV-2 to similarly infect these cell types. However, it has not yet been shown that SARS-CoV-2 infection of these cells is productive or simply alters their cytokine expression[31]. However, the ACE2 receptor has been linked to acute lung injury for both influenza and SARS-CoV viruses[48,49].

Links between inflammation and poor clinical outcomes

Coronavirus death is often correlated with pre-existing medical conditions such as diabetes, hypertension, cardiac diseases and obesity[6,50,51]. While the primary effect of SARS-CoV-2 is clearly the lung infection, several secondary effects play a role in the clinical outcome for a given patient. The complex interactions of viral infection, cytokine production, immune response, and pre-existing diseases is an active field of current research. Although the underlying risk factors for an individual to develop ARDS in response to SARS-CoV-2 infection have not yet been elucidated, it appears that a dysregulated immune response is central to this aspect of the disease[2,3,29,52]. In particular, chemokines are released following viral infection, which leads to the invasion of neutrophils and macrophages and release of ROS. IL-6 levels have been associated with more severe disease as patients who required ventilation exhibit increased systemic IL-6 levels, as reported by studies from Germany and China[53-55]. In addition, replication in the lower airways and exposure of endothelial cells may further amplify the inflammatory response[40]. Collectively, this leads to extensive tissue damage and depletion of epithelial cells, which may be connected to lethality[56]. Within the alveolar tissue and systemically, the feedback between viral load, adaptive and innate immune responses, and tissue damage is clearly a complex system. By utilizing a multi-scale framework to implement these interactions, we aim to connect circulating biomarkers, putative treatments, and clinically observed disease progression to pathophysiological changes at the cell and tissue level.

Anticipated data to drive development and validation

It is important that model development takes into account the types of measurements and biological observations that will be available for later model constraint, calibration, and validation. As participation by the virology and pharmacology communities broadens, we anticipate that this list will grow. While we will endeavor to constrain and validate submodels of the model framework independently, we anticipate human clinical data to not fully determine parameters of the model. To address this concern, we will apply a "virtual population" approach and sensitivity analysis to explore model variability within clinically relevant bounds[57,58]. We anticipate the following data:

Organoid data for viral replication and targeted inhibition

Aarthi Narayanan's virology lab is optimizing SARS-CoV-2 cultures in organoid model systems. These 3D model systems infect epithelial cells co-cultured with fibroblasts and endothelial cells and track the viral replication kinetics under control conditions and after treatment by inhibitors. These experiments measure (at various time points) infectious viral titers and genomic copy numbers in supernatants (outside the cells), viral genomic copy numbers in the infected cells¸ host cell death and inflammatory responses, and ATP and mitochondrial disruptions. See Appendix 2 for further detail.

Inflammation, ACE2 binding, and host response data

The international focus on SARS-CoV-2 is generating an unprecedented amount of mechanistic clinical and preclinical data. Randomized controlled interventional trials in general or specific populations will be of particular value to test and refine the model. As of June 30 2020, there were 1,055 trials registered at clinicaltrials.gov under the search term "COVID-19+Drug". Within these 1,055 trials, there are multiple interventions at different points of the pathophysiology, including, but not limited to: broad acting antivirals (e.g., remdesivir), hyperimmune plasma, IL-6 antibody (e.g., tocilizumab), protease inhibitors (e.g., lopinavir/ritonavir), chloroquine/hydroxychloroquine, and Janus kinase inhibitors (e.g., baricitinib). As this platform develops, we anticipate predicting the responses to such therapies and refining the model with emerging data such that the range of clinical responses are captured with adequate fidelity. In addition, data collected from patients or animals during infection, including the presence of various immune cell subsets in lung tissue and systemic markers of inflammation, will serve to differentiate responses to SARS-CoV-2. These data will be similarly integrated to calibrate and validate the model to ensure accurate predictions of therapeutic outcomes based on clinical characteristics.

Relevant prior modeling

Spurred initially by the emergence of HIV and relevant to the present SARS-CoV-2 pandemic, the field of viral dynamics modeling has been instrumental for understanding the evolution of host-virus interactions[59-67], predicting treatment responses[68-72], and designing novel and more effective therapeutic approaches[73-75]. The classic within-host mathematical model of viral infection uses a system of ordinary differential equations (ODEs) to describe the dynamics between uninfected epithelial ("target") cells, infected cells in the eclipse phase, infected cells producing virus, and infectious virus[76]. This basic model has been shown to capture dynamics of both acute and chronic infection[77], and has been extended to also include multiple viral (potentially resistant) strains[73] and various aspects of host immune responses[78,79]. While such cell population-level ODE models generally do not account for single-cell effects, they are effective for detailing viral load, host immune response, and pathology dynamics[80-85]. Moreover, they can often be used to constrain and estimate parameters for more detailed models, develop novel hypotheses, and design confirmatory experiments[86,87].

Some have modeled intracellular virus replication, including detailed models used for understanding replication and intervention points[58,88], typically using systems of ODEs[89,90]. These models often include virus-receptor binding, receptor trafficking, endocytosis, viral uncoating, RNA transcription, protein synthesis, viral assembly, and viral exocytosis. However, to date no such model has been integrated with detailed spatiotemporal models of viral propagation in 3D tissues with dynamical models of immune interactions.

Agent-based models have been used to simulate viral propagation in 2D tissues with simplified models of viral replication in individual cells, particularly in the field of influenza virus infection[91-95], spatial patterns from single-cell infections for a variety of other viral infections[96-98] such as SARS[99], and oncolytic viral therapies[100-103]. These models have generally not included detailed intracellular models of viral replication and individual cell responses to infection. However, they demonstrate the potential for including detailed intracellular models of viral replication in 2D and 3D tissues with the milieu of immune and epithelial cell types expected in actual patients, while also offering the opportunity to test hypotheses on the impact of viral mutagenicity and host cell heterogeneity on disease progression.

Agent-based models have also been used extensively to characterize the inflammatory dysfunction that produces the most severe manifestations of COVID19. The dynamics of forward feedback inflammation-induced tissue damage was examined with an early agent-based model of systemic inflammation[104]; this model was further developed into the Innate Immune Response ABM (IIRABM), which was used to perform in silico trials of anti-mediator/cytokine interventions (not too different from the types being tried for COVID19)[105]. More recently, the IIRABM has been used as a test platform for the application of genetic algorithms[106] and model-based deep reinforcement learning[107] to discover multi-modal and potentially adaptive mediator-directed therapies for acute systemic inflammation; this work is particularly relevant given the attempts to use anti-cytokine biologics during the current COVID19 pandemic. Finally, the IIRABM, as an endothelial-based model, was integrated with models of epithelial dysfunction to simulate individual and multiple organ dysfunction and failure seen with systemic hyper-inflammation[108]. As noted above, there are significant differences between the pathophysiology of bacterial sepsis and that of severe viral infections, but it appears that at some level of tissue damage the dynamics of the innate system come to fore in terms of the clinical significance.

The rapid prototyping approach of this coalition will use a performance-driven agent-based modeling platform[109] to combine detailed intracellular models of viral endocytosis, replication, and exocytosis, disruption of cell processes (e.g., metabolism and compromised membranes) that culminate in cell death, inflammation signaling and immune responses, tissue damage, and other key effects outlined above in a comprehensive, open source simulation platform. We will deploy and refine interactive, web-hosted versions of the model to critical contributions by virologists, infectious disease modelers, and other domain experts. We will frequently update preprints to foster the fastest possible scientific dialog to iteratively refine this community resource.

Related modeling efforts and other future data sources

We are coordinating with related modeling efforts by a number of groups, such as early pilot work by David Odde and colleagues at the University of Minnesota, and early simulation work in Chaste[110,111] (James Osborne and colleagues), Morpheus[112] (Andreas Deutsch and colleagues), CompuCell3D[113], and Biocellion[114] (Ilya Shmulevich and co-workers). Thomas Hillen has hosted a COVID-19 Physiology Reading Group[115] to exchange information and progress. We are in regular contact with these communities to share data and biological hypotheses and to seek feedback, parameter insights, and data and code contributions.

The COVID-19 Cell Atlas[116] organizes a variety of cell-scale datasets relevant to COVID-19; these may be of particular importance to intracellular modeling components of the project. The COVID-19 Disease Map[117] also has a wealth of host-pathogen interaction data. The Human Biomolecular Atlas Program (HuBMAP)[118] is creating detailed maps of the human respiratory system at cell- and molecular-scale resolution; this will be an excellent data source for tissue geometry in later versions of the model.

Methods

PhysiCell: agent-based cell modeling with extracellular coupling

PhysiCell is an open source simulation agent-based modeling framework for multicellular systems in 2D and 3D dynamical tissue environments[109]. (See Metzcar et al. (2019) for a general overview of agent-based modeling

techniques in tissue-scale biology[119].) In this framework, each cell (of any type) is an off-lattice agent with independent cell cycle progression, death processes, volume changes, and mechanics-driven movement. Each cell agent can have independent data and models attached to it, allowing substantial flexibility in adapting the framework to problems in cancer biology, microbiology, tissue engineering, and other fields. PhysiCell is coupled to BioFVM (an open source biological diffusion solver)[120] to simulate the chemical microenvironment. As part of this coupling, each individual agent can secrete or uptake diffusing substrates and track the total amount of material entering and leaving the cell.

Relevant applications of PhysiCell-powered models have included modeling cancer nanotherapy[121], oncolytic virus therapies[122], tissue biomechanical feedbacks during tumor metastatic seeding[123], and cancer immunology[109,124,125]. The platform was built with a focus on computational efficiency and cross-platform compatibility: the same source code can be compiled and run without modification on Linux, OSX, and Windows, and simulations of up to 10 diffusing substrates on 10 mm^3 of tissue with 10^4 to 10^6 cells are routinely performed on desktop workstations. The platform has been combined with high-throughput computing[124] and active learning techniques[125] to power large-scale model exploration on high performance computing resources.

Integration of intracellular models in PhysiCell agents

Custom functions can be attached to individual cell agents to model molecular-scale, intracellular processes and to couple these with cell phenotypic parameters. These internal models are often implemented as systems of ODEs. For example, cell uptake of diffusing substrates can be coupled with a metabolism model that is defined by a system of ODEs, and the resulting energy output can be used to set the cycle progression and necrotic death probability of a cell[126]. For small systems of ODEs, these models are currently coded “by hand” with standard finite difference techniques. More complex models are written in systems biology markup language (SBML)[127] for reliable scientific communication. Development versions of PhysiCell can read and integrate an individual SBML-encoded model in each cell agent using *libRoadrunner*—a highly efficient SBML integrator[128]. Similar approaches have been used to integrate Boolean signaling networks[129] in PhysiCell in the PhysiBoSS extension[130].

These approaches will initially be used to assess (1) viral replication dynamics in each cell agent, (2) cell death responses to viral load, (3) cell responses to interferons, and (4) changes in the virion endocytosis rate based on the availability of ACE2 and its receptor trafficking dynamics.

Cellular Immunity Agent-Based Model (CIABM)

As an independent model component, co-authors An, Becker, and Cockrell are developing CIABM: an agent-based model of immune system activation and expansion in lymph nodes in response to SARS-CoV-2 infections. This model will be coupled with the overall simulator to mechanistically drive immune expansion and infiltration during inflammatory responses.

The CIABM is intended to be a generalizable model of $CD8^+$ T cell dynamics, designed to represent different disease states resulting from different perturbations (i.e., specific infections of specific pathogens, putative vaccines and their administration strategy). This is consistent with our philosophy of pathophysiological unification through modeling. We have developed multiple ABMs related to the immune response and diseases related to inflammation and immune dysfunction[131,132] and will leverage this experience to integrate various aspects of these models as components of the CIABM. Many of these models are based on the IIRABM[131], which is an abstract representation and simulation of the human inflammatory signaling network response to injury; the model has been calibrated such that it reproduces the general clinical trajectories seen in sepsis. The IIRABM operates by simulating multiple cell types and their interactions, including endothelial cells, macrophages, neutrophils, TH0, TH1, and TH2 cells and their associated precursor cells. The simulated system dies when total damage (defined as aggregate endothelial cell damage) exceeds 80%; this threshold represents the ability of current medical technologies to keep patients alive (i.e., through organ support machines) in conditions that previously would have been lethal. The IIRABM will be used in the CIABM to represent the innate and host tissue component of the CIABM.

The design principles of the CIABM are 1) $CD8^+$ T-cell dynamics focused detail, 2) incorporation of the IIRABM as the innate-host tissue module, and 3) incorporation of humoral and $CD4^+$ T-cell function at an abstracted level. The justification for aggregating humoral and $CD4^+$ T-cell functions is that they are primarily governed by interactions through the MHC2 complex, and, therefore, represent a distinct sensing/recognition capacity than $CD8^+$MHC1-mediated recognition. While we recognize that CD4-helper activity is known to assist the generation of $CD8^+$ T cells, at the outset of this project we will attempt to see how well we can reproduce our clinically-acquired data without having to explicitly represent CD4-helper function. If we are unable to satisfactorily map CIABM behavior to our experimental/clinical data, we will then add these components.

As a general description, the initial components of the innate immune response represent the end-effector of the system, primarily responsible for interactions influencing tissue damage, microbial killing, and abstracted tissue reconstitution. This component incorporates both pro- and anti-inflammatory components, consistent with a self-contained control structure befitting its role as a highly-evolutionarily conserved, fundamental function of multi-cellular organisms. These agent types are: tissue, viral antigen, polymorphonuclear neutrophil cells (PMNs), macrophages, dendritic cells, naïve and cytotoxic $CD8^+$ T cells, and regulatory T cells.

HPC-driven model exploration and parameterization

The concurrent growth and advancements in the three areas of 1) mechanistic simulation modeling, 2) advanced, AI-driven model exploration algorithms, and 3) high-performance computing (HPC) provides the opportunity for large-scale exploration of the complex design spaces in detailed dynamical simulation models. However, if we do not take deliberate efforts to formally facilitate this intersection across our research communities, we risk producing a series of disparate individual efforts, limited in interoperability, transparency, reproducibility and scalability. The EMEWS (extreme model exploration with Swift) framework[133] was developed to directly address this issue and to provide a broadly applicable cyberinfrastructure to lower the barriers for utilization of advanced, large-scale model exploration on HPC resources. The EMEWS paradigm allows for the direct exploitation of cutting edge statistical and machine learning algorithms that make up the vibrant ecosystem of free and open source libraries that are continually added to and updated as research frontiers are expanded, all while controlling simulation workflows that can be run anywhere from desktops to campus clusters and to the largest HPC resources.

We have utilized EMEWS for learning-accelerated exploration of the parameter spaces of agent-based models of immunosurveillance against heterogeneous tumors[124,125]. The approach allowed for iterative and efficient discovery of optimal control and regression regions within biological and clinical constraints of the multi-scale biological systems. We have applied EMEWS across multiple science domains[134-137] and developed large-scale algorithms to improve parameter estimation through approximate Bayesian computation (ABC) approaches[138]. These approaches, applied to the multi-scale modeling of SARS-CoV-2 dynamics, will provide the ability to robustly characterize model behaviors and produce improved capabilities for their interpretation.

nanoHUB platform

The nanoHUB platform (nanohub.org)[139] is a free, cloud-based service offering lectures, tutorials, and, of particular interest to us, interactive Web-based simulation tools. As its name implies, it is primarily focused on nanoscale science education and research. To make their simulation tools easier to use, nanoHUB provides a custom toolkit for developing graphical user interfaces (GUIs). However, since 2017, they have adopted and promoted the use of Jupyter notebooks[140], with accompanying Python modules to provide GUI widgets and visualization. Cloud-based computing and data analysis platforms are well established now, in both academic and commercial settings. Those platforms, such as nanoHUB, that provide easy-to-use web-based GUIs and APIs and offer affordable pricing will likely have their rate of adoption continue to increase, especially among researchers who may lack the expertise or resources to install complex pieces of software.

xml2jupyter and cloud deployment of PhysiCell models

Compiled PhysiCell models generate executable software that runs at the command line. Model parameters are set by editing XML (extensible markup language) configuration files, and the models save data as a combination of vector graphics outputs (scalable vector graphics: SVG) and XML and MATLAB data (.mat) files based on the draft MultiCellDS data standard[141].

To facilitate rapid cloud-hosted dissemination of PhysiCell-powered models on the nanoHUB platform, we developed *xml2jupyter* to automatically generate a Jupyter-based GUI for any PhysiCell model[142]. The Jupyter notebook includes widgets to set parameters, initiate a simulation run, and visualize diffusing substrates and cell agents. In turn, we also developed a protocol to deploy the PhysiCell model and the Jupyter notebook interface on nanoHUB as a cloud-hosted, interactive model. This allows developers to rapidly convert a locally executable command-line model to a cloud-hosted shared model with graphical interface in a matter of minutes to hours (depending upon testing speed on nanoHUB).

In our rapid prototyping, we use rapidly-generated nanoHUB apps for scientific communication across disciplines; virologists, pharmacologists, and other domain experts can explore and visualize the model prototypes without need to download, compile, or understand the code. This facilitates faster multidisciplinary dialog and helps to draw in broader community feedback and contributions.

Modular design

The model is being evolved with a modular architecture. The overall model and each individual model component (submodel) have a separate GitHub software repository in the pc4COVID-19 GitHub organization, available at https://github.org/pc4COVID-19.

Each submodel repository consists of a *master* branch that matches the latest numbered release and a *development* branch. Contributors will fork the development branch, complete their milestones, and submit a pull request to incorporate their progress in the development branch. Whenever a submodel team is ready to make a numbered release, they will use a pull request from the development branch to the master branch and create a numbered release.

The overall model framework and each submodel will keep a versioned design document to include:

- A unique name for the model component
- A clear version number and last update timestamp
- A list of contributors, including 1-2 chief scientists who serve as primary points of contact
- A “plain English” description of the primary purpose of the component
- A statement of model inputs with units of measure
- A clear statement of the biological hypotheses and assumptions of the component
- A record of the current mathematical form of the model (generally maintained in a separate Overleaf LaTeX document), with a snapshot of the equations in the main design document
- Any computational implementation details needed to understand the code
- A link to a GitHub repository
- A list of model parameters, units, biophysical meaning, best estimate, and data source(s) for the parameter estimate (see the discussion in MultiCellDS[141])
- A clear list of model outputs with units
- A set of qualitative and/or quantitative **unit** tests to ensure proper functionality of the module.

A snapshot of this design document will be included in each release of the (sub)model.

The overall model releases will include a clear list of the version of each submodel included in its release.

Coalition structure

After group discussion and prioritization, coalition members self-assigned themselves to one or more subteams responsible for developing the submodels. Each *subteam* has 1-2 chief scientists in charge of managing development, while a technical contact approves pull requests from the subteam’s contributors and coordinates with

the integration team (see below). The submodel chief scientist(s) meet regularly with their team to assign tasks, set milestones, and assess when to make a release. The submodel chief scientist(s) also coordinate their progress with the other submodel teams.

The *integration team*—consisting of the overall leads (as of April 1, 2020: Paul Macklin, Randy Heiland, and Yafei Wang) and other contributors—is responsible for developing and maintaining the overall integrated model, integrating and testing updated submodels, and providing technical support to the subteams.

The *core team* consists of the overall leads and the chief scientists. They meet to coordinate progress of the submodels, refine project scope, exchange ideas on model hypotheses, evaluate community feedback, and plan overall strategy. They cooperate with the overall leads to create model releases (which will always bundle the most stable version of each submodel), update the nanoHUB models, and update the *bioRxiv* preprint.

The current list of subteams can be found in **Box 3.**

Three main phases of community-driven development

Phase 1: Building the coalition and model infrastructure

In the first phase, the overall and integration leads build the overall tissue model structure (a model that integrates several independent *submodels*) and create "placeholder" models that serve as working proof-of-concept starting points for further expansion. This phase also builds and organizes the subteams responsible for the submodels and provides them with training and documentation on the model and submodel architecture.

We anticipate that Phase 1 will require six-to-eight weeks, although Phases 1 and 2 may overlap as individual subteams assume full leadership of their submodel code repositories.

Phase 2: Community-driven development

In this phase, the integration team transitions the primary development of each of the submodels to appropriate domain experts in the subteams, to ensure that each submodel reflects the best available science. During this phase, the integration team supports each subteam in mathematical model development, PhysiCell implementation, and nanoHUB deployment for rapid subteam testing, dissemination, and community feedback on the submodels.

The integration team continues to lead overall model integration, testing, and deployment as a cloud-hosted model, and development of further infrastructure (e.g., HPC investigations) and PhysiCell and xml2jupyter refinements needed by the subteams (e.g., full support for SBML for molecular-scale model integration).

Once the integrated model can qualitatively produce expected viral and immune behaviors (as determined by the core group) and receives no major domain expert or community critiques, the major goal of the coalition (and this paper) will be met: to create a SARS-CoV-2 modeling framework suitable for subsequent calibration, validation, and exploration by the community. It will be submitted to scientific peer review, disseminated to the community, and maintained. This will mark the conclusion of Phase 2.

We anticipate that Phase 2 will require three to nine months.

Phase 3: widespread scientific use and model maintenance

Once the overall model and submodels are largely complete, the model will be a mature, open source community resource available for use in scientific investigations. Moreover, due to our iterative approach, we envision that teams will have begun using earlier versions of the model for investigations by this point. The integration team will transition to supporting parallel investigations by independent groups using the models, and aggregating and sharing best data, parameter estimation, and results. The integration team and subteams will coordinate to encourage full scientific publication of the overall model and the submodels, and resulting scientific investigations.

This phase will also focus on code hardening, documentation, and development of training and outreach materials. This phase is critical for *knowledge capture*, so that the model remains usable beyond the involvement of the original teams and can be rapidly adapted to emerging health challenges in the future. We also envision continued refinement of the model to reflect improved biological knowledge.

Integration: Coordinates overall project and leads multiscale model integration and dissemination.
Chief scientist: Paul Macklin
Technical contact(s): Randy Heiland, Yafei Wang
Members: Paul Macklin, Randy Heiland, Michael Getz, Yafei Wang

Viral Replication: Builds the submodel of viral replication (and release) within individual cells.
Chief scientist(s): Jim Faeder
Technical contact(s): Yafei Wang, Ali Sinan Saglam
Members: Jim Faeder, Yafei Wang, Paul Macklin, Ali Sinan Saglam

Infected cell response: Builds the submodel of individual cell responses to infection, such as secretion of chemokines and apoptosis.
Chief scientist(s): Jason Shoemaker, James Glazier, Sara Hamis, Fiona Macfarlane
Technical contact(s): Jordan Weaver, Josua Aponte, Sara Hamis, Fiona Macfarlane
Members: Jason Shoemaker, Jim Faeder, Penny Morel, James Glazier, Ashok Prasad, Elsje Pienaar, Jordan Weaver, T.J. Sego, Josua Aponte, Yafei Wang, Sara Hamis, Fiona Macfarlan

Pharmacodynamics: Modifies the submodels to simulate pharmacologic interventions.
Chief scientist(s): Robert Stratford, Morgan Craig
Technical contact(s): Tarunendu Mapder, Yafei Wang, Sara Hamis, Fiona Macfarlane
Members: Robert Stratford, Morgan Craig, Sara Quinney, Mark AJ Chaplain, Tarunendu Mapder, Yafei Wang, Sara Hamis, Fiona Macfarlane, Richard F. Bergstrom

Receptor trafficking: Builds the submodel of ACE2 receptor trafficking, including virus binding and endocytosis.
Chief scientist(s): Padmini Rangaman
Technical contact(s): Andy Somogyi
Members: Padmini Rangamani, Andy Somogyi

Tissue immune response: Builds the submodels of individual immune cells and their interactions within an infected tissue.
Chief scientist(s): Morgan Craig, Courtney Davis, Amber Smith, Adrianne Jenner, Penny Morel
Technical contact(s): Adrianne Jenner
Members: Adrianne Jenner, Courtney Davis, Morgan Craig, Amber Smith, Penny Morel, Sofia Alfonso, Rosemary Aogo, Elsje Pienaar, Dennis Hou

Lymph node: Builds the submodel of immune cell expansion at nearby lymph nodes to drive immune cell recruitment.
Chief scientist(s): Gary An, Tarunendu Mapde
Technical contact(s): TBD
Members: Gary An, Chase Cockrell, Marc-Andre Rousseau, James Glazier, T.J. Sego, Tarunendu Mapde, Juliano Ferrari Gianlupi

Tissue damage: Builds models of tissue damage (and potentially recovery).
Chief scientist(s): Ashlee Ford Versypt, Amber Smith
Technical contact(s): TBD
Members: Amber Smith, Ashlee Ford Versypt, Thomas Hillen, Mohammad Aminul Islam

Drug testing/experiment: Explores drug inhibiting virus endocytosis and replication in cell culture
Chief scientist(s): Aarthi Narayanan
Technical contact(s): Kenneth Risner
Members: Aarthi Narayanan, Kenneth Risner

SBML integration: Refines PhysiCell integration with libRoadrunner to support direct execution of SBML models
Chief scientist(s): Randy Heiland
Technical contact(s): Randy Heiland, Andy Somogyi
Members: Andy Somogyi, Randy Heiland, Furkan Kurtoglu, Pablo Maygrundter, Jim Faeder

Visualization and analytics: Refines standalone and integrated visualization and analytics for nanoHUB apps.
Chief scientist(s): Randy Heiland, Amber Smith, Courtney Davis
Technical contact(s): Randy Heiland, Dennis Hou
Members: Randy Heiland, Amber Smith, Courtney Davis , Hadi Taghvafard, Andy Somogyi, Furkan Kurtoglu, Pablo Mayrgundter, Dennis Hou

Box 3: Current subteams.

Iterative development

We use ***rapid prototyping*** using lessons learned from each step to drive iteration towards improving the model.

Each submodel undergoes its own development sprints, contained within a broader development cycle for the overall integrated model (See **Fig. 0.1**.).

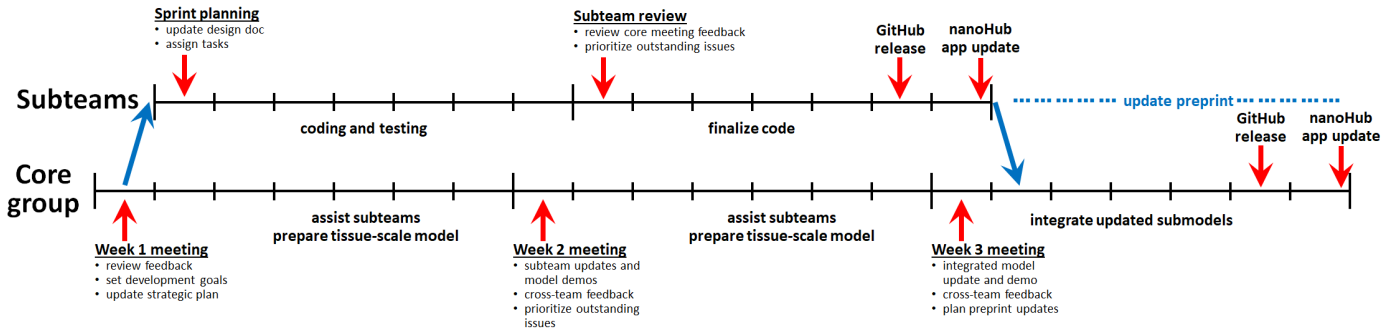

Fig 0.1: Overall development cycle: Throughout the overall development cycle, the core team (integration leads + subteam leads) set priorities and coordinate work of the subteams. Each subteam performs a short sprint to update its submodel. At the end of the 3-week cycle, the integration team bundles the most up-to-date submodels for the next overall model release, while the subteams update the preprint and refine domain knowledge and mathematics for the next sprint.

Overall integrated model development cycle

We aim for a 3-week development cycle for the overall integrated model, although early development cycles may last longer to accommodate building computational infrastructure, development of new core features to support model development, and training.

Start of cycle

The design cycle starts with an initial core team meeting where we discuss feedback from prior design cycles and set priorities for the current design cycle. In particular, we discuss:

- What changes are needed to the submodels? Prioritize changes that can be made within a 7-10 day sprint.
- What changes are needed in the overall integrative framework to facilitate the improved submodels? Set framework goals for early and mid-cycle development.
- Are any funding, personnel, scope, or other changes needed?

Within the working week, the subteams meet to further set and accomplish their sprint goals. (See **Submodel design cycle**). The integration team (1) works on refinements to the PhysiCell and nanoHUB frameworks to facilitate subteam work, (2) provides technical consulting to the subteams to implement their model refinements, and (3) makes any final edits needed to the preprint from the last design cycle.

Mid-cycle advances

The design cycle continues with a core team meeting to discuss the current subteam model sprints:

- Each team gives a brief report on their model advances and a live demo of either the standalone C++ code or a nanoHUB submodel app.
- The teams “cross-pollinate” to exchange ideas and give feedback on each of the submodels.
- The core team decides on any additional changes needed to continue the design cycle.
- The integration team and subteam chief scientists set final deadlines to end the sprints and release the updated submodels.

Within the working week, the subteams continue and complete their developing and testing for their respective sprints, create new submodel releases on GitHub, and update their submodel nanoHUB apps. The integration team continues support for the subteam work and completes any changes to the overall integrative model needed for the upcoming integration.

As the subteams advance towards their releases, the integration team updates and tests the respective sub-models in the overall framework and updates the overall nanoHUB app.

End of cycle

The design cycle nears completion with a core team meeting to discuss integration and preprinting:

- The integration team gives an update on current integration testing.
- The team coordinates any remaining submodel releases.
- The team sets plans for updating the preprint.

Within the working week, the **subteams** complete their releases (if not already complete in week 2) and begin revising the preprint. They also begin testing the integrated model as it comes online to integrate new simulation results and insights into the preprint.

The **integration team** updates the submodels, performs final testing, and creates both GitHub and nanoHUB releases. Once complete, the integration team joins the subteams on preprint updates.

Submodel design cycle

Each submodel is developed in parallel with a unified design cycle (a 7-to-14-day software *sprint*) in coordination with the other subteams during the weekly core team meetings and via a dedicated Slack workspace.

Start of sprint

The sprint cycle starts with an initial subteam meeting to communicate the results and priorities of the core team meeting to the subteam. The team edits the submodel design document, discusses any necessary changes to the mathematics and parameter values, and assigns implementation tasks. The team coordinates with the integration team via the Slack workspace for any needed assistance on model implementation.

End of sprint

The design cycle continues with a core team meeting to discuss the current subteam model sprints:

- Each team gives a brief report on their model advances and a live demo of either the standalone C++ code or a nanoHUB submodel app.
- The teams “cross-pollinate” to exchange ideas and give feedback on each of the submodels.
- The core team decides on any additional changes needed to continue the design cycle.
- The integration team and subteam chief scientists set final deadlines to end the sprints and release the updated submodels.

Within the working week, the **subteams** continue and complete their developing and testing for their respective sprints, create new submodel releases on GitHub, and update their submodel nanoHUB aps. The **integration team** continues support for the subteam work and completes any changes to the overall integrative model needed for the upcoming integration.

As the subteams advance towards their releases, the **integration team** updates and tests the respective sub-models in the overall framework and updates the overall nanoHUB app.

See **Appendix 4: Submodel development details** for more implementation details.

Results

Version 1 (March 25-March 31, 2020)

Version 1 was designed as proof of concept rapid prototype to capture essential (but highly simplified) elements of viral endocytosis, protein synthesis, viral assembly, release, and diffusion to infect other cells. The model was

tailored to RNA viruses on a tissue monolayer (modeled as a layer of epithelium over a basement membrane). This version was kept deliberately simple to create an early starting framework to help coalesce community feedback and contributions. It was also designed to test the use of interactive cloud-hosted models to help accelerate feedback by virologists and other domain experts through live demos.

The proof of concept model was created by the overall leads (Macklin, Heiland, Wang) while assembling the modeling coalition as an initial starting point and feasibility test for rapid prototyping. Feedback on this version drove the formulation of the design protocols reported above.

Submodels

The Version 1 model includes the following submodel components:

- **T:** tissue (which contains epithelial and other cells)
- **V:** viral endocytosis, replication, and exocytosis responses
- **VR:** cell response to viral replication, including cell death and IFN synthesis
- **E:** epithelial cell (incorporates V and VR).

The overall model components are summarized in **Fig 1.1**.

Biological hypotheses

In this proof of concept prototype, we modeled a simplified set of biological hypotheses:

1.T.1 Virus diffuses in the microenvironment with low diffusion coefficient
1.T.2 Virus adhesion to a cell stops its diffusion (acts as an uptake term)

1.V.1 Adhered virus undergoes endocytosis and then becomes uncoated
1.V.2 Uncoated virus (viral contents) lead to release of functioning RNA
1.V.3 RNA creates protein at a constant rate, unless it is degraded
1.V.4 Protein is transformed to an assembled virus state
1.V.5 Assembled virus is released by the cell

1.VR.1 As a proxy for viral disruption of the cell, the probability of cell death increases with the total number of assembled virions
1.VR.2 Apoptosed cells lyse and release some or all of their contents

(In the above, X.C.Y denotes prototype X, model component C, biological hypothesis Y, allowing us to easily refer to any individual hypothesis or assumption in discussion and community feedback.) In the next version of this model, we will use the design document protocols for each of these components.

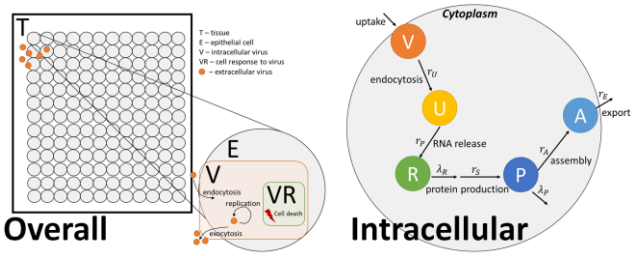

Fig. 1.1: Version 1 model schematic: ***Left:*** In the overall model structure, a ***tissue component*** **(T)** contains multiple ***epithelial cells*** **(E)**. Viral particles diffuse through this domain and can enter the cells (by adhering as an uptake term) or be exported by cells. Each cell includes an intracellular ***virus*** model **(V)** for viral replication kinetics and a ***viral response*** model **(VR)** which uses a pharmacodynamic model to control cell apoptotic response to viral load. ***Right:*** Each epithelial cell individually models its viral kinetics: adhered virions complete endocytosis, are uncoated, functionalize their RNA, synthesize viral components, and assemble them into virions that are subsequently exported to the external tissue compartment (T).

Unit tests

The first prototype should demonstrate the following behaviors for a single cell infected by a single virion:

- The virion progresses to the uncoated state.
- The uncoated virion progresses to the RNA state.
- With export and death off, RNA produces protein.
- With export and death turned off, protein produces and accumulates assembled virus (linearly).

- With export off and death on, cell undergoes apoptosis with increasing likelihood as assembled virus accumulates.
- With export on and death on, surrounding cells get infected and create virion.
- Cells nearest the initial cell are infected first.
- Apoptosis is most frequent nearest to the initial infected cell.

Translation to mathematics, rules, and model components

Extracellular virion transport (Tissue submodel ***T***)

To rapidly implement extracellular viral transport using existing model capabilities, we approximated the process as diffusion with a small diffusion coefficient as in prior nanoparticle models. Using the standard BioFVM formulation[120], if ρ is the concentration or population density of virions (virions / μm^3), then the population balance is modeled as a partial differential equation (PDE) for diffusion, decay, and sources and sinks from interactions with cells:

$$\frac{\partial \rho}{\partial t} = D\nabla^2\rho - \lambda\rho + \sum_{\text{cells } i} \delta(\mathbf{x} - \mathbf{x}_i)(-U_i V_i \rho + E_i), \quad (1)$$

where D is the diffusion coefficient, λ is the net decay rate (which can include other removal processes), δ is the Dirac delta function, $\mathbf{x}_i$ is the position of the center of cell i, U is the uptake rate (by adhering to ACE2 and initiating endocytosis), V is the volume of cell i, and E is the virion export rate from the cell. Note that in the default BioFVM implementation, uptake processes are spread across the volume of a cell.

Note that virus propagation may require more explicit modeling of cell-cell surface contact in later versions, and cilia-driven advective transport and virion deposition (e.g., through airway transport).

Intracellular viral replication dynamics (Virus intracellular model ***V***)

Within each cell, we track *V* (adhered virions in the process of endocytosis), *U* (uncoated viral RNA and proteins), R (viral RNA ready for protein synthesis; R = 1 denotes the total mRNA of one virion), P (synthesized viral proteins; P = 1 denotes sufficient viral protein to assemble a complete virion), and A (total assembled virions ready for exocytosis). Virion import (a source term for V) is handled automatically by the mass conservation terms for PhysiCell in the PDE solutions.

We model these dynamics of internalized virions through a simplified system of ODEs:

$$\frac{dV}{dt} = -r_U V \quad (2)$$

$$\frac{dU}{dt} = r_U V - r_P U \quad (3)$$

$$\frac{dR}{dt} = r_P U - \lambda_R R \quad (4)$$

$$\frac{dP}{dt} = r_S R - r_A P - \lambda_P P \quad (5)$$

$$\frac{dA}{dt} = r_A P \quad (6)$$

Here, r_U is the viral uncoating rate, r_P is the rate of preparing uncoated viral RNA for protein synthesis, r_S is the rate of protein synthesis, r_A is the rate of virion assembly, λ_R is the degradation rate of RNA, and λ_P is the degradation rate of viral protein. We model exocytosis by setting the net export *E* of the assembled virions, in

units of virions per time:

$$E = r_E A, \tag{7}$$

where r_E is the assembled virus export rate.

Cell response (Viral response submodel ***VR***)

In this proof of concept prototype, we modeled apoptotic response to cell disruption but did not model interferon processes. As a simplification, we modeled cell disruption as correlated with assembled virions *A*, and we used a Hill function to relate the apoptosis rate of a cell to *A*:

$$e = \frac{A^n}{A_H^n + A^n} \tag{8}$$

where e is the effect, n is the Hill coefficient, and A_H is the amount of virions at which half of the maximum effect is achieved. After calculating this effect *e*, we set the apoptotic death rate as

$$r_{\text{death}} = r_{\max} e \tag{9}$$

where $r_{\max}$ is the maximum apoptosis rate (at full effect, $e = 1$). As analyzed for agent-based models with stochastic death rates[109,143], in any time interval [*t*, *t*+Δ*t*], the cell has probability $r_{\text{death}} \Delta t$ of apoptosing, and the mean cell survival time (for fixed *e* and thus fixed r_{death}) is $1/r_{\text{death}}$.

In PhysiCell, we can set the lysing cells to release any fraction ($0 \leq f_{\text{release}} \leq 1$) of *V*, *A*, *U*, *R*, and *P* into the extracellular environment as diffusing substrates.

Other implementation notes

To differentiate between incoming imported and exported virions within the computational implementation, we modeled two diffusing fields (for extracellular concentrations of *V* and *A*). However, the models only require extracellular *V*. At the end of each computational step (advancing by one diffusional time step), we iterate through each voxel and transfer all of the extracellular diffusing *A* to *V*. We also created diffusing fields for uncoated virions, RNA, and viral proteins, although these were removed from later model versions.

Software release

The core model associated with the v1 prototype is Version 0.1.3. The nanoHUB app associated with the v1 prototype is Version 1.0. GitHub releases and Zenodo snapshots are given in the Appendix.

Cloud-hosted model

We rapidly created and deployed a cloud-hosted model with an interactive web-based GUI running on nanoHUB (nanohub.org) using xml2jupyter Version 1.1[142]. The web-hosted model can be run at:

https://nanohub.org/tools/pc4COVID-19.

This workflow uses a Python script that converts a PhysiCell configuration file (in XML) into a Jupyter notebook and adds additional Python modules for the GUI. The automated process of converting a standalone PhysiCell model into an interactive Jupyter notebook version (a GUI) takes just a few minutes. The resulting GitHub repository is shared with the nanoHUB system administrators who install it for testing as an online, executable model (an "app"). After we perform usability and other testing and finalize documentation, it is published and becomes available for public use. The whole process (including the initial development of the core PhysiCell model) took less than 12 hours for the Version 1 GUI on nanoHUB (**Fig. 1.2**).

Fig. 1.2: Version 1 on nanoHUB: A. The *About* tab includes background information on the model, run directions, and a legend. **B.** The *Config basics* tab allows users to set the domain size. (These should be not be edited in this version.) **C.** The *Microenvironment* tab lets users set diffusion and decay coefficients, as well as initial and boundary conditions. The track_in_agents option must be enabled for the model to work correctly. **D.** The *User Params* tab sets key model parameters. **E-F.** Sample outputs in the *Out: Plots* tab. Users can scroll the "frame" tab to advance the simulation time and choose whether to plot the cells, a diffusing substrate, or both. These plots display a sheet of epithelium (circles are individual cells). Brighter yellow cells contain more assembled virion. Black cells are apoptotic, and clear spaces show tissue damage (where cells have apoptosed and have been removed.) This version of the nanoHUB model was released at DOI 10.21981/19BB-HM69.

Model behavior: what does the current version teach us?

Except as noted below, all simulation results use the v1 model default parameters, which are supplied in the XML configuration parameter file of the version 0.1.2 core model repository.

In all plots, dark blue cells have 0 assembled virus, pale blue cells have 1-9 assembled virions, grey cells have 10-99 assembled virions, light yellow cells have 100-999 assembled virions, and bright yellow cells contain 1000 or more assembled virions. Black cells are apoptotic, and white spaces show regions devoid of cells (extensive tissue damage). See the legend in **Fig. 1.2** (A) and the caption in **Fig. 1.3** (A).

Behavior with default parameters

Running the overall model (with virus release turned on and off as appropriate for the respective unit tests) shows that the v1 prototype satisfies all the qualitative unit tests. A single cell is infected with a virion in the center of the tissue. Over time, the virion is uncoated to create functionalized RNA, which is synthesized to viral proteins and assembled to functional virus. The graphical output shows this center cell turning to a bright yellow as assembled virions accumulate. By enabling the substrate plot, we can see the diffusive field of virions first has zero concentration (no virions have been released), but as the first cell's viral production increases, it releases virus particles that begin diffusing into the domain (**Fig. 1.3 A**).

Over time, neighboring cells also become infected and progress towards a higher viral load (increasingly bright shades of yellow). The infection propagates outward from the initially infected cell into the remaining tissue. As each cell's viral load (here measured as number of assembled virions) increases, the viral response model calculates the increasing effect e, and cells have greater probability of apoptosis. Cells nearest to the initial site of infection apoptose earliest. As these cells degrade, they are removed from the simulation, leading to the creation

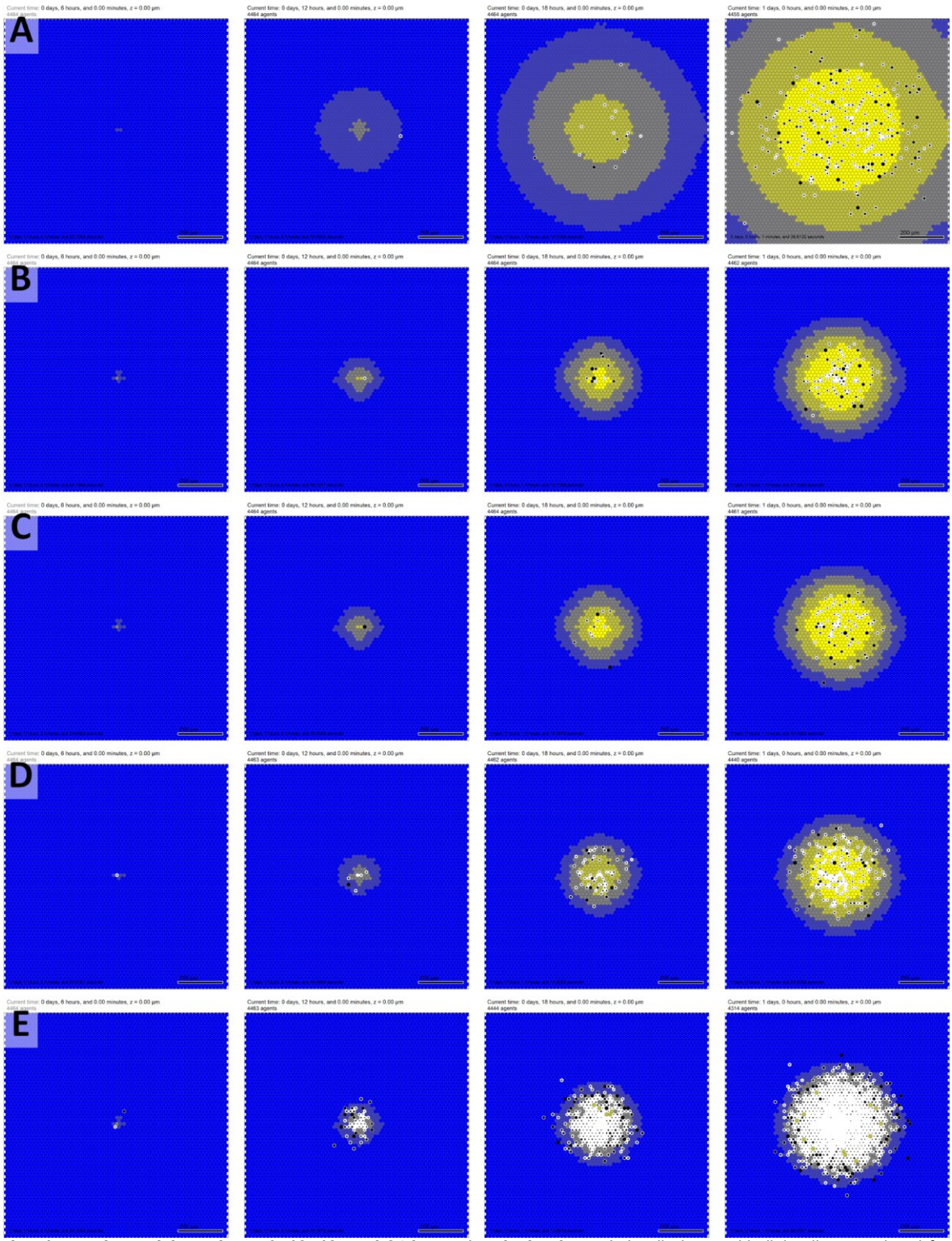

Fig. 1.3: Version 1 sample model results at 6, 12, 18, and 24 hours (vertical columns). In all plots, epithelial cells are colored from blue (no assembled virions) to bright yellow (1000 or more virions). Black cells are apoptotic, and white regions show damaged tissues where apoptotic cells have degraded to expose (unmodeled) basement membrane. Bar: 200 μm. **A.** Simulation time course for the default parameters. Note the spread of the infection from an initial infected cell at the center, with apoptotic death events focused near the center. **B.** Decreasing the diffusion coefficient of virions by a factor of 10 drastically reduces the rate of spread, although focusing exocytosed virions in a smaller diffusion distance increases the number of virions infecting nearby cells, leading to faster apoptosis. **C.** Allowing apoptosed cells to release their assembled virions at lysis had a negligible effect for these parameters, given the dominant effects of releasing virions throughout the cell survival times. **D.** Decreasing the tolerance (half max) of cells to assembled virions prior to apoptosis accelerates tissue damage but does not drastically accelerate the spread of the infection. **E.** Increasing the apoptosis rate (or decreasing the survival time) for infected cells drastically increases tissue degradation.

of a degraded, cell-free region near the center of the tissue. This degraded region spreads outwards from the

initial site of infection over time.

See **Fig. 1.3 A** for a simulation with default parameters. The nanoHUB distribution of this model takes approximately 60-90 seconds to execute.

Impact of the virion diffusion coefficient

We tested the effect of the viral diffusion coefficient by reducing it from 900 μm^2/min to 90 μm^2/min. Because the viral particles spread more slowly after their release, the overall spread of the infection is slowed (**Fig. 1.3 B**). We left D = 90 μm^2/min for all subsequent investigations of the v1 model.

Impact of the viral release at cell death

We tested the effect of releasing all assembled viral particles at the time of cell death by setting $f_{release}$ = 1. For this set of model parameters, the release of assembled virions had a negligent impact of the overall spread of infection: Compare the final frame of **Fig. 1.3 B** (no release: $f_{release}$ = 0) to **Fig. 1.3 C** (complete release: $f_{release}$ = 1). This is because cells release far more virions during their infected lifetimes, so the effect is dominant over the one-time release of virions at cell death. We expect this behavior would change if the cells exocytosed virions more slowly.

Impact of the cell tolerance to viral load

We decreased the cell tolerance to viral load by decreasing the A_H of Equation 8 from 500 virions to 10, while leaving $f_{release}$ = 1. As expected, cell death and tissue damage occurred much more quickly under these parameters (**Fig. 1.3 D**). Interestingly (and contrary to intuition), this did not significantly alter the rate at which the infection spread through the tissue. Compare the final frame of **Fig. 1.3 C** (higher tolerance to viral load) to **Fig. 1.3 D** (lower tolerance to viral load). This shows the importance of creating spatiotemporal models of viral replication in tissues, as the balance of competing processes can lead to unexpected dynamics at the tissue, organ, and organism levels.

Impact of the cell survival time under high viral loads

We decreased the cell tolerance to viral load further by decreasing the mean cell survival time under high viral loads, which is equivalent to increasing the maximum apoptosis rate r_{max}. Following prior analyses[109,143], $1/r_{max}$ is the mean expected survival time as $A \to \infty$. We increased r_{max} from 0.001 min^{-1} (1000 minute expected lifetime at high loads) to 0.01 min^{-1} (100 minute expected lifetime at high viral loads). This drastically accelerated the rate of tissue damage, leaving much more basement membrane (the assumed surface under the epithelial monolayer) exposed (**Fig. 1.3 E**). In a later version of this model framework, we would expect this to lead to earlier onset of fluid leakage, edema, and ultimately adverse respiratory outcomes such as ARDS. Interestingly, this did not significantly increase the rate of spread of the infection. Compare the final frame of **Fig. 1.3 D** (higher tolerance to viral load) to **Fig. 1.3 E** (lower tolerance to viral load).

Selected feedback from domain experts and the community

We gathered feedback from the multidisciplinary community, several of whom joined the coalition for future work. We summarize the feedback below.

A virologist noted that more detail on endocytosis, viral uncoating, and synthesis would expose more actionable points in the replication cycle. Preliminary SARS-CoV-2 experiments in her laboratory suggest that the time course (and thus general order of magnitude of rate parameters) is very similar to Venezuelan equine encephalitis virus (VEEV) dynamics measured earlier[21,22]. The exponential progression matches observations: the first cell is infected with one virion and so at first produces virus slowly, but neighboring cells can be infected with multiple virions and thus create virus particles more quickly.

A community member identified typographical errors in the original documentation but verified that that mathematics in the C++ implementation were not affected. He emphasized the importance of implementing RNA decay (as a rate limiting step in virus replication) and the importance of integrating ACE2 receptor trafficking (as a rate

limiting step in virus adhesion and endocytosis).

A mathematician noted the potential to simplify the model by removing the diffusing *U, R,* and *P* fields and reported bugs in the initialization (where no cells are initially infected for some domain sizes, due to hard-coding of the initial seeding). Other mathematicians emphasized the importance of varying virion "uptake" with ACE2 receptor availability and hence the need to integrate receptor trafficking.

A mathematical biologist noted prior work on other respiratory viruses will help estimate parameters and build initial immunologic regulation models. Lung pathology and disease severity are closely tied to the immunologic reaction, and prior data and images from influenza will help with calibrating spatial considerations. She expects animal and drug data available for SARS-CoV-2 in the coming months. She noted the importance of distinguishing between mild and severe infections and ARDS. Matching the output to data will be imperative, with one quick possibility to make this match data and distinguish between possibilities is to plot the resulting viral load. She suggested that it would be helpful to show multi focal points of initial infection seeding (possibly of different initial seeding size) that merge together over time, which would match observations of lung histology. Future work will have a better impact if the models uses a true lung tissue geometry with immune cells limiting the peripheral spread. The current model seems more relevant to in vitro growth of a single plaque, which may be scrutinized.

A quantitative systems pharmacologist pointed out the need for clearer scoping and diagrams to clearly lay out the design of each submodel component. We will need procedures to choose future incorporations and changes of scope. He also pointed out the need to understand what happens if you bind up a lot of ACE2 with receptor; there are early insights online[144].

A bioengineer with tissue damage and inflammation expertise noted that the diffusion coefficient of 900 μm^2/min = 15 μm^2/s = 1.5e-11 m^2/s is not particularly small; prior analyses[145] considered virion diffusion in an lung epithelial monolayer for influenza with D = 3.18e-15m^2/s estimating from experimental data. The virions for SARS-CoV-2 could be more mobile though; it is uncertain. There are data[146] about the diffusion coefficient for albumin in tissue being on the order of 10-50 μm^2/s. She stated that it makes sense for a virion (radius of 25-100 nm) to move more slowly than a protein with radius < 5 nm unless "diffusive transport" in the model is encompassing an active or facilitated transport mode beyond just classic diffusion. She also noted that her laboratory has looked a lot at the renin-angiotensin-system systemically and in kidneys: the kinetics of AngII, ACE, and ACE2 in the lungs would be of interest for connecting the next iteration of the ACE2 receptor model to connect to ARDS. Pfizer may also have relevant related models.

A mathematical biologist with expertise in infectious diseases noted that the model could study immune responses and the impact of mucosal structure in future versions. She suggested quantifying damage or disease metrics. She also noted that ultimately it would be useful to note which parameter estimates might be species-specific and which are not, to be able to switch between experimental and clinical systems, e.g., it is worth recording if current estimates are from human, macaque, etc. She also noted that it may be important to determine if apoptotic cells are replaced or if there is permanent damage (in the model). If the model is run longer, it would be worthwhile to translate the visual sense of damage to a quantitative metric.

An independent team of clinically-focused modelers noted their work on modeling immune expansion in "off screen" lymph nodes and offered to link their model to our immune infiltration functions.

A mathematical biologist with a focus on model and data standards noted the need for clearly specifying each model's assumptions, inputs, and outputs to drive robust parallel development. He noted that it is critical to consider information flow between submodels and revise these data flows as the iterations proceed. He suggested that we state separate execution of submodels as a key design goal to support parallel development. Lastly, he noted that software should be released in conjunction with validation data and methodologies.

Core team discussion and priorities for v2

The core team met by virtual conference on April 1, 2020 to discuss the first preprint, model results, and feedback. The core team set as priorities (1) to formalize design specifications for each individual model component and interfaces between components, (2) form teams responsible for each component, (3) focus v2 development on refactoring into this modular format, (3) begin development of the submodels, and (4) begin refine parameter

estimates. The clearer specification and organization of submodels was the top priority. As time permits, it was also viewed as important to begin a receptor trafficking model.

The core team agreed to keep working via the dedicated Slack workspace to rapidly coalesce on the submodel teams. Each subteam has a separate channel in the workspace.

Version 2 (April 1-May 9, 2020)

Version 2 incorporated key v1 feedback, with a focus on introducing a more modular design, improving default model parameters, better initialization options, and a new ACE2 receptor trafficking submodel. This design cycle lasted longer due in part to work spent on subteam organization. As with Version 1, the Version 2 model was developed by the overall leads (Macklin, Heiland, Wang) to refine key model infrastructure for the forming subteams. (See the discussion in **Three main phases of community-driven development**.)

Version 2 also began work to test the design documents that were first discussed by the core team during the v1 model feedback. The interactive nanoHUB model included new usability refinements, notably an option to animate the model outputs.

Model changes

The v2 model was expanded to include the following submodel components (**Fig. 2.1**):

- **T:** tissue (which contains epithelial and other cells)
- **RT:** ACE2 receptor trafficking (including virus endocytosis)
- **V:** viral endocytosis, replication, and exocytosis responses
- **VR:** cell response to viral replication, including cell death and IFN synthesis
- **E:** epithelial cell (incorporates RT, V and VR).

Based on community feedback, the default virion diffusion coefficient was reduced by a factor of 10 to 90 μm^2/min. We may reduce this parameter further based upon oncolytic virus therapy modeling experience by Morgan Craig and Adrianne Jenner.

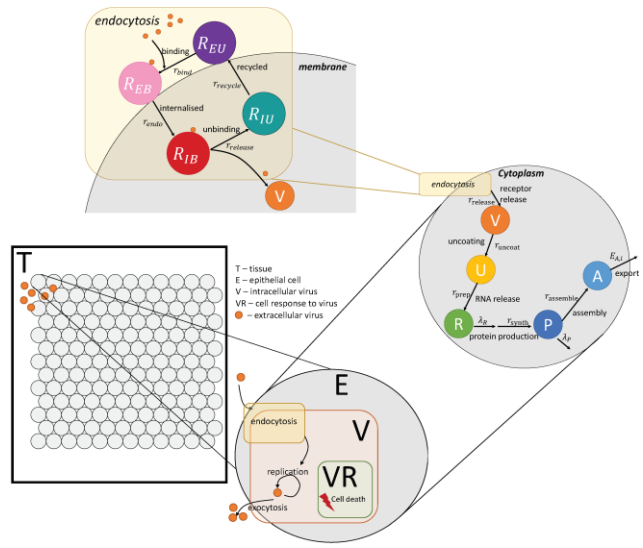

Fig. 2.1: Version 2 model schematic: In the overall model structure, a ***tissue component*** **(T)** contains multiple ***epithelial cells*** **(E)**. Viral particles diffuse through this domain and can enter the cells (by adhering as an uptake term) or be exported by cells. Each cell includes an ACE2 ***receptor trafficking*** model (**RT**) where virus can bind an unoccupied surface receptor, which is endocytosed to release its virion and eventually return to the surface. Each cell's ***virus lifecycle*** model **(V)** simulates viral replication kinetics, and its ***viral response*** model **(VR)** uses a dose-response model to control cell apoptotic response to viral load.

Biological hypotheses

The v2 model was similar to v1 with a simplified set of biological hypotheses:

2.T.1	Virus diffuses in the microenvironment with low diffusion coefficient
2.T.2	Virus adhesion to a cell stops its diffusion (acts as an uptake term)
2.RT.1	Virus adheres to unbound external ACE2 receptor to become external (virus)-bound ACE2 receptor
2.RT.2	Bound external ACE2 receptor is internalized (endocytosed) to become internal bound ACE2 receptor
2.RT.3	Internalized bound ACE2 receptor releases its virion and becomes unbound internalized receptor; the released virus is available for use by the viral lifecycle model **V**

2.RT.4	Internalized unbound ACE2 receptor is returned to the cell surface to become external unbound receptor
2.RT.5	Each receptor can bind to at most one virus particle
2.V.1	Internalized virus (previously released in 2.RT.3) is uncoated
2.V.2	Uncoated virus (viral contents) lead to release of functioning RNA
2.V.3	RNA creates viral protein at a constant rate unless it degrades
2.V.4	Viral protein is transformed to an assembled virus state
2.V.5	Assembled virus is released by the cell (exocytosed)
2.VR.1	As a proxy for viral disruption of the cell, the probability of cell death increases with the total number of assembled virions
1.VR.2	Apoptosed cells lyse and release some or all of their contents

(In the above, X.C.Y denotes prototype X, model component C, biological hypothesis Y, allowing us to easily refer to any individual hypothesis or assumption in discussion and community feedback.) In the next version of this model, we will use the design document protocols for each of these components.

Unit tests

The v2 prototype had no changes in qualitative unit tests; once the ACE2 receptor trafficking model works correctly, the model will behave as in v1.

Translation to mathematics, rules and model components

Extracellular virion transport (Tissue submodel ***T***)

There were no changes in this integration-scale tissue model (T) for v2.

ACE2 receptor trafficking (submodel ***RT***)

For each cell, we track R_{EU} (external unbound ACE2 receptors), R_{EB} (external virus-bound receptors), R_{IB} (internalized virus-bound receptor), and R_{IU} (internalized unbound receptor). We model hypotheses 2.RT.1-2.RT.5 as a system of ordinary differential equations:

$$\frac{dR_{EU}}{dt} = -r_{\text{bind}} n_V R_{EU} + r_{\text{recycle}} R_{IU} \tag{10}$$

$$\frac{dR_{EB}}{dt} = r_{\text{bind}} n_V R_{EU} - r_{\text{endo}} R_{EB} \tag{11}$$

$$\frac{dR_{IB}}{dt} = r_{\text{endo}} R_{EB} - r_{\text{release}} R_{IB} \tag{12}$$

$$\frac{dR_{IU}}{dt} = r_{\text{release}} R_{IB} - r_{\text{recycle}} R_{IU} \tag{13}$$

As in the v1 virus model, we estimate n_V (the number of extracellular virions interacting with the cell) based upon consistency with the BioFVM implementation and set

$$r_{\text{bind}} n_V R_{EU} = U_i V_i \rho \tag{14}$$

where U is the cellular uptake rate and V is the volume of the cell, and so

$$n_V \approx V_i \rho \tag{15}$$

$$U_i = r_{\text{bind}} R_{\text{EU}} \tag{16}$$

Thus, the virus endocytosis rate varies with the availability of unbound externalized ACE2 receptor, as expected. To link with the viral replication submodel, the unbinding of virus from internalized receptor must act as a source term for the internalized virus:

$$\text{Source}_V = r_{\text{release}} R_{IB} \tag{17}$$

Intracellular viral replication dynamics (Virus lifecycle model ***V***)

We make a small modification to the internalized virus model to account for the coupling with the receptor trafficking model:

$$\frac{dV}{dt} = \text{Source}_V - r_U V \tag{18}$$

$$\frac{dU}{dt} = r_U V - r_P U \tag{19}$$

$$\frac{dR}{dt} = r_P U - \lambda_R R \tag{20}$$

$$\frac{dP}{dt} = r_S R - r_A P - \lambda_P P \tag{21}$$

$$\frac{dA}{dt} = r_A P - E_A \tag{22}$$

We model exocytosis by setting the export rate E_A of the assembled virions, in units of virions per time:

$$E = r_E A \tag{23}$$

Cell response (Viral response submodel ***VR***)

There were no changes from the v1 model.

Initialization

In v2, we added the option to specify the *multiplicity of infection (MOI):* the ratio of initial virions to number of epithelial cells. These virions are placed randomly in the extracellular space. We use a default MOI = 0.01 to model a fine mist of virions landing on the tissue. Users can also set an option to only infect the centermost cell, which sets $V = 1$ for that cell.

Refined parameter estimates

Detailed experimental characterization of ACE2 receptor trafficking in SARS-CoV[147] permits an initial estimation of key model parameters. This experimental work reported that endocytosed receptors were observed in 3 hours post infection, and that 10 hours later (13 hours elapsed time), receptors were observed in vesicles. This estimates the time scale of binding and endocytosis to be on the order of 3 hours, and that virion release occurs on the order of 10 hours. Thus:

$$\frac{1}{r_{\text{bind}} R_{EU}(0)} + \frac{1}{r_{\text{endo}}} \sim 3 \text{ hours} \tag{24}$$

and

$$\frac{1}{r_{\text{release}}} \sim 10 \text{ hours}. \tag{25}$$

Supposing that binding is relatively fast compared to endocytosis, we set $\frac{1}{r_{\text{bind}} R_{EU}(0)} \sim 1 \text{ min}$, and so $\frac{1}{r_{\text{endo}}} \sim 3 \text{ hours}$. Recycled receptors were observedwithin 14 hours (1 hour after the appearance of endocytosed receptors), so we set $\frac{1}{r_{\text{recycle}}} \sim 1 \text{ hour}$. Assuming there are 1,000 to 10,000 ACE2 receptors per cell, we set the parameters (to order of magnitude) at

$$r_{\text{bind}} = 0.001 \text{ min}^{-1} \tag{26}$$

$$r_{\text{endo}} = 0.01 \text{ min}^{-1} \tag{27}$$

$$r_{\text{release}} = 0.001 \text{ min}^{-1} \tag{28}$$

$$r_{\text{recycle}} = 0.01 \text{ min}^{-1} \tag{29}$$

$$r_{\text{bind}} = 0.001 \text{ min}^{-1} \tag{30}$$

The report observed expression of viral proteins by 18 hours (5 hours after viral release from endocytosed ACE2 receptors). Assuming that $r_{\text{uncoat}} \sim r_{\text{prep}} \sim r_{\text{synth}}$, each parameter has magnitude 0.01 min^{-1}. We similarly set $r_{\text{assemble}} = r_{\text{exo}} = 0.01 \text{ min}^{-1}$ in the v2 model.

Other implementation notes

To differentiate between incoming imported and exported virions within the computational implementation, we modeled two diffusing fields (for extracellular concentrations of *V* and *A*). However, the models only require extracellular *V*. At the end of each computational step (advancing by one diffusional time step), we iterate through each voxel and transfer all of the extracellular diffusing *A* to *V*. We also created diffusing fields for uncoated virions, RNA, and viral proteins, although these were removed from later model versions.

By setting the virus uptake rate *U* as noted above, PhysiCell (via BioFVM) automatically removes the correct amount of virions from the extracellular diffusing field and places them in an internalized virus particle variable *n*. By PhysiCell's automated mass conservation:

$$\Delta n = \Delta t \, r_{\text{bind}} n_V R_{EU} = \Delta t \, U_i V_i \rho. \tag{31}$$

If *n* was previously set to zero, then the current value of *n* represents Δn. By assumption 2.RT.5, Δn is equal to the change in the number of external virus-bound receptors (one virion per receptor). Thus, these receptors (Δn) represent the net increase in bound external receptors. So at each time step, we:

1) Increase R_{EB} by *n*
2) Decrease R_{EU} by *n*
3) Set *n* = 0 (because these virions have been "delivered" to the receptor trafficking model)

Software release

The core model associated with the v2 prototype is Version 0.2.1. The nanoHUB app associated with the v2 prototype is Version 2.1. GitHub releases and Zenodo snapshots are given in the Appendix.

The cloud-hosted interactive model can be run at https://nanohub.org/tools/pc4COVID-19.

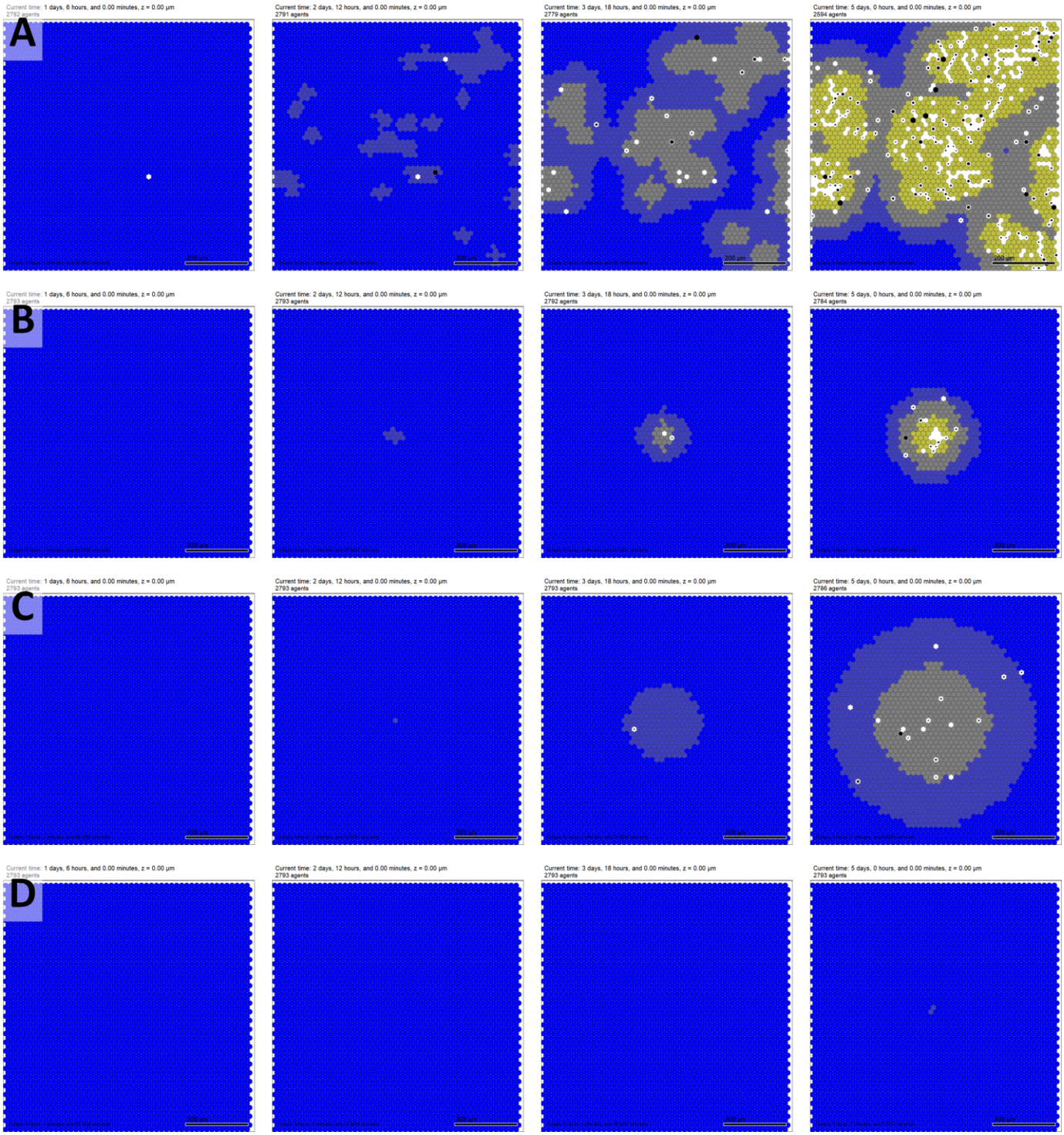

Fig. 2.2: Version 2 sample model results at 30, 60, 120, and 180 hours. In all plots, epithelial cells are colored from blue (no assembled virions) to bright yellow (1000 or more virions). Black cells are apoptotic, and white regions show damaged tissues where apoptotic cells have degraded to expose (unmodeled) basement membrane. Bar: 200 μm. **A.** Simulation time course using the new initialization with an MOI (multiplicity of infection) of 0.01. As virions land randomly on the tissue, they initiate multiple infections that spread and merge. **B.** After infecting a single cell (with the new default parameters), the infected region (plaque) spreads radially as in the v1 model, but at a slower rate. As before, tissue degradation (black apoptotic cells and white cleared tissue) has greatest frequency near the original site of infection. **C.** If the number of ACE2 receptors is cut by a factor of 10, fewer virions infect cells, leading to slower viral replication. However, the reduced rate of virus binding and endocytosis leaves more extracellular viral particles to disperse, leading to a larger spread of the region of infection. **D.** Decreasing instead the rate of virus release from internalized ACE2 receptor drastically slows the viral dynamics.

Model behavior: what does the current version teach us?

Except as noted below, all simulation results use the v2 model default parameters, which are supplied in the XML configuration parameter file of the version 0.2.1 core model repository.

In all plots, dark blue cells have 0 assembled virus, pale blue cells have 1-9 assembled virions, grey cells have 10-99 assembled virions, light yellow cells have 100-999 assembled virions, and bright yellow cells contain 1000 or more assembled virions. Black cells are apoptotic, and white spaces show regions devoid of cells (extensive tissue damage).

Infection by a single virus versus a dispersion of virions

Compared to the previous method of initially infecting a single cell with a single virion, the v2 model simulation using the new MOI initialization (MOI=0.01) showed viral particles nucleating multiple infections spread as independent plaques that later merge (**Fig. 2.2 A** and **Fig. 2.2 B**). For higher MOIs, some cells can be infected by more than one virion, leading to faster viral replication.

Targeting the endocytosis cascade versus targeting ACE2 receptor

As more subcellular mechanisms are added to the model, we can ask *what if* questions about potential pharmacologic interventions[9]. Using the v2 model, we first investigated the impact of reducing the number of ACE2 receptors on each cell by a factor of 10 (e.g., by an intervention that targets ACE2 receptor or reduces its expression). We found that while this reduced the number of viral particles infecting each cell (thus slowing replication in individual cells), it paradoxically *accelerated* the spread of the infected region through the tissue (**Fig. 2.2 C**). This phenomenon can be understood by dimensional analysis: the effective transport length scale L of the virus particle is $L = \sqrt{\frac{D}{U}}$, where U is the uptake rate of the viral particles. In the v2 model, U is proportional to the number of unbound external ACE2 receptors. If this number is reduced, then the length scale increases, leading to a faster dissemination of virus particles, exposing more tissue to virus particles, and ultimately infecting more cells earlier in the disease time course. On the other hand, with slower viral replication in individual cells, tissue damage may be delayed. (**Fig. 2.2 D**).

We similarly investigated whether decreasing the rate of viral release from virus-bound endocytosed receptors by reducing $r_{release}$ by a factor of 10. This drastically impaired the spread of the infection: ACE2 receptors trapped and internalized more viral particles, which then replicated more slowly, thus reducing the severity of the infection.

Selected feedback from domain experts within the coalition and the community

The core team reviewed the v2 model and project progress on weekly between April 8, 2020 and May 4, 2020.

The team discussed the potential need for an improved viral replication model. In particular, for low virus counts early in cellular infection, the continuum hypothesis needed for ordinary differential equations may not hold, and non-physical behaviors (e.g., infection by less than a single virus) may prevent the eradication of infections in the model. A discrete modeling approach may be required, although limiting mass transfers (e.g., from R_{EU} to R_{EB}) to integer amounts could also help address this issue. The core team also reaffirmed the need to create a simplified immune system model to continue progress.

The core team also identified needed refinements in xml2jupyter, particularly the ability to run additional analytics on simulation outputs and visualize the results in the Jupyter notebook interface.

The core team formed the subteams, identified chief scientists, and organized the first rounds of subteam meetings. The core team also discussed the need to include subteam updates in the weekly core meetings. This was first implemented in the May 4, 2020 call, and the development cycle discussed above reflects these community-driven changes to team management.

We received additional feedback from the community from a postdoctoral fellow at Barcelona Supercomputing

Center (BSC), who noted the number of virion particles should be constrained to integer values. He also suggested a branch of the sub-models may be reimplemented as stochastic differential equation. In addition, the fellow pointed out that BSC is developing COVID-19 molecular disease maps, mainly by curating interactions between viral and cellular proteins from several data sources and domain experts. It may be possible to "translate" these process descriptions to activity flow models for Boolean network simulations in PhysiBoSS[130]. Future collaborations could test the COIVD-19 tissue simulator developed by this coalition in PhyiBoSS.

Core team discussion and priorities for v3

The highest priority for v3 is to start transitioning the development of the submodels to the subteams, thus moving the project from Phase 1 to Phase 2. In particular, the team was keen to implement a basic immune model.

Version 3 (May 10 - July 27, 2020)

Version 3 focused on implementing a realistic representation of the tissue-level immune response to SARS-CoV-2 and transitioning development of the submodels to the subteams. Due to the complexity of the immune system, a significant portion of time was spent developing a realistic minimal model of the immune response.

This also represents the first model release to begin the transition from Phase 1 to Phase 2: the immune team took on primary development of the C++ for their submodel. This development cycle also performed software hardening on the core PhysiCell toolkit to facilitate complex immune behaviors (particularly phagocytosis and CD8$^+$ T cell attacks on infected cells) while improving multithreading safety and cross-platform compatibility. Moreover, we performed a code refactoring to take advantage of new *cell definition* functionality in PhysiCell 1.7.1, which eased the development of the immune model with multiple cell types.

Key hypotheses

The overall aim of this submodel is to include features of the immune response to SARS-CoV-2 that are specific to the local tissue environment. The main immune cellular components included at this stage are tissue-resident macrophages, infiltrating neutrophils, and CD8$^+$ T cells, which are recruited as the infection progresses. The general pattern of events that this model encompasses are summarized here. When epithelial cells in the tissue become infected with SARS-CoV-2, they secrete chemokines that cause macrophages to migrate towards them following a chemokine gradient. In addition, the infected cells may die as a result of the infection (see the cell response model ***VR***), and dead cells will release factors that cause macrophages to migrate towards them. Macrophages phagocytose dead cells and remove them from the tissue. When macrophages encounter dead cells, they begin to secrete pro-inflammatory cytokines, and phagocytose any dead cell material they find. The result of pro-inflammatory cytokine secretion is the in-

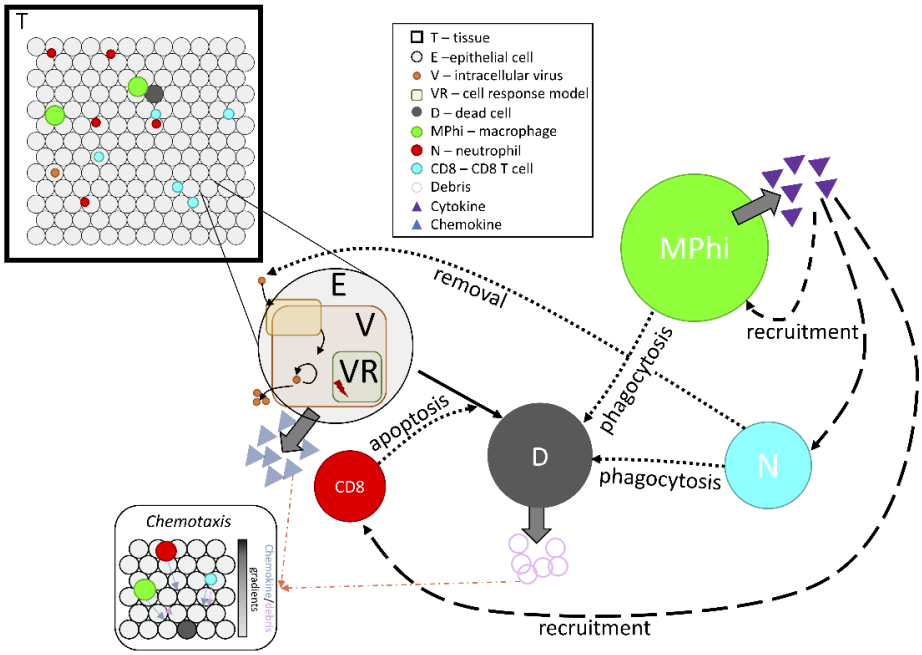

Fig. 3.1: Immune submodel schematic. Immune cells (macrophages, neutrophils, and CD8$^+$ T cells) patrol within the *tissue component* (T), containing multiple *epithelial cells* (E). Cells infected by virus secrete chemokine, which attracts immune cells along the chemokine gradient. CD8$^+$ T cells induce apoptosis in infected cells, creating dead cells that are phagocytosed by macrophages and neutrophils that are attracted along debris gradients. Upon activation, macrophages secrete cytokine that recruits other immune cell types.

filtration of neutrophils into the tissue. Neutrophils are short-lived cells and are replenished in the tissue as long as pro-inflammatory cytokines are still being produced. $CD8^+$ T cells, presumed to be specific for SARS-CoV-2, enter the tissue at a later time, and their role is to kill infected cells. $CD8^+$ T cell entry is dependent upon the presence of pro-inflammatory cytokines. Death of an infected cell is more likely after prolonged contact with one or more $CD8^+$ T cells. $CD8^+$ T cells may also interact with macrophages that have phagocytosed dead cells or virus as these macrophages will now be able to present viral antigens to both $CD4^+$ and $CD8^+$ T cells; however antigen presentation is not directly included in this initial version of the model. As described below, simulations were performed using a field of already infected epithelial cells, and the behavior of the immune cells in this tissue appears to follow the established rules.

Owing to the immune response cascade outlined above, we first integrated macrophages, neutrophils, and $CD8^+$ T cells into the SARS-CoV-2 tissue model. The adaptive immune response in a naïve host begins a few days after innate immune action. For this version, we simplify dynamics by modeling only $CD8^+$ T cells, and we do not yet model antigen presentation via dendritic cells or macrophages. Thus, we assume that $CD8^+$ T cells are recruited around day 4 of infection in response to infected cells and pro-inflammatory cytokine production, where infected cells are killed in response to sustained total contact with one or more $CD8^+$ T cells. It is assumed that immune actions only affect infected cells that are past the eclipse phase and are thus generating virus.

Immune cells travel in a biased correlated random walk along chemical gradients[109]. To control for spatial migration, the submodel contains three diffusing chemicals in addition to free virions: pro-inflammatory cytokines secreted by macrophages, $CD8^+$ T cells, and post-eclipse phase infected cells recruit immune cells into tissue from blood or lymph nodes, which could ultimately be modeled in a separate submodel. We assume all immune cells migrate in the tissue toward infected cells along a chemokine gradient, which is assumed to be secreted by infected cells for simplicity. Infected cells and macrophages also secrete IFN-I, which will reduce viral burst size from neighboring infected cells in future versions of the model.

Model changes

The v2 model was expanded to include the following submodel components (**Fig. 3.1**):

- **T:** tissue (which contains epithelial and other cells, and diffusible factors)
- **RT:** ACE2 receptor trafficking (including virus endocytosis)
- **V:** viral endocytosis, replication, and exocytosis responses
- **VR:** cell response to viral replication, including cell death and IFN synthesis
- **E:** epithelial cell (includes RT, V and VR).
- **D:** dead cell
- **MPhi:** macrophage
- **N:** neutrophil
- **CD8:** $CD8^+$ T cell

Biological hypotheses

The v3 model introduced new assumptions regarding how the infected and dead cells are cleared and how immune cells act in the model (indicated by X.C.Y, where X denotes prototype, C denoted modeling component, and Y denotes a biological hypothesis, for easy reference):

3.T.1	Virus diffuses in the microenvironment with low diffusion coefficient
3.T.2	Virus adhesion to a cell stops its diffusion (acts as an uptake term)
3.T.3	Pro-inflammatory cytokine diffuses in the microenvironment
3.T.4	Pro-inflammatory cytokine is taken up by recruited immune cells
3.T.5	Pro-inflammatory cytokine is eliminated or cleared
3.T.6	Chemokine diffuses in the microenvironment
3.T.7	Chemokine is taken up by immune cells during chemotaxis
3.T.8	Chemokine is eliminated or cleared
3.T.9	Debris diffuses in the microenvironment
3.T.10	Debris is taken up by macrophages and neutrophils during chemotaxis

3.T.11 Debris is eliminated or cleared

3.RT.1 Virus adheres to unbound external ACE2 receptor to become external (virus)-bound ACE2 receptor
3.RT.2 Bound external ACE2 receptor is internalized (endocytosed) to become internal bound ACE2 receptor
3.RT.3 Internalized bound ACE2 receptor releases its virion and becomes unbound internalized receptor. The released virus is available for use by the viral lifecycle model **V**
3.RT.4 Internalized unbound ACE2 receptor is returned to the cell surface to become external unbound receptor
3.RT.5 Each receptor can bind to at most one virus particle.

3.V.1 Internalized virus (previously released in 2.RT.3) is uncoated
3.V.2 Uncoated virus (viral contents) lead to release of functioning RNA
3.V.3 RNA creates viral protein at a constant rate unless it degrades
3.V.4 Viral protein is transformed to an assembled virus state
3.V.5 Assembled virus is released by the cell (exocytosis)

3.VR.1 After infection, cells secrete chemokine
3.VR.2 As a proxy for viral disruption of the cell, the probability of cell death increases with the total number of assembled virions
3.VR.3 Apoptosed cells lyse and release some or all of their contents

3.E.1 Live epithelial cells undergo apoptosis after sufficient cumulative contact time with adhered $CD8^+$ T cells.
3.E.2 Live epithelial cells follow all rules of RT
3.E.3 Live epithelial cells follow all rules of V
3.E.4 Live epithelial cells follow all rules of VR
3.E.5 Dead epithelial cells follow all rules of D.

3.D.1 Dead cells produce debris

3.Mphi.1 Resident (unactivated) and newly recruited macrophages move along debris gradients.
3.MPhi.2 Macrophages phagocytose dead cells
3.Mphi.3 Macrophages break down phagocytosed materials
3.Mphi.4 After phagocytosing dead cells, macrophages activate and secrete pro-inflammatory cytokines
3.Mphi.5 Activated macrophages can decrease migration speed
3.Mphi.6 Activated macrophages have a higher apoptosis rate
3.Mphi.7 Activated macrophages migrate along chemokine and debris gradients
3.Mphi.8 Macrophages are recruited into tissue by pro-inflammatory cytokines.
3.MPhi.9 Macrophages die naturally and become dead cells.

3.N.1 Neutrophils are recruited into the tissue by pro-inflammatory cytokines
3.N.2 Neutrophils die naturally and become dead cells
3.N.3 Neutrophils migrate locally in the tissue along chemokine and debris gradients
3.N.4 Neutrophils phagocytose dead cells and activate
3.N.5 Neutrophils break down phagocytosed materials
3.N.6 Activated neutrophils reduce migration speed
3.N.7 Neutrophils uptake virus

3.CD8.1 $CD8^+$ T cells are recruited into the tissue by pro-inflammatory cytokines
3.CD8.2 $CD8^+$ T cells apoptose naturally and become dead cells

3.CD8.3 $CD8^+$ T cells move locally in the tissue along chemokine gradients
3.CD8.4 $CD8^+$ T cells adhere to infected cells. Cumulated contact time with adhered $CD8^+$ T cells can induce apoptosis (See 3.E.1)

Unit tests

To confirm the dynamics of the immune model qualitatively reproduce the *in-situ* dynamics, we monitored the population numbers of immune cells (macrophages, neutrophils, $CD8^+$ T cells) over time and compared with our biological expectations.

Translation to mathematics, rules, and model components

There were no changes to the ACE2 receptor trafficking model ***RT*** or the intracellular viral replication dynamics model ***V.***

Extracellular transport (Tissue submodel ***T***)

Extracellular densities of pro-inflammatory cytokine and chemokine were modelled using the standard BioFVM formulation[120], similar to that for extracellular virus (introduced above), i.e.:

$$\frac{\partial \rho}{\partial t} = D\nabla^2\rho - \lambda\rho + \sum_{\text{cells } i} \delta(x - x_i)(S_i(\rho_i^* - \rho) - U_i\rho)V_i, \tag{32}$$

where D is the diffusion coefficient of each substrate, λ is the net decay rate, δ is the discrete Dirac delta function, x_i is the position of the centre of cell i, S_i is the secretion rate of cell i, ρ_i^* is the saturation density at which cell i stops secreting, U_i is the uptake rate of the substrate by cell i, and V_i is the volume of cell i. The concentration ρ, represents the density of pro-inflammatory cytokine ρ_{cytokine}, chemokine $\rho_{\text{chemokine}}$ or dead cell debris ρ_{debris}. Similarly, diffusion, decay, secretion, and uptake parameters are all substrate specific rates, i.e. the diffusion coefficients are $D_{\text{cytokine}}, D_{\text{chemokine}}$ and D_{debris}; the decay rates are $\lambda_{\text{cytokine}}, \lambda_{\text{chemokine}}$ and λ_{debris}; the secretion rates are $S_{\text{cytokine}}, S_{\text{chemokine}}$ and S_{debris}; the uptake rates are $U_{\text{cytokine}}, U_{\text{chemokine}}$ and U_{debris}; and the saturation densities are $\rho^*_{\text{cytokine}}, \rho^*_{\text{chemokine}}$ and ρ^*_{debris}.

Cell response (Viral response submodel ***VR***)

We made a small addition to the cell response model. After infection, cells start secreting chemokine at a rate

$$S_{\text{chemokine}} \min\left(1, \frac{A}{A_H}\right) \tag{33}$$

where A is the intracellular assembled virion count and A_H is the amount of assembled virions at which half of the maximum effect of virus-induced cell apoptosis is achieved. Secretion continues until the cell dies either through lysis or $CD8^+$ T cell induced apoptosis.

Signaling, degradation, and phagocytosis of apoptotic cells (Dead cell dynamics ***D***)

Cells that die release debris that attracts phagocytes and signals that that they can be cleared from the micro-environment. They secret these signals at a rate S_{debris}.

Chemotaxis (Chemotaxis model ***MPhi, N,*** and ***CD8***)

Macrophages and neutrophils undergo chemotaxis up the chemokine gradient and dead-cell debris gradients released by infected cells and dead cells respectively. The velocity of cell chemotaxis is

$$\vec{v}_{\text{mot}} = s_{\text{mot}} \frac{(1-b)\xi + b\vec{b}}{\left|\left|(1-b)\xi + b\vec{b}\right|\right|} \tag{34}$$

where s_{mot} is the speed of chemotaxis (cell-type-specific), $0 \leq b \leq 1$ is the migration bias (also cell-type-specific), ξ is a random unit vector direction in 3D (or 2D) and $\vec{b}$ is the migration bias direction defined by

$$\vec{b} = \frac{\sigma_{chemokine}\nabla\rho_{chemokine} + \sigma_{debris}\nabla\rho_{debris}}{\left|\left|\sigma_{chemokine}\nabla\rho_{chemokine} + \sigma_{debris}\nabla\rho_{debris}\right|\right|} \quad (35)$$

where $\sigma_{chemokine}$ and σ_{debris} are the sensitivity of chemotaxis along either the chemokine or dead-cell debris gradient. $CD8^+$ T cells also undergo chemotaxis, but along the chemokine gradient, i.e. $\sigma_{debris} = 0$ and $\sigma_{chemokine} = 1$. Chemotaxing cells take up chemokine at a rate $U_{chemokine}$.

Phagocytosis dynamics (Phagocytosis of apoptotic cells ***MPhi*** and ***N***)

Once a macrophage or neutrophil has found a cell to phagocytose, it reduces its speed from $s_{mot,a}$ (active chemotaxis speed) to $s_{mot,p}$ (phagocytosis/attached speed) and starts searching locally for material to phagocytose.

If there is a dead cell in contact with a macrophage or neutrophil (i.e., if there is a dead cell in the cell's ~30 μm mechanical interaction voxel as in PhysiCell[109]), the immune cell will phagocytose the dead cell with rate r_{phag}, which is cell-type specific and reflects the efficacy with which each immune cell subtype clears debris. If the immune cell is in contact with a dead cell over a period of $[t, t + \Delta t]$, then the probability of phagocytosis is $r_{phag}\,\Delta t$. When an immune cell phagocytoses a dead cell, the immune cell absorbs the volume of that cell and subsequently increases its volume, i.e., the phagocytosing cell gains:

(a) all of the dead cell's fluid volume;
(b) all of the dead cell's nuclear solid and cytoplasmic solid volume (which are added to the nuclear cytoplasmic solid volume)

This implies that after phagocytosis within time Δt, the volume of a macrophage or neutrophil i that phagocytoses a dead cell j will be given by

$$V_{cs,i}(t + \Delta t) = V_{cs,i}(t) + V_{cs,j}(t) + V_{ns,j}(t), \qquad V_{cf,i}(t + \Delta t) = V_{cf,i}(t) + V_{Vf,j}(t), \quad (36)$$

where $V_{cs,k}$ is the volume of the cytoplasmic solid volume in cell k, $V_{ns,k}$ is the volume of nuclear solid volume in cell k, $V_{cf,k}$ is the cytoplasmic fluid volume in cell k, and $V_{Vf,k}$ is the total fluid volume of cell k. Because this will typically increase the cell's volume above its "target" equilibrium volume, the standard PhysiCell volume model[109] will begin to shrink the cell's volume back towards its resting volume, allowing us to model degradation of phagocytosed materials. After phagocytosing dead material, macrophages start secreting pro-inflammatory cytokines at a rate $S_{cytokine}$.

Neutrophil viral clearance (***N***)

Neutrophils take up extracellular virus at a rate U. We assume this uptake rate is equivalent to the ACE2 receptor binding rate r_{bind}.

Immune cell recruitment (***Mphi, N,*** and ***CD8***)

Macrophages, neutrophils and $CD8^+$ T cells are recruited to the tissue by pro-inflammatory cytokines through capillaries/vasculature in the lung. The density of vasculature accounts for approximately 8.8% of the tissue[148]. Accordingly, at the start of each simulation we randomly assign 8.8% of the tissue voxels as vasculature points through which immune cells arrive randomly throughout the course of the simulation. (Note that the v1-v3 models simulate a single layer of epithelium where immune cells are allowed to move freely through or just above the tissue; this 2-D formulation is implemented as a single layer of 3D voxels[109].)

At regular time intervals Δt_{immune}, we integrate the recruitment signal to determine the number of immune cells recruited to the tissue. The number of cells recruited into the tissue between t and $t + \Delta t_{\text{immune}}$ varies with the pro-inflammatory cytokine recruitment signal across the tissue:

$$\#\text{ of recruited cells} = r_{\text{recruit}} \int_{\Omega} \min\left(1, \max\left(0, \frac{\rho_{\text{cytokine}} - \rho_{\min}}{\rho_{\text{sat}} - \rho_{\min}}\right)\right) dV \;\; \Delta t_{\text{immune}} \quad (37)$$

where Ω is the computational domain, r_{recruit} is the recruitment rate (per volume), $\rho_{\min}$ is the minimum recruitment signal, ρ_{sat} is the maximum (or saturating), and ρ_{cytokine} is the pro-inflammatory cytokine concentration. The value of $\rho_{\min}$, ρ_{sat}, and r_{recruit} are cell-type specific, i.e. macrophages, neutrophils, and CD8⁺ T cells have different minimum and saturating recruitment signal concentrations which results in heterogenous arrival times into the tissue.

Recruited cells are randomly seeded at vessel locations. In the v3 model, we set $\Delta t_{\text{immune}} = 10$ min. Notice that the number of recruited cells scales with duration of the time interval and the size of the tissue.

CD8⁺ T cell induction of infected cell apoptosis (***CD8*** dynamic model)

When a CD8⁺ T cell is in contact with a cell (based on PhysiCell's mechanical interaction testing; see the note in phagocytosis above) with intracellular assembled virion is greater than 1, i.e. $A > 1$, the T cell attempts to attach to the infected cell with an attachment rate r_{attach}. Following prior immune modeling work[124,125], if the cell is in contact for a duration Δt, then the probability of forming an attachment in that time period is $r_{\text{attach}} \Delta t$. While the cells are attached, the immune cell's cumulative CD8⁺ T cell contact time is increased by Δt. The T cell has a mean attachment lifetime T_{attach}. Between t and $t + \Delta t$, the probability of detaching is given by $\Delta t / T_{\text{attach}}$.

We assume that an infected cell will undergo apoptosis after its cumulative attachment time exceeds a threshold $T_{\text{CD8\_contact\_death}}$. This can be either from a single or multiple T cell attachments. All attached T cells detach when a cell undergoes apoptosis. When CD8⁺ T cells adhere to another cell, their motility is turned off, i.e. $s_{mot,p} = 0$, and when they detach from a cell, their speed returns to their active chemotaxis speed $s_{mot,a}$.

Initialization

An initial population of $MPhi_0$ macrophages is seeded randomly throughout the tissue.

Estimates for immune parameters

The diffusion coefficient for the chemokine, pro-inflammatory cytokine, and debris, $D_{\text{chemokine}}, D_{\text{cytokine}}$, and D_{debris}, were set at $555.56\ \mu m^2/min$ which was estimated by Matzavinos ***et al*** as the diffusion coefficient for monoclonal antibodies[149]. This is equivalent to $8 \times 10^{-3}\ cm^2/day$, which is similar to $1.25 \times 10^{-3}\ cm^2/day$ estimated by Liao ***et al.***[150,151]. Decay and secretion rates of the pro-inflammatory cytokine, chemokine, and debris were assumed to be equivalent. Decay rates for the signaling substrates, $\lambda_{chemokine}, \lambda_{cytokine}$ and λ_{debris}, were all set to $1.02 \times 10^{-2}/min$, which was estimated as the decay rate of IL-6 by Buchwalder ***et al.***[152].The secretion rate for each signaling substrate, $S_{chemokine}, S_{cytokine}$ and S_{debris}, was $0.8254/\rho^*\ 1/min$, obtained through fitting the secretion rate of infected cells to the production of IL-6 by infected basal epithelial cells measured by Ye ***et al.***[153] over 25 hour[153]. The uptake rate of pro-inflammatory cytokine, $U_{cytokine}$, was estimated to be $0.0018\ (pg/ml)^{-1}day^{-1}$ from measurements of the binding rate of IL-6 [154]. The chemokine uptake rate, $U_{chemokine}$, was estimated to be $0.0510\ (pgml)^{-1}day^{-1}$ [155]. The uptake rate of debris, U_{debris}, was assumed to be equivalent to that of $U_{chemokine}$, because it acts as a chemoattractant.

Macrophages, neutrophils and CD8⁺ T cells all have different sizes. Macrophages have an average diameter of $21\ \mu m$ [156], giving a total volume of $4849 \mu m^3$. Neutrophils have an average diameter of $14\ \mu m$ [157], giving a total volume of $1437\ \mu m^3$. When activated, CD8⁺ T cells have a diameter of 0.7 $9.7\ \mu m$[158], giving a total volume of $478 \mu m^3$. For all immune cells, the volume of nucleus was assumed to be 10% of the cells total volume[159].

The active migration rate of macrophages and CD8⁺ T cells along the chemokine gradient was $s_{mot,a} = 4 \mu m/min$ based on *in vitro* and *in vivo* measurements of leukocyte chemotaxis rates[160]. We assume these cells have a migration bias of 0.5 (unitless). Neutrophils move faster with stronger bias along the chemokine gradient at $s_{mot} = 19 \mu m/min$, with a bias of 0.91[160]. Once macrophages and neutrophils encounter material to phagocytose, their motility reduces to $s_{mot,p} = 0.4 \mu m/min$ and if a CD8⁺ T cell connects to an infected cell they

are no longer motile, i.e., $s_{mot,p} = 0 \mu m/min$. Cells persist on their given trajectory for 5 minutes before a new trajectory is chosen. All immune cells undergo apoptosis at different rates, with neutrophils undergoing apoptosis on average after 18.72 hours[161] (i.e. $a_{I,N} = 8.87 \times 10^{-4}$ min^{-1}), macrophages on average every 3.3 days[162] (i.e. $a_{I,M\Phi} = 2.083 \times 10^{-4}$ min^{-1}) and CD8$^+$ T on average every 2.5 days (i.e. $a_{I,T} = 2.778 \times 10^{-4}$ min^{-1})[163].

Macrophages are well known for their capability in phagocytosing dead cell debris[164]. As such, we set the probability of a macrophage phagocytosing a dead cell in its neighborhood to $p_{phag,M\Phi} = 1$. To account for the fact that neutrophils split their time between phagocytosing dead cells and taking up virus[165], we set the probability that neutrophils phagocytose dead cells as $p_{phag,N} = 0.7$.

For the recruitment of immune cells, parameters were chosen to achieve immunologically reasonable arrival times for the immune cell subsets. Neutrophil and macrophage infiltration into tissue is faster than T cell infiltration, with neutrophils and macrophages arriving within 1 to 2 days after infection[166] and CD8$^+$ T cells arriving closer to 4-5 days after infection[167]. The minimum and saturated signal concentrations, ρ_{min} and ρ_{sat}, for macrophages and neutrophils were, therefore, assumed to be equivalent and fixed as $\rho_{min} = 0.1\ \text{substrate}/\mu m^3$ and $\rho_{sat} = 0.3\ \text{substrate}/\mu m^3$. Whereas, CD8$^+$ T cells had higher signal concentrations for their minimum and saturated recruitment signals, i.e. $\rho_{min} = 0.4\ \text{substrate}/\mu m^3$ and $\rho_{sat} = 0.7\ \text{substrate}/\mu m^3$. The recruitment rate for the different immune types was assumed to be equivalent, i.e. $r_{\text{recruit}} = 4 \times 10^{-9}\ \text{cells}/\text{min}/\mu m^3$ and the immune recruitment rate time-step was $\Delta t_{immune} = 10\ \text{min}$.

Direct observations of CD8$^+$ T cell-infected cell interactions and quantification of infected cell fate revealed that death required a median of 3.5 distinct CD8$^+$ T cell contacts. Killed infected cells have a cumulative median contact time of 50 min and individual contacts between CD8$^+$ T cells and infected cells lasts on average 8.5 min[168]. We therefore set $T_{\text{CD8\_contact\_death}} = 50\ \text{min}$.

Other implementation notes

This simplified immune model does not yet include many key immune agents, including dendritic cells, natural killer (NK) cells, B cells, antibodies, the complement system, and most cytokines. No anti-inflammatory cytokines are modeled, nor can this model return to homeostasis following potential infection clearance. Dynamics of cytokine binding and unbinding to receptors are also omitted. The model does not yet incorporate known SARS-CoV-2 immune evasion techniques, such as a delayed IFN-I response and lymphopenia (decreased CD8$^+$ T cells) from early in infection. In addition, the antigen-presentation from macrophages and subsequent activation process of CD4$^+$ and CD8$^+$ T cells has been omitted. Many of these important mechanisms are planned for inclusion in future versions. See further discussion in v3 modeling results below.

Software release

The core model associated with the v3 prototype is Version 0.2.1. The nanoHUB app associated with the v3 prototype is Version 3.2. GitHub releases and Zenodo snapshots are given in the Appendix.

The cloud-hosted interactive model can be run at https://nanohub.org/tools/pc4COVID-19.

Model behavior: what does the current version teach us?

Except as noted below, all simulation results use the v3 model default parameters, which are supplied in the XML configuration parameter file of the version 0.3.2 core model repository.

In all plots, dark blue cells have 0 assembled virus, pale blue cells have 1-9 assembled virions, grey cells have 10-99 assembled virions, light yellow cells have 100-999 assembled virions, and bright yellow cells contain 1000 or more assembled virions. Black cells are apoptotic, and white spaces show regions devoid of cells (extensive tissue damage). Unactivated macrophages are green, activated macrophages are magenta, CD8$^+$ T cells are red, and neutrophils are cyan. Apoptotic immune cells are light orange.

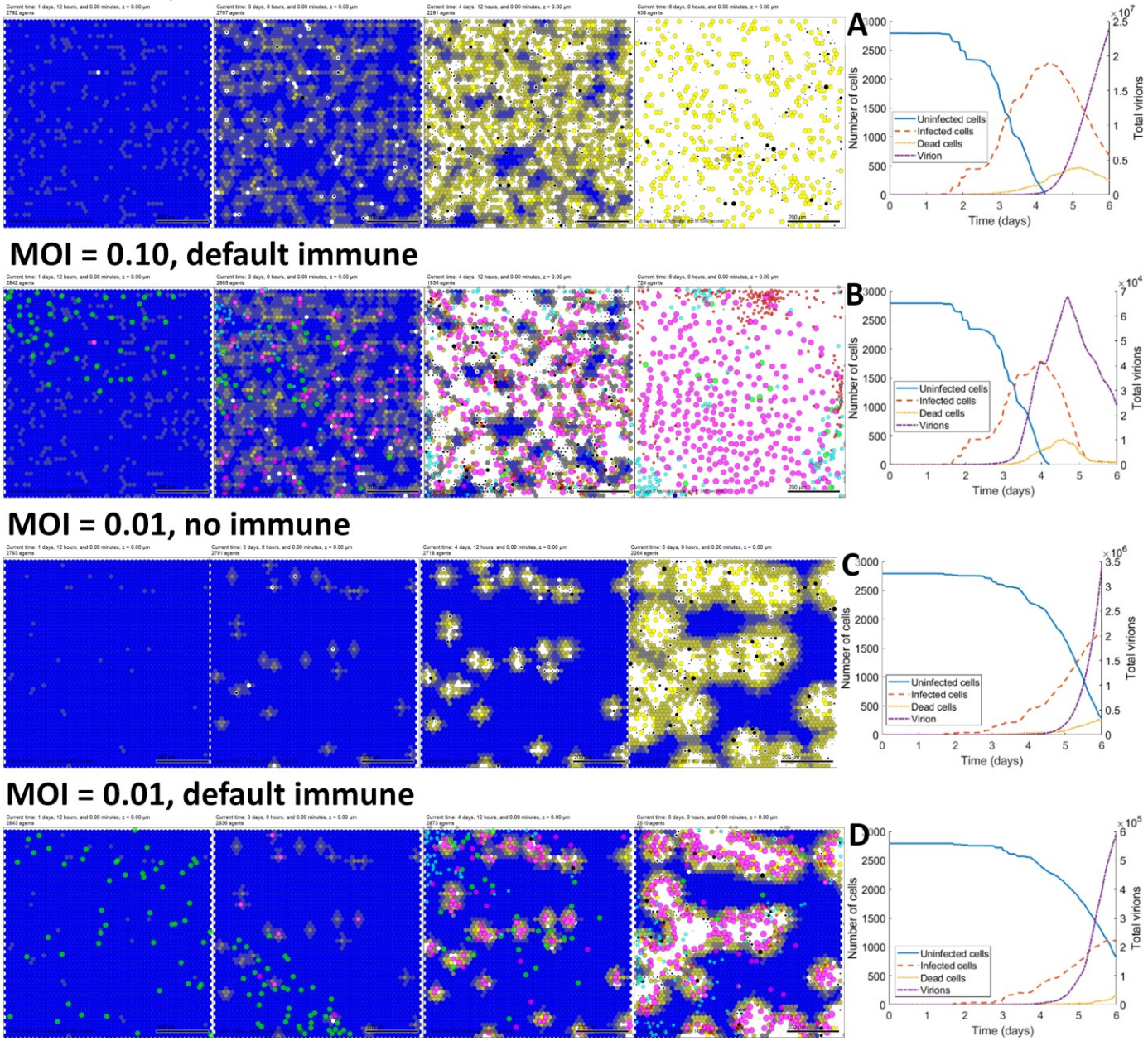

Fig. 3.2: Version 3 model at 46, 72, 108, and 144 hours (default immune settings). In all plots, epithelial cells are colored from blue (no assembled virions) to bright yellow (1000 or more virions). Black cells are apoptotic, and white regions show damaged tissues where apoptotic cells have degraded to expose (unmodeled) basement membrane. Green cells are macrophages, magenta cells are activated macrophages, cyan cells are neutrophils, and red cells are $CD8^+$ T cells. Bar: 200 μm.

Rows 1-2: Simulated dynamics starting with an MOI (multiplicity of infection) of 0.10 without an immune response (**Row 1**) and with an immune response (**Row 2**). **Plots A-B** show uninfected (blue), infected (orange), and dead (yellow) cell counts and total extracellular virion (purple) without an immune response (**A**) and with an immune response (**B**). The immune response clears infected and dead cells more quickly and limits the maximum extracellular viral load, but the underlying tissue is completely destroyed.

Rows 3-4: Simulated dynamics starting with an MOI (multiplicity of infection) of 0.01 without an immune response (**Row 3**) and with an immune response (**Row 4**). **Plots C-D** show uninfected, infected, and dead cell counts and total extracellular virion without an immune response (**C**) and with an immune response (**D**) (same coloring as A-B). The immune response slows the spread of the infection and increases uninfected cell survival.

Impact of adding the immune response (default parameters)

Figs. 3.2-3.5 demonstrate the results of simulating SARS-Cov-2 infection under different parameter regimes. **Fig. 3.2** simulates the dynamics without and with an immune response for a MOI of 0.10 (top results) and 0.01 (bottom results), using the default immune parameters. When the MOI is 0.10, most of tissue is destroyed, either

by the virus (**Fig. 3.2 top row**) or the immune system (**Fig. 3.2 second row**). Reducing the MOI allows some of the tissue to survive the infection in the absence (**Fig. 3.2, third row**) or presence (**Fig. 3.2, fourth row**) of the immune response. All subsequent model results will show a MOI of 0.01 to highlight differences in dynamics to changes in immune parameters. As discussed below, this may not be necessary once the interferon response in infected cells is added to the model.

At high MOI, macrophages are rapidly activated (**Fig. 3.2, first panel in row 2**), and the release of inflammatory cytokines results in the infiltration of $CD8^+$ T cells by day 3 (**Fig. 3.2, second panel in row 2**). The $CD8^+$ T cells kill all infected cells and the tissue is destroyed. At low MOI (0.01), the number of tissue cells surviving is greater (**Fig. 3.2, fourth row, panel 4**). However, macrophage activation is delayed, which further delays the infiltration of $CD8^+$ T cells. At the end of the simulation, on day 6, there is a large number of infected cells (**Fig. 3.2 D**), and the viral titers are still rising. This suggests that, under these default conditions, the lower MOI simply delays the

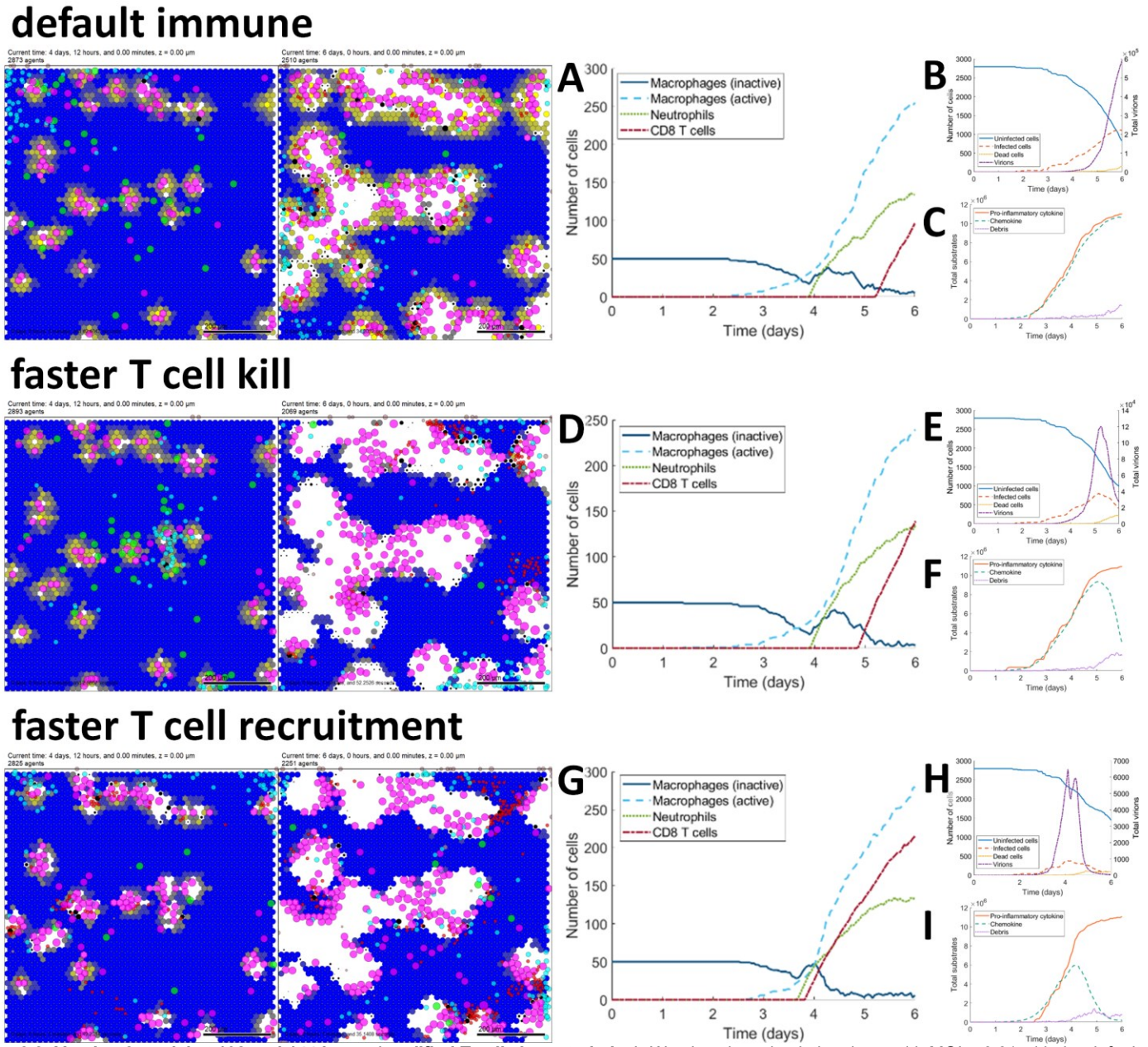

Fig. 3.3: Version 3 model at 108 and 144 hours (modified T cell characteristics). We show late simulation times with MOI = 0.01 with the default immune parameters (**top row**), faster T cell killing (**middle row**), and faster T cell recruitment (**bottom row**). **A, D, and G** plot immune cell dynamics, **B, E, and H** plot infected cell and virion dynamics, and **C, F, and I** plot changes in signaling factors for each simulated scenario. Faster T cell killing and faster T cell recruitment both slow infection dynamics and (nearly) control the infection by 6 days. Cells are colored as in Fig. 3.2.

infection; the tissue is completely destroyed if the simulation is continued beyond 6 days, as seen with the higher MOI of 0.10 (result not shown).

Changing T cell parameters

In the initial model v3 simulation results introduced in **Fig. 3.2**, it appeared that the dynamics of $CD8^+$ T cell recruitment and activation relative to viral replication might be important. Thus, we varied some of the immune cell parameters to determine whether the survival of the tissue could be improved. **Fig. 3.3 (second row)** shows the results when the rate of $CD8^+$ T cell killing was doubled by reducing the threshold contact time for cell death from 50 min to 25 min. Even macrophage, neutrophil, and $CD8^+$ T cell recruitment were slightly reduced compared to the default parameters (compare **Fig. 3.3 D** to **Fig. 3.3 A**), the increased ability of $CD8^+$ T cells to kill infected cells results in fewer infected cells and the viral titers are falling (**Fig. 3.3 B and E**).

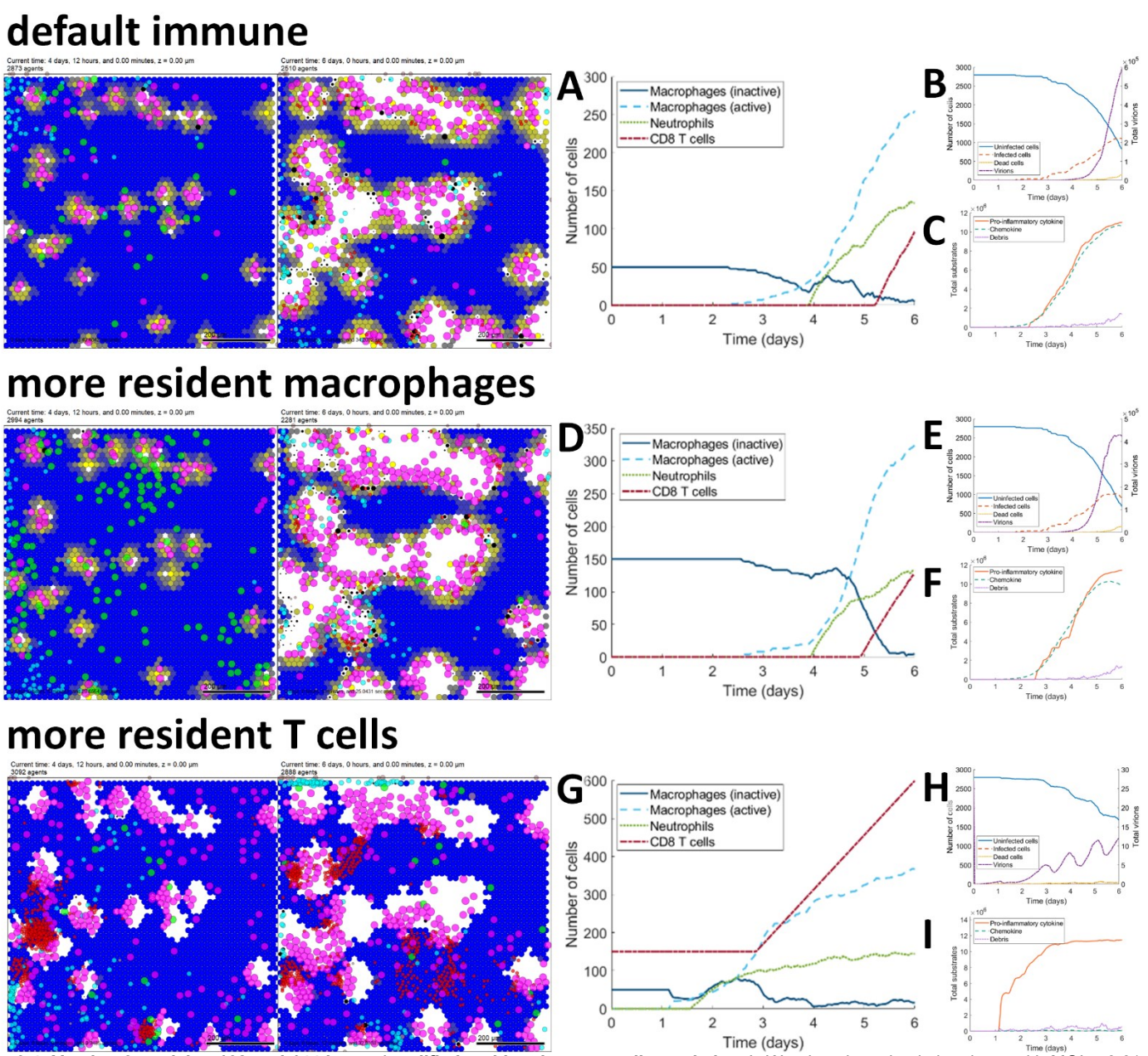

Fig. 3.4: Version 3 model at 108 and 144 hours (modified resident immune cell populations). We show late simulation times with MOI = 0.01 with the default immune parameters (**top row**), increased resident macrophages (**middle row**), and addition of resident T cells (**bottom row**). **A, D, and G** plot immune cell dynamics, **B, E, and H** plot infected cell and virion dynamics, and **C, F, and I** plot changes in signaling factors for each simulated scenario. Increasing the resident macrophage population did not appreciably inhibit the infection, while introducing resident T cells reduced viral titers and better controlled the infection. Cells are colored as in Fig. 3.2.

We also increased the recruitment rate of $CD8^+$ T cells to the tissue in response to inflammatory cytokines by reducing $\rho_{\min}$ from 0.4 to 0.1, and by reducing ρ_{sat} from 0.7 to 0.4; see **Fig. 3.3 (third row)**. This resulted in greater sparing of tissue, and the virus was completely cleared under these conditions (**Fig. 3.3 H**).

Changing resident immune cell populations

We also investigated whether the outcome would be influenced by the number of macrophages and T cells that might be resident within the tissue at the time of infection. We first increased the initial number of macrophages from 50 to 150 (**Fig. 3.4, second row**). Interestingly, this did not result in an improved outcome over that seen with the default parameters (compare **Fig. 3.4, top row**). $CD8^+$ T cell recruitment was enhanced (**Fig. 3.4 D**) but the viral load was continuing to increase at day 6 (**Fig. 3.4 B**), suggesting that increased number of macrophages did not result in more virus control. This could be because in the present model macrophages essentially removed dead cells and do not have a role in killing infected cells. Moreover, because the model's macrophages cannot activate until dead infected cells are present, increasing the number of macrophages cannot trigger a faster immune response. This suggests that after reaching a minimal number of macrophages, adding more resident macrophages has a minimal impact on improving immune response.

In contrast, the presence of resident T cells (**Fig. 3.4, bottom row**) did result in an improved outcome, with more tissue spared and essentially no viral replication (**Fig. 3.4 H**). The final viral count on day 6 was under 15 as T cells were able to kill every infected cell before it could release a significant amount of assembled virions (**Fig. 3.4 H**). This drastically slowed the spread of the infection through the tissue. We also note that the faster T cell killing resulted in earlier accumulation of apoptotic cells, leading to faster activation of macrophages and hence accelerated immune cell recruitment (**Fig. 3.4 G**).

The addition of an interferon response (which could prevent nearby cells from endocytosing these few virions)

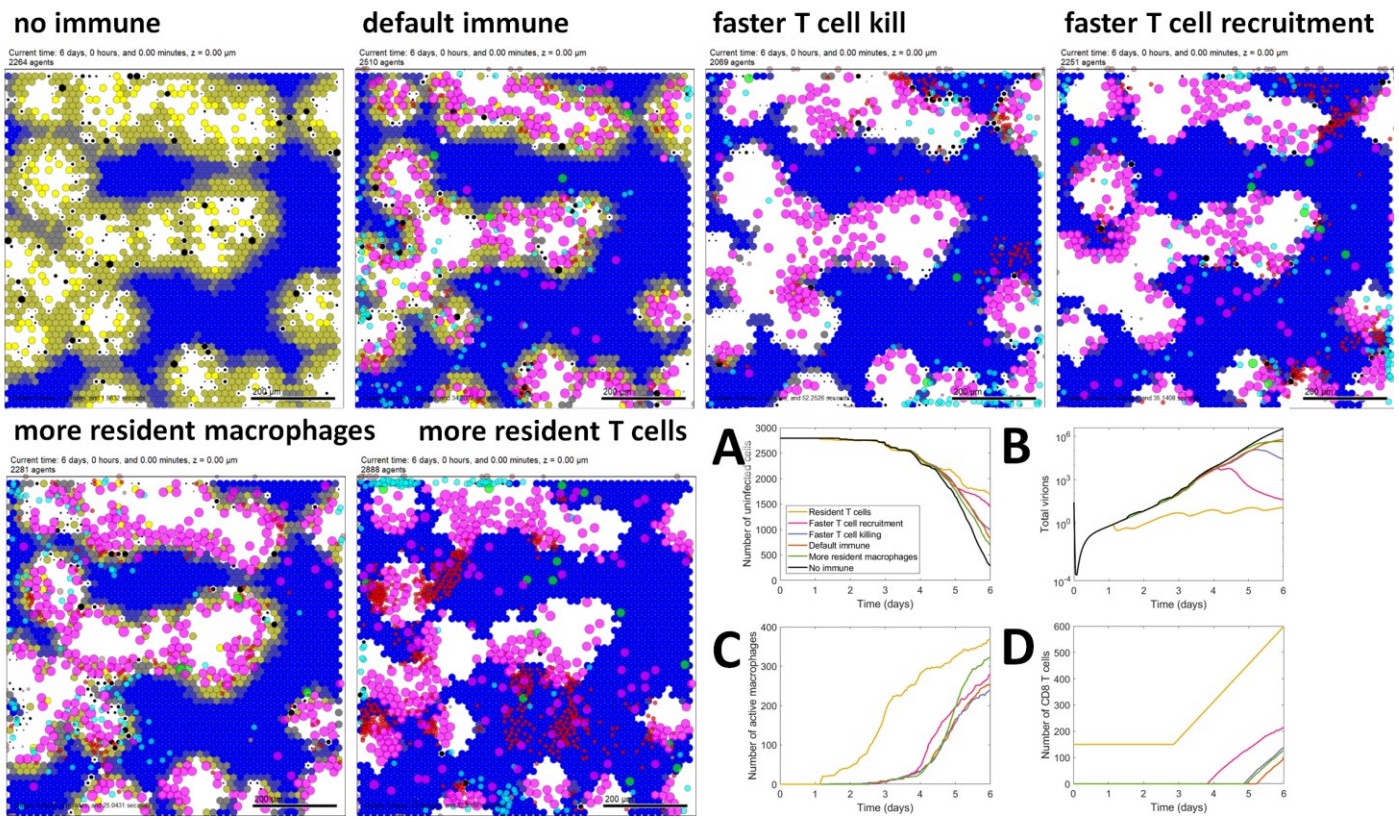

Fig. 3.5: Comparison of version 3 model runs. We show late simulation times with MOI = 0.01 with the default immune parameters (**top row**), increased resident macrophages (**middle row**), and addition of resident T cells (**bottom row**). **A, D, and G** plot immune cell dynamics, **B, E, and H** plot infected cell and virion dynamics, and **C, F, and I** plot changes in signaling factors for each simulated scenario. Increasing the resident macrophage population did not appreciably inhibit the infection, while introducing resident T cells reduced viral titers and better controlled the infection. Cells are colored as in Fig. 3.2.

or antibodies (which could directly neutralize the released virions) could potentially completely control the infection in future versions of the model.

Further comparison of v3 model results

When we compare these simulations side by side (**Fig. 3.5**) we can see that the two scenarios with the best outcomes are those in which the recruitment rate of T cells is increased and when resident T cells are included. These resulted in the largest amount of surviving uninfected tissue (**Fig. 3.5 A**) as well as viral clearance (**Fig. 3.5 B**). It is interesting to note that the increase in recruitment resulted in T cells arriving in the tissue only one day earlier than the default scenario (**Fig. 3.5 D**), but this had a dramatic effect. Under these conditions, the virus expanded but was cleared within 6 days of infection. This model provides a mechanism to explore how $CD8^+$ T cell recruitment could be enhanced in COVID-19 patients. While the presence of resident T cells prevented the viral infection from propagating there was still a significant amount of tissue loss in the current model.

Discussion of v3 model results

The inclusion of the basic tissue immune system to the model has provided some interesting new avenues for research. It is important to note some of the caveats with the existing model. In order to be able to reliably see the beneficial effect of the immune response we had to reduce the viral MOI tenfold. This was because at the higher MOI, either the virus killed the tissue in the absence of the immune response, whereas when the immune response was present it was the immune response that destroyed the tissue (although in this model, the immune cells only destroyed infected cells and did not damage uninfected cells). It is important to note that the present model does not include the cellular interferon response, which would have the effect of slowing viral replication and making more cells resistant to viral infection. When this aspect is included, it is possible that the MOI will not need to be reduced to the same degree.

The results of the simulations so far suggest that controlling the recruitment of $CD8^+$ T cells is a critical parameter leading to viral clearance and reduced tissue destruction. Recent single cell RNA sequencing studies of cells from bronchoalveolar lavage fluid from COVID-19 patients have demonstrated that individuals with moderate disease have increased numbers of $CD8^+$ T cells infiltrating the lungs compared to those with severe disease[169]. This suggests that aspects of the model that can influence this parameter should be explored further. This could include the addition of a more detailed lymph node model in which the kinetics of activation and proliferation of specific $CD8^+$ T cells can be explored.

The presence of resident $CD8^+$ T cells prior to infection effectively prevented viral replication, although at the cost of some tissue damage. It is known that resident memory $CD8^+$ T cells in the lung can provide protection from subsequent infection[170]. It is possible that certain individuals infected with SARS-CoV-2 have been exposed to related coronaviruses and recent studies have observed that up to 40% of unexposed individuals have detectable T cell responses to SARS-CoV-2 proteins[171,172]. Moreover, presence of $CD8^+$ T cells is plausible in uninfected tissues that are adjacent to infected tissues: an initial infection may resemble the default scenario of extensive damage, but the recruited $CD8^+$ T cells could provide protection to nearby tissues from such damage. In the present simulations, it was assumed that all of the resident $CD8^+$ T cells could recognize SARS-CoV-2, but, in reality, only a small fraction of these T cells would be specific for the virus. This can be explored in future simulations.

The fact that increasing the macrophage number did not affect the outcome could reflect the fact that in the present model, these cells have no role in removing infected cells and only remove cells once they have died. Thus, they do not influence the infection beyond secreting inflammatory cytokines that are necessary for the recruitment of $CD8^+$ T cells and neutrophils to the tissue. In subsequent model versions it may be possible to add an interaction between macrophages that have taken up virus and/or dead infected cells with $CD8^+$ T cells. This interaction could further activate macrophages and allow them to kill infected cells before they die.

Selected feedback from domain experts within the coalition and the community

During the extensive v3 model development cycle, the modeling coalition met weekly to discuss and refine the model assumptions and record feedback for future work. Several members presented results at virtual seminars

and virtual conferences; feedback from audience questions and interactions are also reflected here.

Several members noted that because the ACE2 and viral replication dynamics models use ODEs, it is possible that a cell in a low extracellular viral concentration could endocytose less than one full virion. These cells (with < 1 endocytosed virion) can still synthesize viral proteins and assemble virions in the current ODE model, leading to artificially fast viral propagation in the tissue. Future model versions must compensate for this by only allowing integer numbers of virions to uncoat and replicate. Moreover, for a coated virus such as SARS-CoV-2, we must ensure that only live cells release assembled virions; this is the default model setting in v3 (lysed cells release 0% of their assembled virions by default settings).

It was also widely noted the antiviral effects of interferons should be incorporated to more accurately model the rate of spread of an infection. This is of critical importance in light of recent news reports that interferon beta treatment is emerging as a treatment option[173,174]. Within infected cells, further feedbacks (e.g., on endocytosis) may be needed to prevent further re-infection of those cells. We may also need to model heterogeneity in cells' susceptibility to infection and cytokine production. Cytokine production by infected cells may or may not vary with the amount of virus in those cells.

While the initial immune model in v3 was able to address open questions on the effect of T cells, further work is needed, including explicit cross-talk and feedback between pro- and anti-inflammatory cytokines. Future models should include more neutrophil behaviors, including their own secretion of pro-inflammatory cytokines.

Future immune models should also include activation of antigen-presenting cells (APCs) and T helper cells. Macrophages that have taken up dead infected cells should present antigens to $CD4^+$ and $CD8^+$ T cells. Interactions of macrophages with $CD4^+$ T cells should render them capable of killing infected cells, particularly those with antibodies bound to their surface.

While lymphopenia is a topic of significant clinical interest[175,176], there is currently no mechanism for it in the model. This could be addressed by linking T cell death to the level of inflammatory cytokines, since the degree of lymphopenia has been correlated with levels of IL-6, IL-10 and TNF-α[175]. Also, the current model only captures a "cytokine storm" in the sense that as more macrophages are recruited, they also secrete pro-inflammatory cytokines, leading to an accelerated accumulation of cytokines as macrophages accumulate. Future models will need to address this more mechanistically.

In terms of the model development process, we found that there may need to be more flexibility in the length of each development cycle. The transition from Phase 1 to Phase 2 of the project requires substantial training of new developers and creation of software infrastructure. The two-to-three week development cycle noted above is more appropriate to late Phase 2 when all this infrastructure is in place and model changes are more minor from one version to the next.

Core team discussions and priorities for v4

In the next development cycle, we plan to introduce type I IFN secretion and its antiviral effects in nearby uninfected cells, particularly reduced receptor endocytosis and viral replication. This will allow us to investigate recent reports on interferon beta

We also plan to introduce a refined, expert-driven model of viral replication to avoid the model artifacts discussed above and to ensure that cells can only replicate virus if they are infected by at least one *whole* virion, that they can only replicate viral proteins if they have at least one full set of viral RNA coated, and they can only assemble virions if they have at least one set of replicated viral proteins. Adding discrete / integer checks on these behaviors may introduce delays analogous to delay differential equations that improve model realism.

We plan to continue refining the immune response submodel as addressed above, with a focus on improving pro- and anti-inflammatory responses and adding missing immune cell types. We plan to link this with a new lymph node model that will more mechanistically regulate T cell expansion, "education" and recruitment.

Discussion

Within three weeks of the World Health Organization's declaration of a global pandemic of COVID-19[177], community-based prototyping built upon an existing PhysiCell 3D cell-modeling framework to rapidly develop Version 1 of an intracellular and tissue-level model of SARS-CoV-2[109]. A growing coalition of domain experts from across STEM fields are working together to ensure accuracy and utility of this agent-based model of intracellular, extracellular, and multicellular SARS-CoV-2 infection dynamics. Version 1 development underscored the necessity of clearly explaining model components, defining scope, and communicating progress as it occurs for invaluable real-time feedback from collaborators and the broader community. This rapid prototyping already helped in growing the coalition and recruiting complementary expertise; for instance, a team modeling lymph node dynamics and immune infiltration joined during the Version 1 cycle after seeing initial progress.

The version 1 prototype also showed the scientific benefit of rapid prototyping: even a basic coupling between extracellular virion transport, intracellular replication dynamics, and viral response (apoptosis) showed the direct relationship between the extracellular virion transport rate and the spread of infection in a tissue. More importantly, it showed that for viruses that rapidly create and exocytose new virions, release of additional assembled virions at the time of cell death does not significantly speed the spread of infection. Moreover, decreasing the cell tolerance to viral load does not drastically change the rate at which the infection spreads, but it does accelerate the rate of tissue damage and loss, which could potentially trigger edema and ARDS earlier. This suggests that working to slow apoptosis may help preserve tissue integrity and delay adverse severe respiratory responses. That such a simple model could already point to actionable hypotheses for experimental and clinical investigations points to the value of rapid model iteration and investigation, rather than waiting for a "perfect" model that incorporates all processes with mechanistic molecular-scale detail.

Version 2 showed promise of increasing mechanistic details to evaluate potential inhibitors. For example, it was found that that reducing the expression of ACE2 receptors could paradoxically lead to faster spread of the infection across the tissue, although the individual infected cells would replicate virus more slowly. On the other hand, taking advantage of high receptor expression but interfering with viral release from internalized receptors may help slow infectious dynamics. Generally, adding sufficient actionable cell mechanisms to the model framework allows us to ask pharmacologically-driven questions on potential pharmacologic interventions, and how these findings are affected by heterogeneity, stochasticity, and the multiscale interactions in the simulated tissue.

Version 3 allowed our first investigations of immune system responses. We found that T cell behaviors are critical to controlling the spread of an infection through the tissue. In particular, rapid recruitment as well as the presence of "educated" $CD8^+$ T cells prior to infection (e.g., after responding to infection in a nearby tissue) had a significant protective effect, even in the current model that does not explicitly model antibodies. This is consistent with emerging studies that link T cell responses to patients with the best recovery[169,171,172].

As work on future versions progresses, teams will work in parallel on submodels to add, parameterize, and test new model components. It will be important to balance the need for new functionality with the requirement for constrained scope, while also balancing the importance of model validation with timely dissemination of results. Thus, this preprint will be updated with every development cycle to invite feedback and community contributions. Between cycles, the most up-to-date information about this model can be found at http://COVID-19.physicell.org.

Getting involved

To get involved, we welcome biological expertise, especially related to model assumptions, hypotheses, infection dynamics, and interpretation of results. Mathematical contributions to the underlying model or model analysis and data contributions for crafting, parameterizing, and validating model predictions are particularly sought.

We encourage the community to test the web-hosted hosted model at https://nanohub.org/tools/pc4COVID-19. This model will be frequently updated to reflect progress, allowing the public to take advantage of this rapid prototyping effort.

We avidly encourage the community to test the model, offer feedback, and join our growing coalition via Google survey (https://forms.gle/12vmLR7aiMTHoD5YA), by direct messaging Paul Macklin on Twitter (@MathCancer),

or by joining the pc4COVID-19 Slack workspace (invitation link). Updates will frequently be disseminated on social media by Paul Macklin (@MathCancer), the PhysiCell project (@PhysiCell), the Society for Mathematical Biology subgroup for Immunobiology and Infection Subgroup (@smb_imin), and others.

We also encourage developers to watch the pc4COVID-19 GitHub organization and to contribute bug reports and software patches to the corresponding (sub)model repositories. See https://github.com/pc4COVID-19

We are encouraged by the fast recognition of the computational and infectious disease communities that we can make rapid progress against COVID-19 if we pool our expertise and resources. Together, we can make a difference in understanding viral dynamics and suggesting treatment strategies to slow infection, improve immune response, and minimize or prevent adverse immune responses. We note that this work will not only help us address SARS-CoV-2 but will also provide a framework for readiness for future emerging pathogens.

Acknowledgements

PM thanks the Jayne Koskinas Ted Giovanis Foundation for Health and Policy for generous support. PM, RH, and YW thank the National Institutes of Health (U01-CA232137-01) for support. PM, RH, JAG, YW, and JFG thank the National Science Foundation for funding and resources via the nanoBIO Node for nanoHUB (1720625). AS thanks the NIH for support from the NIAID (R01 AI139088). MC and AJ were supported under NSERC Discovery Grant RGPIN-2018-04546. ANFV acknowledges support from the NIH (R35-GM133763). We thank the NCN CP for fast-tracked deployment of models on nanoHUB.

We thank the scientific community for model feedback, including Simon Parkinson, Richard Allen (Pfizer Inc.), David Dai (Pfizer Inc.), Rohit Rao (Pfizer Inc.), and the co-authors of this manuscript. We thank Furkan Kurtoglu (Indiana University) for contributions to SBML integration efforts and other multiscale design aspects. We thank Mark Chaplain for his assistance in coordinating with the UK Royal Society's RAMP Initiative.

All the authors dedicate this work in memory of Bing Liu, our co-author, colleague, and friend. His insights and community-minded contributions are sorely missed.

Appendices

Appendix 1: Code availability

All code is being made available as open source under the standard 3-Clause BSD license. Users should cite this preprint (or the final published paper, as the case may be).

Core model releases

Version 1 model

Version 0.1.0 (released March 26, 2020)

GitHub: https://github.com/pc4COVID-19/COVID-19/releases/tag/0.1.0
Notes: First release.

Version 0.1.1 (released March 26, 2020)

GitHub: https://github.com/pc4COVID-19/COVID-19/tree/0.1.1
Notes: Minor bugfixes and first inclusion of “math” directory.

Version 0.1.2 (released March 26, 2020)

GitHub: https://github.com/pc4COVID-19/COVID-19/releases/tag/0.1.2
Zenodo: https://doi.org/10.5281/zenodo.3733336
Notes: First release with Zenodo integration. Last release in 0.1.x chain (v1 model chain).

Version 0.1.3 (released April 1, 2020)

GitHub: https://github.com/pc4COVID-19/COVID-19/tree/0.1.3
Zenodo: https://doi.org/10.5281/zenodo.3737166
Notes: First release after transferring the COVID-19 tissue-level model (overall model) from Paul Macklin's personal GitHub account to the new pc4COVID-19 GitHub organization.

Version 2 model

Version 0.2.0 (released April 9, 2020)

GitHub: https://github.com/pc4COVID-19/COVID-19/tree/0.2.0
Zenodo: https://doi.org/10.5281/zenodo.3747011
Notes: First v2 prototype. Introduced modular design and ACE2 receptor trafficking

Version 0.2.1 (released April 10, 2020)

GitHub: https://github.com/pc4COVID-19/COVID-19/tree/0.2.1
Zenodo: https://doi.org/10.5281/zenodo.3747011
Notes: Minor bugfixes for cell visualization.

Version 3 model

Version 0.3.0 (released July 3, 2020)

GitHub: https://github.com/pc4COVID-19/COVID-19/tree/0.3.0
Zenodo: http://doi.org/10.5281/zenodo.3929320
Notes: First v3 prototype. First integration of new immune submodel. Upgrade to PhysiCell Version 1.7.1, allowing use of XML-based cell definitions to define the behavior of immune cell types. Upgrade to PhysiCell Version 1.7.2 beta to improve multithreaded performance, add new cell-cell interaction features, and fix concurrency issues on some platforms.

Version 0.3.1 (released July 3, 2020)

GitHub: https://github.com/pc4COVID-19/COVID-19/tree/0.3.1
Zenodo: http://doi.org/10.5281/zenodo.3929726
Notes: This release improves parameter estimates for digestion of phagocytosed material and has an immune model refinement to prevent runaway macrophage death.

Version 0.3.2 (released July 15, 2020)

GitHub: https://github.com/pc4COVID-19/COVID-19/tree/0.3.2
Zenodo: https://dx.doi.org/10.5281/zenodo.3946820
Notes: This release simplifies the macrophage rules.

nanoHUB cloud-hosted model releases

The latest version can always be accessed directly at https://nanohub.org/tools/pc4COVID-19

Version 1 model

Version 1.0 (released March 26, 2020):

GitHub: https://github.com/rheiland/pc4COVID-19/releases/tag/v1.0

Zenodo: http://doi.org/10.5281/zenodo.3733276
nanoHUB DOI: http://dx.doi.org/doi:10.21981/19BB-HM69
Notes: First published version.

Version 2 model

Version 2.1 (released April 14, 2020):

GitHub: https://github.com/pc4COVID-19/pc4COVID-19/releases/tag/v2.1
Zenodo: http://doi.org/10.5281/zenodo.3766879
nanoHUB DOI: http://dx.doi.org/doi:10.21981/2B1H-GX51
Notes: Second published version. Moved GitHub repository to the pc4COVID-19 GitHub organization. Added another tab in the GUI for generating animation of cells (from SVG output files).

Version 3 model

Version 3.0 (released July 3, 2020):

GitHub: https://github.com/pc4COVID-19/pc4COVID-19/tree/v3.0
Zenodo: http://doi.org/10.5281/zenodo.392953 9
nanoHUB DOI: http://dx.doi.org/doi:10.21981/V52J-0S03
Notes: The major change to the GUI in this release is the addition of a “Cell Types” tab. This allows editing parameters associated with <cell_definitions> in the configuration file. This version also includes a <style> block in the Jupyter notebook that fixed an unwanted scrollbar in the lengthy About tab.

Version 3.1 (released July 3, 2020):

GitHub: https://github.com/pc4COVID-19/pc4COVID-19/tree/v3.1
Zenodo: http://doi.org/10.5281/zenodo.3929960
nanoHUB DOI: http://dx.doi.org/doi:10.21981/YNWZ-GE50
Notes: Minor updates to “About” text, e.g., explaining nature of stochastic results. Edits to immune_submodels.cpp (see details in the core model repository).

Version 3.2 (released July 21, 2020):

GitHub: https://github.com/pc4COVID-19/pc4COVID-19/tree/v3.2
Zenodo: http://doi.org/10.5281/zenodo.3954019
nanoHUB DOI: http://dx.doi.org/doi:10.21981/843E-JE78
Notes: Update to use core model 0.3.2

Appendix 2: Organoid platform details

Aarthi Narayanan’s virology lab is optimizing SARS-CoV-2 cultures in organoid model systems. The viral replication kinetics will be assessed by infection of different lung epithelial, fibroblast and endothelial cells, in addition to standard cell lines such as Vero cells, which are one of the cell lines in use for inhibitor assessment studies. Primary cells and/or cell lines will be infected with SARS-CoV-2 at increasing multiplicities of infection (MOI) and infectious viral titers in the supernatants assessed by plaque assays at multiple time points post infection (pi). This will stretch from ~3 hours post infection (phi) to 48 hpi depending on the cell type and the MOI.

In parallel, the viral genomic copy numbers will be assessed in the same supernatant samples by qRT-PCR with virus specific primers. This will provide information on how the production of infectious virions compares with the number of genomic copies available outside the cell. If the numbers are skewed in the direction of genomic copies (which may happen in the context of some kinds of inhibitors), it will shed light on the mechanisms of inhibition involving inhibition of infectivity of progeny virions.

The viral genomic copy numbers inside the cells will also be assessed by qRT-PCR and compared to the genomic copies outside the cell. This will provide direction on the efficacy of particle packaging and the extent of

production of infectious versus noninfectious virus. While it will not provide directly pertinent information about the possibility of heterogeneity of released virus populations and quasispecies, it can provide initial clues in that direction, which can then trigger more specific questions and relevant approaches. These approaches will be pursued for cell lines, primary cells and, hopefully, subsequently transitioned to organoid platforms.

From a host response point of view, we will pursue two aspects: host cell death and inflammatory responses. For cell survival and death measurements, we will employ an assay that measures ATP activity in cells (hence a reflection of a live cell) in the context of infection and inhibitor treatments. For inflammatory responses, we will assess supernatants for inflammatory mediators by ELISA (multiplexed). The cells will be lysed to obtain RNA, which will be queried for transcription of several genes associated with inflammatory responses using gene expression arrays (multiplexed).

Additional host response events will include mitochondrial activity and ROS production assessments in the context of infection and inhibitor treatments. The impact of anti-inflammatory strategies on mitochondrial activity and cell survival will be assessed to determine correlations between viral replication dependent and independent events.

Appendix 3: Overall design cycle development details

In each prototyping or design cycle:

1. The core team sets priorities for the design iteration:
    a. Discuss feedback and identify highest priority model refinements.
    b. Collaborate to update the submodel design documents to address feedback.
    c. Update the overall model design document as needed.
    d. Assess new data to refine parameter estimates.
    e. Refine submodel input/output formats as necessary.
    f. Assess next release dates for the submodels.
2. Submodel teams meet to refine their code and put out their next releases. The chief scientists communicate releases to the overall leads.
3. The integration team integrates the latest submodel releases into a new release candidate for the overall model.
    a. Address any bug reports.
    b. Test new or altered functions.
    c. Satisfy all qualitative and/or quantitative unit tests.
    d. Qualitatively test the model for new or improved behaviors over the last iteration.
4. The integration team prepares a software release:
    a. Update documentation.
    b. Create a new numbered release on GitHub.
    c. Update list of available validation data and best parameter estimates.
    d. Create a Zenodo snapshot.
    e. Announce on Twitter (via @PhysiCell, @MathCancer, and @SMB_imin).
5. The integration team updates the cloud-hosted model for multidisciplinary testing:
    a. Update the nanoHUB app repository with new code.
    b. Run xml2jupyter to update the Jupyter interface.
    c. Update project on nanoHUB, test/refine until successful release.
    d. Update documentation, numbered GitHub release, Zenodo snapshot of deployed model.
    e. Perform live demos with domain experts and community to gather feedback.
6. The whole team seeks additional community feedback via Twitter and the pc4COVID-19 Slack workspace. The team integrates comments received from scientific peer review as appropriate.

7. The core team evaluates progress:
    a. Distill feedback to assess the need for new model hypotheses, behaviors, or components.
    b. Assess which biological behaviors are currently exhibited by the model.
    c. Refine the design protocol (e.g., with refined model specification methods) as necessary.
    d. Assess the need for an additional design iteration.
8. Update preprint for scientific dissemination. Return to Step 1 if there is substantial feedback, or if the core team determines that further refinements are within project scope.

Appendix 4: Submodel development details

In each software sprint, each submodel team will

1. Set priorities for the design iteration:
    a. Discuss feedback and identify highest priority model refinements.
    b. Refine model assumptions and hypotheses.
    c. Assess new data to refine parameter estimates.
2. “Translate” biological hypotheses into agent model rules and other mathematical model components:
    a. Run the new hypotheses and rules by domain experts as their time permits.
    b. Define new qualitative and/or quantitative unit tests for new behaviors and functions.
    c. Assign implementation tasks.
3. Perform computational implementation of refined mathematical model (and submodels):
    a. Address any bug reports.
    b. Add or modify functions based on new rules in steps 1-2.
    c. Test new or altered functions.
    d. Satisfy all qualitative and/or quantitative unit tests.
    e. Qualitatively test the model for new or improved behaviors over the last iteration.
4. Create a software release:
    a. Update documentation.
    b. Create a new numbered release on GitHub.
    c. Update list of available validation data and best parameter estimates.
    d. Create a Zenodo snapshot.
    e. Communicate with the core team on the software release.
5. Create a cloud-hosted submodel for multidisciplinary testing:
    a. Update the nanoHUB app repository with new code.
    b. Run xml2jupyter to update the Jupyter interface.
    c. Update project on nanoHUB, test/refine until successful release.
    d. Update documentation, numbered GitHub release, and Zenodo snapshot of deployed model.
    e. Perform live demos with the core team as needed.

While waiting for the start of the next software sprint, each submodel team will

1. Perform model evaluation:
    a. Distill feedback to assess the need for new model hypotheses, behaviors, or components.
    b. Assess which biological behaviors are currently exhibited by the model.
    c. Refine the design protocol (e.g., with refined model specification methods) as necessary.
    d. Assess the need for an additional design iteration.
2. Help update the preprint for scientific dissemination.

In the next software sprint, return to Step 1 if there is substantial feedback, or if the core team determines that further refinements are within project scope.

References

1 Dong, E., Du, H. & Gardner, L. An interactive web-based dashboard to track COVID-19 in real time. *The Lancet Infectious Diseases*, doi:10.1016/s1473-3099(20)30120-1 (2020).

2 Rozenblatt-Rosen, O. *et al.* The Human Tumor Atlas Network: Charting Tumor Transitions across Space and Time at Single-Cell Resolution. *Cell* **181**, 236-249, doi:10.1016/j.cell.2020.03.053 (2020).

3 Zhou, P. *et al.* A pneumonia outbreak associated with a new coronavirus of probable bat origin. *Nature* **579**, 270-273, doi:10.1038/s41586-020-2012-7 (2020).

4 Bouadma, L., Lescure, F.-X., Lucet, J.-C., Yazdanpanah, Y. & Timsit, J.-F. Severe SARS-CoV-2 infections: practical considerations and management strategy for intensivists. *Intensive Care Medicine* **46**, 579-582, doi:10.1007/s00134-020-05967-x (2020).

5 Yang, X. *et al.* Clinical course and outcomes of critically ill patients with SARS-CoV-2 pneumonia in Wuhan, China: a single-centered, retrospective, observational study. *The Lancet Respiratory Medicine*, doi:10.1016/s2213-2600(20)30079-5 (2020).

6 Zhou, F. *et al.* Clinical course and risk factors for mortality of adult inpatients with COVID-19 in Wuhan, China: a retrospective cohort study. *The Lancet* **395**, 1054-1062, doi:10.1016/s0140-6736(20)30566-3 (2020).

7 Zhang, J.-j. *et al.* Clinical characteristics of 140 patients infected with SARS-CoV-2 in Wuhan, China. *Allergy*, doi:10.1111/all.14238 (2020).

8 Liang, W. *et al.* Cancer patients in SARS-CoV-2 infection: a nationwide analysis in China. *The Lancet Oncology* **21**, 335-337, doi:10.1016/s1470-2045(20)30096-6 (2020).

9 Macklin, P. When Seeing Isn't Believing: How Math Can Guide Our Interpretation of Measurements and Experiments. *Cell Systems* **5**, 92-94, doi:10.1016/j.cels.2017.08.005 (2017).

10 Macklin, P. Key challenges facing data-driven multicellular systems biology. *GigaScience* **8**, doi:10.1093/gigascience/giz127 (2019).

11 Wrapp, D. *et al.* Cryo-EM structure of the 2019-nCoV spike in the prefusion conformation. *Science* **367**, 1260-1263, doi:10.1126/science.abb2507 (2020).

12 Hoffmann, M. *et al.* SARS-CoV-2 Cell Entry Depends on ACE2 and TMPRSS2 and Is Blocked by a Clinically Proven Protease Inhibitor. *Cell* **181**, 271-280.e278, doi:10.1016/j.cell.2020.02.052 (2020).

13 Sahin, A. R. 2019 Novel Coronavirus (COVID-19) Outbreak: A Review of the Current Literature. *Eurasian Journal of Medicine and Oncology*, doi:10.14744/ejmo.2020.12220 (2020).

14 White, K. A., Enjuanes, L. & Berkhout, B. RNA virus replication, transcription and recombination. *RNA Biology* **8**, 182-183, doi:10.4161/rna.8.2.15663 (2014).

15 Stark, G. R., Kerr, I. M., Williams, B. R. G., Silverman, R. H. & Schreiber, R. D. How Cells Respond to Interferons. *Annual Review of Biochemistry* **67**, 227-264, doi:10.1146/annurev.biochem.67.1.227 (1998).

16 Perry, A. K., Chen, G., Zheng, D., Tang, H. & Cheng, G. The host type I interferon response to viral and bacterial infections. *Cell Research* **15**, 407-422, doi:10.1038/sj.cr.7290309 (2005).

17 Spiegel, M. *et al.* Inhibition of Beta Interferon Induction by Severe Acute Respiratory Syndrome Coronavirus Suggests a Two-Step Model for Activation of Interferon Regulatory Factor 3. *Journal of Virology* **79**, 2079-2086, doi:10.1128/jvi.79.4.2079-2086.2005 (2005).

18 Hale, B. G., Randall, R. E., Ortín, J. & Jackson, D. The multifunctional NS1 protein of influenza A viruses. *Journal of General Virology* **89**, 2359-2376, doi:10.1099/vir.0.2008/004606-0 (2008).

19 Danthi, P. Viruses and the Diversity of Cell Death. *Annual Review of Virology* **3**, 533-553, doi:10.1146/annurev-virology-110615-042435 (2016).

20 Yue, Y. *et al.* SARS-Coronavirus Open Reading Frame-3a drives multimodal necrotic cell death. *Cell Death & Disease* **9**, doi:10.1038/s41419-018-0917-y (2018).

21 Keck, F. *et al.* Altered mitochondrial dynamics as a consequence of Venezuelan Equine encephalitis virus infection. *Virulence* **8**, 1849-1866, doi:10.1080/21505594.2016.1276690 (2017).

22 Keck, F. *et al.* Mitochondrial-Directed Antioxidant Reduces Microglial-Induced Inflammation in Murine In Vitro Model of TC-83 Infection. *Viruses* **10**, doi:10.3390/v10110606 (2018).

23 Thiel, V. *et al.* Lack of Innate Interferon Responses during SARS Coronavirus Infection in a Vaccination and Reinfection Ferret Model. *PLoS ONE* **7**, e45842, doi:10.1371/journal.pone.0045842 (2012).

24 Widagdo, W., Okba, N. M. A., Stalin Raj, V. & Haagmans, B. L. MERS-coronavirus: From discovery to intervention. *One Health* **3**, 11-16, doi:10.1016/j.onehlt.2016.12.001 (2017).
25 Channappanavar, R. *et al.* Dysregulated Type I Interferon and Inflammatory Monocyte-Macrophage Responses Cause Lethal Pneumonia in SARS-CoV-Infected Mice. *Cell Host & Microbe* **19**, 181-193, doi:10.1016/j.chom.2016.01.007 (2016).
26 Channappanavar, R. *et al.* IFN-I response timing relative to virus replication determines MERS coronavirus infection outcomes. *Journal of Clinical Investigation* **129**, 3625-3639, doi:10.1172/jci126363 (2019).
27 Al-Hazmi, A. Challenges presented by MERS corona virus, and SARS corona virus to global health. *Saudi Journal of Biological Sciences* **23**, 507-511, doi:10.1016/j.sjbs.2016.02.019 (2016).
28 Yuen, K.-Y. *et al.* Comparative replication and immune activation profiles of SARS-CoV-2 and SARS-CoV in human lungs: an ex vivo study with implications for the pathogenesis of COVID-19. *Clinical Infectious Diseases*, doi:10.1093/cid/ciaa410 (2020).
29 Qin, C. *et al.* Dysregulation of Immune Response in Patients with COVID-19 in Wuhan, China. *SSRN Electronic Journal*, doi:10.2139/ssrn.3541136 (2020).
30 Jamilloux, Y. *et al.* Should we stimulate or suppress immune responses in COVID-19? Cytokine and anti-cytokine interventions. *Autoimmunity Reviews* **19**, 102567, doi:10.1016/j.autrev.2020.102567 (2020).
31 Prompetchara, E., Ketloy, C. & Palaga, T. Immune responses in COVID-19 and potential vaccines: Lessons learned from SARS and MERS epidemic. *Asian Pacific Journal of Allergy and Immunology*, doi:10.12932/ap-200220-0772 (2020).
32 Channappanavar, R. & Perlman, S. Pathogenic human coronavirus infections: causes and consequences of cytokine storm and immunopathology. *Seminars in Immunopathology* **39**, 529-539, doi:10.1007/s00281-017-0629-x (2017).
33 Nahrendorf, M., Pittet, M. J. & Swirski, F. K. Monocytes: Protagonists of Infarct Inflammation and Repair After Myocardial Infarction. *Circulation* **121**, 2437-2445, doi:10.1161/circulationaha.109.916346 (2010).
34 Fung, S.-Y., Yuen, K.-S., Ye, Z.-W., Chan, C.-P. & Jin, D.-Y. A tug-of-war between severe acute respiratory syndrome coronavirus 2 and host antiviral defence: lessons from other pathogenic viruses. *Emerging Microbes & Infections* **9**, 558-570, doi:10.1080/22221751.2020.1736644 (2020).
35 Siu, K. L. *et al.* Severe acute respiratory syndrome Coronavirus ORF3a protein activates the NLRP3 inflammasome by promoting TRAF3-dependent ubiquitination of ASC. *The FASEB Journal* **33**, 8865-8877, doi:10.1096/fj.201802418R (2019).
36 Chen, I. Y., Moriyama, M., Chang, M.-F. & Ichinohe, T. Severe Acute Respiratory Syndrome Coronavirus Viroporin 3a Activates the NLRP3 Inflammasome. *Frontiers in Microbiology* **10**, doi:10.3389/fmicb.2019.00050 (2019).
37 Camp, J. V. & Jonsson, C. B. A Role for Neutrophils in Viral Respiratory Disease. *Frontiers in Immunology* **8**, doi:10.3389/fimmu.2017.00550 (2017).
38 Weitnauer, M., Mijošek, V. & Dalpke, A. H. Control of local immunity by airway epithelial cells. *Mucosal Immunology* **9**, 287-298, doi:10.1038/mi.2015.126 (2015).
39 Crane, M. J., Lee, K. M., FitzGerald, E. S. & Jamieson, A. M. Surviving Deadly Lung Infections: Innate Host Tolerance Mechanisms in the Pulmonary System. *Frontiers in Immunology* **9**, doi:10.3389/fimmu.2018.01421 (2018).
40 Teijaro, John R. *et al.* Endothelial Cells Are Central Orchestrators of Cytokine Amplification during Influenza Virus Infection. *Cell* **146**, 980-991, doi:10.1016/j.cell.2011.08.015 (2011).
41 Liu, J. *et al.*, doi:10.1101/2020.02.16.20023671 (2020).
42 Liu, J. *et al.*, doi:10.1101/2020.02.10.20021584 (2020).
43 Shokri, S., Mahmoudvand, S., Taherkhani, R. & Farshadpour, F. Modulation of the immune response by Middle East respiratory syndrome coronavirus. *Journal of Cellular Physiology* **234**, 2143-2151, doi:10.1002/jcp.27155 (2018).
44 Kong, W. p. *et al.* Modulation of the Immune Response to the Severe Acute Respiratory Syndrome Spike Glycoprotein by Gene-Based and Inactivated Virus Immunization. *Journal of Virology* **79**, 13915-13923, doi:10.1128/jvi.79.22.13915-13923.2005 (2005).
45 Cruz, J. L. G. *et al.* Alphacoronavirus Protein 7 Modulates Host Innate Immune Response. *Journal of Virology* **87**, 9754-9767, doi:10.1128/jvi.01032-13 (2013).

46 Liu, L. *et al.* Anti–spike IgG causes severe acute lung injury by skewing macrophage responses during acute SARS-CoV infection. *JCI Insight* **4**, doi:10.1172/jci.insight.123158 (2019).
47 Leong, A. S. Y. *et al.* Multiple organ infection and the pathogenesis of SARS. *Journal of Experimental Medicine* **202**, 415-424, doi:10.1084/jem.20050828 (2005).
48 Yang, P. *et al.* Angiotensin-converting enzyme 2 (ACE2) mediates influenza H7N9 virus-induced acute lung injury. *Scientific Reports* **4**, doi:10.1038/srep07027 (2014).
49 Kuba, K. *et al.* A crucial role of angiotensin converting enzyme 2 (ACE2) in SARS coronavirus–induced lung injury. *Nature Medicine* **11**, 875-879, doi:10.1038/nm1267 (2005).
50 Madjid, M., Safavi-Naeini, P., Solomon, S. D. & Vardeny, O. Potential Effects of Coronaviruses on the Cardiovascular System: A Review. *JAMA Cardiol*, doi:10.1001/jamacardio.2020.1286 (2020).
51 Wadman, M., Couzin-Frankel, J., Kaiser, J. & Matacic, C. A rampage through the body. *Science* **368**, 356-360, doi:10.1126/science.368.6489.356 (2020).
52 Stebbing, J. *et al.* COVID-19: combining antiviral and anti-inflammatory treatments. *The Lancet Infectious Diseases* **20**, 400-402, doi:10.1016/s1473-3099(20)30132-8 (2020).
53 Herold, T. *et al.*, doi:10.1101/2020.04.01.20047381 (2020).
54 Zhang, C., Wu, Z., Li, J.-W., Zhao, H. & Wang, G.-Q. The cytokine release syndrome (CRS) of severe COVID-19 and Interleukin-6 receptor (IL-6R) antagonist Tocilizumab may be the key to reduce the mortality. *International Journal of Antimicrobial Agents*, 105954, doi:10.1016/j.ijantimicag.2020.105954 (2020).
55 Schett, G., Sticherling, M. & Neurath, M. F. COVID-19: risk for cytokine targeting in chronic inflammatory diseases? *Nature Reviews Immunology*, doi:10.1038/s41577-020-0312-7 (2020).
56 Sanders, C. J. *et al.* Compromised respiratory function in lethal influenza infection is characterized by the depletion of type I alveolar epithelial cells beyond threshold levels. *American Journal of Physiology-Lung Cellular and Molecular Physiology* **304**, L481-L488, doi:10.1152/ajplung.00343.2012 (2013).
57 Allen, R. J., Rieger, T. R. & Musante, C. J. Efficient Generation and Selection of Virtual Populations in Quantitative Systems Pharmacology Models. *CPT: Pharmacometrics & Systems Pharmacology* **5**, 140-146, doi:10.1002/psp4.12063 (2016).
58 Cassidy, T. & Craig, M. Determinants of combination GM-CSF immunotherapy and oncolytic virotherapy success identified through in silico treatment personalization. *PLOS Computational Biology* **15**, doi:10.1371/journal.pcbi.1007495 (2019).
59 Nowak, M. *et al.* Antigenic diversity thresholds and the development of AIDS. *Science* **254**, 963-969, doi:10.1126/science.1683006 (1991).
60 Wei, X. *et al.* Viral dynamics in human immunodeficiency virus type 1 infection. *Nature* **373**, 117-122, doi:10.1038/373117a0 (1995).
61 Rosenbloom, D. I. S., Hill, A. L., Laskey, S. B. & Siliciano, R. F. Re-evaluating evolution in the HIV reservoir. *Nature* **551**, E6-E9, doi:10.1038/nature24634 (2017).
62 Reeves, D. B. *et al.* A majority of HIV persistence during antiretroviral therapy is due to infected cell proliferation. *Nature Communications* **9**, doi:10.1038/s41467-018-06843-5 (2018).
63 Koelle, K., Farrell, A. P., Brooke, C. B. & Ke, R. Within-host infectious disease models accommodating cellular coinfection, with an application to influenza†. *Virus Evolution* **5**, doi:10.1093/ve/vez018 (2019).
64 Perelson, A. S., Neumann, A. U., Markowitz, M., Leonard, J. M. & Ho, D. D. HIV-1 Dynamics in Vivo: Virion Clearance Rate, Infected Cell Life-Span, and Viral Generation Time. *Science* **271**, 1582-1586, doi:10.1126/science.271.5255.1582 (1996).
65 Smith, A. M. & Ribeiro, R. M. Modeling the Viral Dynamics of Influenza A Virus Infection. *Critical Reviews™ in Immunology* **30**, 291-298, doi:10.1615/CritRevImmunol.v30.i3.60 (2010).
66 Smith, A. M. & Perelson, A. S. Influenza A virus infection kinetics: quantitative data and models. *Wiley Interdisciplinary Reviews: Systems Biology and Medicine* **3**, 429-445, doi:10.1002/wsbm.129 (2011).
67 Smith, A. M., McCullers, J. A. & Adler, F. R. Mathematical model of a three-stage innate immune response to a pneumococcal lung infection. *Journal of Theoretical Biology* **276**, 106-116, doi:10.1016/j.jtbi.2011.01.052 (2011).
68 Bonhoeffer, S., May, R. M., Shaw, G. M. & Nowak, M. A. Virus dynamics and drug therapy. *Proceedings of the National Academy of Sciences* **94**, 6971-6976, doi:10.1073/pnas.94.13.6971 (1997).

69 Hill, A. L., Rosenbloom, D. I. S., Fu, F., Nowak, M. A. & Siliciano, R. F. Predicting the outcomes of treatment to eradicate the latent reservoir for HIV-1. *Proceedings of the National Academy of Sciences* **111**, 13475-13480, doi:10.1073/pnas.1406663111 (2014).

70 Rosenbloom, D. I. S., Hill, A. L., Rabi, S. A., Siliciano, R. F. & Nowak, M. A. Antiretroviral dynamics determines HIV evolution and predicts therapy outcome. *Nature Medicine* **18**, 1378-1385, doi:10.1038/nm.2892 (2012).

71 Mueller, S. N. *et al.* Mathematical Modeling Predicts that Increased HSV-2 Shedding in HIV-1 Infected Persons Is Due to Poor Immunologic Control in Ganglia and Genital Mucosa. *Plos One* **11**, e0155124, doi:10.1371/journal.pone.0155124 (2016).

72 Perelson, A. S. *et al.* Decay characteristics of HIV-1-infected compartments during combination therapy. *Nature* **387**, 188-191, doi:10.1038/387188a0 (1997).

73 Kirtane, A. R. *et al.* Development of an oral once-weekly drug delivery system for HIV antiretroviral therapy. *Nature Communications* **9**, doi:10.1038/s41467-017-02294-6 (2018).

74 Schiffer, J. T. & Gottlieb, S. L. Biologic interactions between HSV-2 and HIV-1 and possible implications for HSV vaccine development. *Vaccine* **37**, 7363-7371, doi:10.1016/j.vaccine.2017.09.044 (2019).

75 Schiffer, J. T. *et al.* Mathematical modeling of herpes simplex virus-2 suppression with pritelivir predicts trial outcomes. *Science Translational Medicine* **8**, 324ra315-324ra315, doi:10.1126/scitranslmed.aad6654 (2016).

76 Perelson, A. S. Modelling viral and immune system dynamics. *Nature Reviews Immunology* **2**, 28-36, doi:10.1038/nri700 (2002).

77 Hill, A. L., Rosenbloom, D. I. S., Nowak, M. A. & Siliciano, R. F. Insight into treatment of HIV infection from viral dynamics models. *Immunological Reviews* **285**, 9-25, doi:10.1111/imr.12698 (2018).

78 Wang, Y., Zhou, Y., Brauer, F. & Heffernan, J. M. Viral dynamics model with CTL immune response incorporating antiretroviral therapy. *Journal of Mathematical Biology* **67**, 901-934, doi:10.1007/s00285-012-0580-3 (2012).

79 Schiffer, J. T. & Corey, L. Rapid host immune response and viral dynamics in herpes simplex virus-2 infection. *Nature Medicine* **19**, 280-288, doi:10.1038/nm.3103 (2013).

80 Jenner, A. L., Yun, C.-O., Kim, P. S. & Coster, A. C. F. Mathematical Modelling of the Interaction Between Cancer Cells and an Oncolytic Virus: Insights into the Effects of Treatment Protocols. *Bulletin of Mathematical Biology* **80**, 1615-1629, doi:10.1007/s11538-018-0424-4 (2018).

81 Möhler, L., Flockerzi, D., Sann, H. & Reichl, U. Mathematical model of influenza A virus production in large-scale microcarrier culture. *Biotechnology and Bioengineering* **90**, 46-58, doi:10.1002/bit.20363 (2005).

82 Schulze-Horsel, J., Schulze, M., Agalaridis, G., Genzel, Y. & Reichl, U. Infection dynamics and virus-induced apoptosis in cell culture-based influenza vaccine production—Flow cytometry and mathematical modeling. *Vaccine* **27**, 2712-2722, doi:10.1016/j.vaccine.2009.02.027 (2009).

83 Banks, H. T., Bortz, D. M. & Holte, S. E. Incorporation of variability into the modeling of viral delays in HIV infection dynamics. *Mathematical Biosciences* **183**, 63-91, doi:10.1016/s0025-5564(02)00218-3 (2003).

84 Culshaw, R. V., Ruan, S. & Webb, G. A mathematical model of cell-to-cell spread of HIV-1 that includes a time delay. *Journal of Mathematical Biology* **46**, 425-444, doi:10.1007/s00285-002-0191-5 (2003).

85 Li, M. Y. & Shu, H. Impact of Intracellular Delays and Target-Cell Dynamics on In Vivo Viral Infections. *SIAM Journal on Applied Mathematics* **70**, 2434-2448, doi:10.1137/090779322 (2010).

86 Smith, A. M. Validated models of immune response to virus infection. *Current Opinion in Systems Biology* **12**, 46-52, doi:10.1016/j.coisb.2018.10.005 (2018).

87 Smith, A. M. Host-pathogen kinetics during influenza infection and coinfection: insights from predictive modeling. *Immunological Reviews* **285**, 97-112, doi:10.1111/imr.12692 (2018).

88 Guedj, J. *et al.* Modeling shows that the NS5A inhibitor daclatasvir has two modes of action and yields a shorter estimate of the hepatitis C virus half-life. *Proceedings of the National Academy of Sciences* **110**, 3991-3996, doi:10.1073/pnas.1203110110 (2013).

89 Heldt, F. S., Frensing, T. & Reichl, U. Modeling the Intracellular Dynamics of Influenza Virus Replication To Understand the Control of Viral RNA Synthesis. *Journal of Virology* **86**, 7806-7817, doi:10.1128/jvi.00080-12 (2012).

90 Sidorenko, Y. & Reichl, U. Structured model of influenza virus replication in MDCK cells. *Biotechnology and Bioengineering* **88**, 1-14, doi:10.1002/bit.20096 (2004).
91 Fachada, N., Lopes, V. V. & Rosa, A. Simulating antigenic drift and shift in influenza A. 2093, doi:10.1145/1529282.1529744 (2009).
92 Levin, D. *et al.* A spatial model of the efficiency of T cell search in the influenza-infected lung. *Journal of Theoretical Biology* **398**, 52-63, doi:10.1016/j.jtbi.2016.02.022 (2016).
93 Beauchemin, C., Samuel, J. & Tuszynski, J. A simple cellular automaton model for influenza A viral infections. *Journal of Theoretical Biology* **232**, 223-234, doi:10.1016/j.jtbi.2004.08.001 (2005).
94 Beauchemin, C. Probing the effects of the well-mixed assumption on viral infection dynamics. *Journal of Theoretical Biology* **242**, 464-477, doi:10.1016/j.jtbi.2006.03.014 (2006).
95 Beauchemin, C., Forrest, S. & Koster, F. T. Modeling Influenza Viral Dynamics in Tissue. **4163**, 23-36, doi:10.1007/11823940_3 (2006).
96 Akpinar, F., Inankur, B., Yin, J. & Lyles, D. S. Spatial-Temporal Patterns of Viral Amplification and Interference Initiated by a Single Infected Cell. *Journal of Virology* **90**, 7552-7566, doi:10.1128/jvi.00807-16 (2016).
97 Bauer, A. L., Beauchemin, C. A. A. & Perelson, A. S. Agent-based modeling of host–pathogen systems: The successes and challenges. *Information Sciences* **179**, 1379-1389, doi:10.1016/j.ins.2008.11.012 (2009).
98 Medyukhina, A., Timme, S., Mokhtari, Z. & Figge, M. T. Image-based systems biology of infection. *Cytometry Part A* **87**, 462-470, doi:10.1002/cyto.a.22638 (2015).
99 Bankhead, A. *et al.* A simulation framework to investigate in vitro viral infection dynamics. *Journal of Computational Science* **4**, 127-134, doi:10.1016/j.jocs.2011.08.007 (2013).
100 Wilke, C. O. *et al.* Complex Spatial Dynamics of Oncolytic Viruses In Vitro: Mathematical and Experimental Approaches. *PLoS Computational Biology* **8**, e1002547, doi:10.1371/journal.pcbi.1002547 (2012).
101 Sun, G.-Q. *et al.* Spatiotemporal Dynamics of Virus Infection Spreading in Tissues. *Plos One* **11**, e0168576, doi:10.1371/journal.pone.0168576 (2016).
102 Jenner, A. L., Frascoli, F., Coster, A. C. F. & Kim, P. S. Enhancing oncolytic virotherapy: Observations from a Voronoi Cell-Based model. *Journal of Theoretical Biology* **485**, 110052, doi:10.1016/j.jtbi.2019.110052 (2020).
103 Quintela, B. M. *et al.* An Age-based Multiscale Mathematical Model of the Hepatitis C Virus Life-cycle During Infection and Therapy: Including Translation and Replication. **60**, 508-511, doi:10.1007/978-981-10-4086-3_128 (2017).
104 An, G. Agent-based computer simulation and sirs: building a bridge between basic science and clinical trials. *Shock* **16**, 266-273, doi:10.1097/00024382-200116040-00006 (2001).
105 An, G. In silico experiments of existing and hypothetical cytokine-directed clinical trials using agent-based modeling*. *Critical Care Medicine* **32**, 2050-2060, doi:10.1097/01.ccm.0000139707.13729.7d (2004).
106 Hunt, C. A., Cockrell, R. C. & An, G. Examining the controllability of sepsis using genetic algorithms on an agent-based model of systemic inflammation. *PLOS Computational Biology* **14**, e1005876, doi:10.1371/journal.pcbi.1005876 (2018).
107 Petersen, B. K. *et al.* Deep Reinforcement Learning and Simulation as a Path Toward Precision Medicine. *Journal of Computational Biology* **26**, 597-604, doi:10.1089/cmb.2018.0168 (2019).
108 An, G. Introduction of an agent-based multi-scale modular architecture for dynamic knowledge representation of acute inflammation. *Theoretical Biology and Medical Modelling* **5**, doi:10.1186/1742-4682-5-11 (2008).
109 Ghaffarizadeh, A., Heiland, R., Friedman, S. H., Mumenthaler, S. M. & Macklin, P. PhysiCell: An open source physics-based cell simulator for 3-D multicellular systems. *PLoS Comput Biol* **14**, e1005991, doi:10.1371/journal.pcbi.1005991 (2018).
110 Cooper, F. *et al.* Chaste: Cancer, Heart and Soft Tissue Environment. *Journal of Open Source Software* **5**, 1848, doi:10.21105/joss.01848 (2020).
111 Prlic, A. *et al.* Chaste: An Open Source C++ Library for Computational Physiology and Biology. *PLoS Computational Biology* **9**, e1002970, doi:10.1371/journal.pcbi.1002970 (2013).

112 Starruß, J., de Back, W., Brusch, L. & Deutsch, A. Morpheus: a user-friendly modeling environment for multiscale and multicellular systems biology. *Bioinformatics* **30**, 1331-1332, doi:10.1093/bioinformatics/btt772 (2014).
113 Sego, T. J. *et al.* A Modular Framework for Multiscale Spatial Modeling of Viral Infection and Immune Response in Epithelial Tissue. *bioRxiv*, 2020.2004.2027.064139, doi:10.1101/2020.04.27.064139 (2020).
114 Kang, S., Kahan, S., McDermott, J., Flann, N. & Shmulevich, I. Biocellion: accelerating computer simulation of multicellular biological system models. *Bioinformatics* **30**, 3101-3108, doi:10.1093/bioinformatics/btu498 (2014).
115 Hillen, T. *COVID-19 Physiology Group*, <https://sites.google.com/ualberta.ca/cov-pg/home> (2020).
116 *COVID-19 Cell Atlas*, <https://www.covid19cellatlas.org/> (2020).
117 Ostaszewski, M. *et al.* COVID-19 Disease Map, building a computational repository of SARS-CoV-2 virus-host interaction mechanisms. *Scientific Data* **7**, doi:10.1038/s41597-020-0477-8 (2020).
118 Hu, B. C. The human body at cellular resolution: the NIH Human Biomolecular Atlas Program. *Nature* **574**, 187-192, doi:10.1038/s41586-019-1629-x (2019).
119 Metzcar, J., Wang, Y., Heiland, R. & Macklin, P. A Review of Cell-Based Computational Modeling in Cancer Biology. *JCO Clin Cancer Inform* **3**, 1-13, doi:10.1200/CCI.18.00069 (2019).
120 Ghaffarizadeh, A., Friedman, S. H. & Macklin, P. BioFVM: an efficient, parallelized diffusive transport solver for 3-D biological simulations. *Bioinformatics* **32**, 1256-1258, doi:10.1093/bioinformatics/btv730 (2016).
121 Wang, Y., Heiland, R. & Macklin, P. *pc4nanobio: cancer nanotherapy simulator [nanoHUB app, Version 0.9.1]*, <https://nanohub.org/resources/pc4nanobio> (2019).
122 Jenner, A. L. *Replication Competent Oncolytic Virus expressing secretable trimeric TRAIL: hypothesis testing [nanoHUB app, Version 0.3]*, <https://nanohub.org/resources/iu399sp19p101> (2019).
123 Wang, Y., Heiland, R. & Macklin, P. *Physicell: liver tissue mechanobiology [nanoHUB app, Version 1.2]*, <https://nanohub.org/resources/pc4livermedium> (2019).
124 Ozik, J. *et al.* High-throughput cancer hypothesis testing with an integrated PhysiCell-EMEWS workflow. *BMC Bioinformatics* **19**, 483, doi:10.1186/s12859-018-2510-x (2018).
125 Ozik, J., Collier, N., Heiland, R., An, G. & Macklin, P. Learning-accelerated discovery of immune-tumour interactions. *Mol Syst Des Eng* **4**, 747-760, doi:10.1039/c9me00036d (2019).
126 Wang, Y. *et al.* Rapid community-driven development of a SARS-CoV-2 tissue simulator. *bioRxiv*, 10.1101/2020.1104.1102.019075, doi:10.1101/2020.04.02.019075 (2020).
127 Hucka, M. *et al.* The systems biology markup language (SBML): a medium for representation and exchange of biochemical network models. *Bioinformatics* **19**, 524-531, doi:10.1093/bioinformatics/btg015 (2003).
128 Somogyi, E. T. *et al.* libRoadRunner: a high performance SBML simulation and analysis library. *Bioinformatics* **31**, 3315-3321, doi:10.1093/bioinformatics/btv363 (2015).
129 Stoll, G. *et al.* MaBoSS 2.0: an environment for stochastic Boolean modeling. *Bioinformatics* **33**, 2226-2228, doi:10.1093/bioinformatics/btx123 (2017).
130 Letort, G. *et al.* PhysiBoSS: a multi-scale agent-based modelling framework integrating physical dimension and cell signalling. *Bioinformatics* **35**, 1188-1196, doi:10.1093/bioinformatics/bty766 (2019).
131 Cockrell, C. & An, G. Sepsis reconsidered: Identifying novel metrics for behavioral landscape characterization with a high-performance computing implementation of an agent-based model. *J Theor Biol* **430**, 157-168, doi:10.1016/j.jtbi.2017.07.016 (2017).
132 Cockrell, R. C. & An, G. Examining the controllability of sepsis using genetic algorithms on an agent-based model of systemic inflammation. *PLOS Computational Biology* **14**, e1005876, doi:10.1371/journal.pcbi.1005876 (2018).
133 Ozik, J., Collier, N. T., Wozniak, J. M. & Spagnuolo, C. in *2016 Winter Simulation Conference (WSC)* 206-220 (2016).
134 Ozik, J., Collier, N. T., Wozniak, J. M., Macal, C. M. & An, G. Extreme-Scale Dynamic Exploration of a Distributed Agent-Based Model With the EMEWS Framework. *IEEE Transactions on Computational Social Systems* **5**, 884-895, doi:10.1109/tcss.2018.2859189 (2018).

135 Wozniak, J. M. *et al.* CANDLE/Supervisor: a workflow framework for machine learning applied to cancer research. *BMC Bioinformatics* **19**, doi:10.1186/s12859-018-2508-4 (2018).
136 Khanna, A. S. *et al.* A modeling framework to inform preexposure prophylaxis initiation and retention scale-up in the context of 'Getting to Zero' initiatives. *Aids* **33**, 1911-1922, doi:10.1097/qad.0000000000002290 (2019).
137 Tatara, E. *et al.* in *2019 Winter Simulation Conference (WSC)* 1008-1019 (2019).
138 Rutter, C. M., Ozik, J., DeYoreo, M. & Collier, N. Microsimulation model calibration using incremental mixture approximate Bayesian computation. *The Annals of Applied Statistics* **13**, 2189-2212, doi:10.1214/19-aoas1279 (2019).
139 Madhavan, K. *et al.* nanoHUB.org: cloud-based services for nanoscale modeling, simulation, and education. *Nanotechnology Reviews* **2**, doi:10.1515/ntrev-2012-0043 (2013).
140 Kluyver, T. *et al.* in *ELPUB.* 87-90.
141 Friedman, S. H. *et al.* MultiCellDS: a community-developed standard for curating microenvironment-dependent multicellular data [**Preprint**]. *bioRxiv* **090456**, doi:10.1101/090456 (2016).
142 Heiland, R., Mishler, D., Zhang, T., Bower, E. & Macklin, P. xml2jupyter: Mapping parameters between XML and Jupyter widgets. *J Open Source Softw* **4**, doi:10.21105/joss.01408 (2019).
143 Macklin, P., Edgerton, M. E., Thompson, A. M. & Cristini, V. Patient-calibrated agent-based modelling of ductal carcinoma in situ (DCIS): from microscopic measurements to macroscopic predictions of clinical progression. *J Theor Biol* **301**, 122-140, doi:10.1016/j.jtbi.2012.02.002 (2012).
144 Lowe, D. *Angiotensin and the Coronavirus*, <https://blogs.sciencemag.org/pipeline/archives/2020/03/17/angiotensin-and-the-coronavirus> (2020).
145 Beauchemin, C., Forrest, S. & Koster, F. T. 23-36 (Springer Berlin Heidelberg).
146 Sniekers, Y. H. & van Donkelaar, C. C. Determining Diffusion Coefficients in Inhomogeneous Tissues Using Fluorescence Recovery after Photobleaching. *Biophysical Journal* **89**, 1302-1307, doi:10.1529/biophysj.104.053652 (2005).
147 Wang, H. *et al.* SARS coronavirus entry into host cells through a novel clathrin- and caveolae-independent endocytic pathway. *Cell Research* **18**, 290-301, doi:10.1038/cr.2008.15 (2008).
148 Pienaar, E. *et al.* A computational tool integrating host immunity with antibiotic dynamics to study tuberculosis treatment. *Journal of Theoretical Biology* **367**, 166-179, doi:10.1016/j.jtbi.2014.11.021 (2015).
149 Matzavinos, A. Mathematical modelling of the spatio-temporal response of cytotoxic T-lymphocytes to a solid tumour. *Mathematical Medicine and Biology* **21**, 1-34, doi:10.1093/imammb/21.1.1 (2004).
150 Liao, K.-L., Bai, X.-F. & Friedman, A. The role of CD200–CD200R in tumor immune evasion. *Journal of Theoretical Biology* **328**, 65-76, doi:10.1016/j.jtbi.2013.03.017 (2013).
151 Secomb, T. W., Liao, K.-L., Bai, X.-F. & Friedman, A. Mathematical Modeling of Interleukin-27 Induction of Anti-Tumor T Cells Response. *PLoS ONE* **9**, doi:10.1371/journal.pone.0091844 (2014).
152 Buchwalder, P.-A., Buclin, T., Trinchard, I., Munafo, A. & Biollaz, J. Pharmacokinetics and Pharmacodynamics of IFN-β1a in Healthy Volunteers. *Journal of Interferon & Cytokine Research* **20**, 857-866, doi:10.1089/10799900050163226 (2000).
153 Ye, S., Lowther, S., Stambas, J. & Sandri-Goldin, R. M. Inhibition of Reactive Oxygen Species Production Ameliorates Inflammation Induced by Influenza A Viruses via Upregulation of SOCS1 and SOCS3. *Journal of Virology* **89**, 2672-2683, doi:10.1128/jvi.03529-14 (2015).
154 Tenhumberg, S. *et al.* Structure-guided Optimization of the Interleukin-6 Trans-signaling Antagonist sgp130. *Journal of Biological Chemistry* **283**, 27200-27207, doi:10.1074/jbc.M803694200 (2008).
155 Arnaud, P. Les différents interférons : Pharmacologie, mécanismes d'action, tolérance et effets secondaires. *La Revue de Médecine Interne* **23**, 449S-458S, doi:10.1016/s0248-8663(02)00659-8 (2002).
156 Krombach, F. *et al.* Cell size of alveolar macrophages: an interspecies comparison. *Environmental Health Perspectives* **105**, 1261-1263, doi:10.1289/ehp.97105s51261 (1997).
157 *Blood and Bone Marrow Pathology*. (2011).
158 Du, M., Kalia, N., Frumento, G., Chen, F. & Zhang, Z. Biomechanical properties of human T cells in the process of activation based on diametric compression by micromanipulation. *Medical Engineering & Physics* **40**, 20-27, doi:10.1016/j.medengphy.2016.11.011 (2017).

159 Heyden, S. & Ortiz, M. Investigation of the influence of viscoelasticity on oncotripsy. *Computer Methods in Applied Mechanics and Engineering* **314**, 314-322, doi:10.1016/j.cma.2016.08.026 (2017).
160 Trepat, X., Chen, Z. & Jacobson, K. in *Comprehensive Physiology* (2012).
161 Craig, M., Humphries, A. R. & Mackey, M. C. An upper bound for the half-removal time of neutrophils from circulation. *Blood* **128**, 1989-1991, doi:10.1182/blood-2016-07-730325 (2016).
162 Eftimie, R. & Eftimie, G. Tumour-associated macrophages and oncolytic virotherapies: a mathematical investigation into a complex dynamics. *Letters in Biomathematics* **5**, S6-S35, doi:10.30707/LiB5.2Eftimiea (2018).
163 Kim, P. S., Lee, P. P. & Levy, D. Modeling regulation mechanisms in the immune system. *Journal of Theoretical Biology* **246**, 33-69, doi:10.1016/j.jtbi.2006.12.012 (2007).
164 Klöditz, K. & Fadeel, B. Three cell deaths and a funeral: macrophage clearance of cells undergoing distinct modes of cell death. *Cell Death Discovery* **5**, doi:10.1038/s41420-019-0146-x (2019).
165 Selders, G. S., Fetz, A. E., Radic, M. Z. & Bowlin, G. L. An overview of the role of neutrophils in innate immunity, inflammation and host-biomaterial integration. *Regenerative Biomaterials* **4**, 55-68, doi:10.1093/rb/rbw041 (2017).
166 Brandes, M., Klauschen, F., Kuchen, S. & Germain, Ronald N. A Systems Analysis Identifies a Feedforward Inflammatory Circuit Leading to Lethal Influenza Infection. *Cell* **154**, 197-212, doi:10.1016/j.cell.2013.06.013 (2013).
167 Janeway Jr, C. A., Travers, P. T., Walport, P. & Shlomchik, M. J. *Immunobiology*. 5th edn, (Garland Science, 2001).
168 Halle, S. *et al.* In Vivo Killing Capacity of Cytotoxic T Cells Is Limited and Involves Dynamic Interactions and T Cell Cooperativity. *Immunity* **44**, 233-245, doi:10.1016/j.immuni.2016.01.010 (2016).
169 Liao, M. *et al.* Single-cell landscape of bronchoalveolar immune cells in patients with COVID-19. *Nature Medicine* **26**, 842-844, doi:10.1038/s41591-020-0901-9 (2020).
170 McMaster, S. R., Wilson, J. J., Wang, H. & Kohlmeier, J. E. Airway-Resident Memory CD8 T Cells Provide Antigen-Specific Protection against Respiratory Virus Challenge through Rapid IFN-γ Production. *The Journal of Immunology* **195**, 203-209, doi:10.4049/jimmunol.1402975 (2015).
171 Grifoni, A. *et al.* Targets of T Cell Responses to SARS-CoV-2 Coronavirus in Humans with COVID-19 Disease and Unexposed Individuals. *Cell* **181**, 1489-1501.e1415, doi:10.1016/j.cell.2020.05.015 (2020).
172 Sette, A. & Crotty, S. Pre-existing immunity to SARS-CoV-2: the knowns and unknowns. *Nature Reviews Immunology* **20**, 457-458, doi:10.1038/s41577-020-0389-z (2020).
173 Wadman, M. Can boosting interferons, the body's frontline virus fighters, beat COVID-19? *Science*, doi:10.1126/science.abd7137 (2020).
174 Rowlatt, J. *Coronavirus: Protein treatment trial 'a breakthrough'*, <https://www.bbc.com/news/health-53467022> (2020).
175 Diao, B. *et al.* Reduction and Functional Exhaustion of T Cells in Patients With Coronavirus Disease 2019 (COVID-19). *Frontiers in Immunology* **11**, doi:10.3389/fimmu.2020.00827 (2020).
176 Mathew, D. *et al.*, doi:10.1101/2020.05.20.106401 (2020).
177 Organization, W. H. *WHO Director-General's opening remarks at the media briefing on COVID-19 - 11 March 2020*, <https://www.who.int/dg/speeches/detail/who-director-general-s-opening-remarks-at-the-media-briefing-on-covid-19---11-march-2020> (2020).